MHD COMBINED CONVECTION IN A CHANNEL WITH CAVITY USING NANOFLUIDS

by

Md. Abul Kalam Azad
Student No. 0411093007P
Registration No. 0411093007, Session: April- 2011

MASTER OF PHILOSOPHY
IN
MATHEMATICS

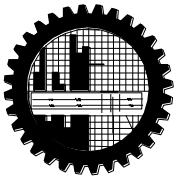

Department of Mathematics
BANGLADESH UNIVERSITY OF ENGINEERING AND TECHNOLOGY, DHAKA-1000
December 11, 2016

The thesis entitled **"MHD COMBINED CONVECTION IN A CHANNEL WITH CAVITY USING NANOFLUIDS"**, submitted by **Md. Abul Kalam Azad**, Roll no: 0411093007P, Registration No. 0411093007, Session April/2011 has been accepted as satisfactory in partial fulfillment of the requirement for the degree of Master of Philosophy in Mathematics on December 11, 2016.

BOARD OF EXAMINERS

1. _____
Dr. Salma Parvin — Chairman (Supervisor)
Associate Professor
Department of Mathematics, BUET, Dhaka-1000

2. _____
Dr. Md. Mustafa Kamal Chowdhury — Member (Co- Supervisor)
Professor (Retired)
Department of Mathematics, BUET, Dhaka-1000

3. _____
Head — Member (Ex-Officio)
Department of Mathematics
BUET, Dhaka-1000

4. _____
Dr. Md. Abdul Maleque — Member
Professor
Department of Mathematics, BUET, Dhaka-1000

5. _____
Dr. Mohammad Ferdows — Member (External)
Associate Professor
Department of Applied Mathematics,
University of Dhaka, Dhaka – 1000.

CANDIDATE'S DECLARATION

I hereby announce that the work which is being presented in this thesis entitled '**MHD COMBINED CONVECTION IN A CHANNEL WITH CAVITY USING NANOFLUIDS**' submitted in partial fulfillment of the requirements for the degree of **Master of Philosophy** in Mathematics on December 11, 2016, Bangladesh University of Engineering and Technology, Dhaka-1000 is my own work with proper citation and acknowledgement.

It is hereby declared that this thesis or any part of it has not been submitted elsewhere for any degree or diploma.

Md. Abul Kalam Azad
M. Phil Student
Department of Mathematics
December 11, 2016

CERTIFICATE OF RESEARCH

This is to certify that the work entitled '**MHD COMBINED CONVECTION IN A CHANNEL WITH CAVITY USING NANOFLUIDS**' has been carried out by **Mr. Md. Abul Kalam Azad** bearing Roll No.: 0411093007P, Registration No.: 0411093007, Session: April/2011, of Department of Mathematics, Bangladesh University of Engineering and Technology, Dhaka-1000, Bangladesh in partial fulfillment of the requirements for the degree of **Master of Philosophy** in Mathematics of the aforementioned University, under our supervision.

7/1/17

Dr. Md. Mustafa Kamal Chowdhury
Co-Supervisor
Department of Mathematics
Bangladesh University of Engineering and Technology (BUET)

07.01.17

Dr. Salma Parvin
Supervisor
Department of Mathematics
Bangladesh University of Engineering and Technology (BUET)

Dedicated

to

My Parents and Kids

ACKNOWLEDGEMENT

All praises for Almighty ALLAH, Whose uniqueness, oneness and wholeness is unchallengeable and without His help no work would have been possible to accomplish the goal.

I am especially indebted to my supervisor Assoc. prof. Dr. Salma Parvin, Department of Mathematics, Bangladesh University of Engineering and Technology and Co Supervisor Prof. Dr. Md. Mustafa Kamal Chowdhury, Department of Mathematics, Bangladesh University of Engineering and Technology for their guidance and encouragement throughout my study. I have experienced an excellent academic study under their supervision and their invaluable recommendations and support helped me to plan my further academic studies in the best way.

I am thankful from the core of my heart to faculty members of the Department of Mathematics, Bangladesh University of Engineering and Technology, especially, to Prof. Dr. Md. Abdul Alim, Head, Department of Mathematics, Prof. Dr. Md. Abdul Maleque, Prof. Dr. Md. Abdul Hakim Khan, Prof. Dr. Md. Elias, Prof. Dr. Md. Manirul Alam Sarker, Prof. Dr. Md. Zafar Iqbal Khan, Assoc. Prof. Dr. Ms. Rehena Nasrin and all other teachers of this department for their guidance and supports.

I am also very grateful to Prof. Dr. Md. Mustafizur Rahman, Department of Mathematics, Bangladesh University of Engineering and Technology for giving me an initiative for this study. Without his inspiring guidance, remarkable suggestions, constant encouragement, keen interest, constructive criticism and friendly discussions, this thesis could not have been possible.

I am grateful to all my colleagues in AIBA as well as IIUC for their encouragement and helping mentality in all affairs especially in my research work.

Last but not least, I must acknowledge the love and affection of my family members who prayed for my success and well-being. I am grateful to them for their never-ending love, patience and encouragement.

ABSTRACT

Heat Transfer Enhancement in presence of magnetic field on combined convective flow in a horizontal channel with a bottom heated open cavity using nanofluids has been studied numerically. The horizontal lower surface is at a uniform temperature T_h while vertical sides of the cavity along with the channel walls are adiabatic. The physical domain is filled with water based nanofluids containing Cu nanoparticles. The fluid enters from left with initial velocity U_i and temperature T_i and exits from right The physical problems are represented mathematically by different sets of governing two-dimensional equations along with the corresponding boundary conditions. Using a class of appropriate transformations, the governing equations along with the boundary conditions are transformed into non-dimensional form, which are then solved by employing a finite-element method based on Galerkin weighted residuals. The investigations are conducted for different values of Rayleigh number Ra (= 10^3 - 10^6), Reynolds number Re (= 100 – 500), Hartmann number Ha (= 0 – 20), solid volume fraction ϕ (= 0% – 15%), and physical parameter, cavity aspect ratio AR (= 0.5 - 2.0). Various characteristics such as streamlines, isotherms and heat transfer rate in terms of the average Nusselt number (Nu_{av}), and average fluid temperature (θ_{av}) are presented for the aforesaid parameters. The results indicate that the mentioned parameters strongly affect the flow phenomenon and temperature field inside the cavity whereas in the channel these effects are less significant. Comparisons with previously published work are performed and the results are found to be in excellent agreement.

TABLE OF CONTENTS

NOMENCLATURE

AR	cavity aspect ratio
B_0	magnetic induction (Wb/m^2)
c_p	specific heat at constant pressure (J/kg.K)
g	gravitational acceleration (ms^{-2})
h	convective heat transfer coefficient ($W/m^2.K$)
H	height of the cavity (m)
Ha	Hartmann number
k	thermal conductivity of fluid ($Wm^{-1}K^{-1}$)
L	length of the cavity (m)
n	dimensional distance either along x or y direction (m)
N	non-dimensional distance either along X or Y direction
N_α	quadratic shape function
Nu	Nusselt number
p	pressure
P	non-dimensional pressure
Pr	Prandtl number
Ra	Rayleigh number
Re	Reynolds number
S_x	surface tractions along X-axis
S_y	surface tractions along Y-axis
T	dimensional fluid temperature (K)
ΔT	dimensional temperature difference (K)
u	velocity in x-direction (m/s)
U	dimensionless horizontal velocity
v	velocity in y-direction (m/s)
V	dimensionless vertical velocity
$\overline{A}$	cavity area (m^2)
x, y	Cartesian coordinates (m)
X, Y	dimensionless Cartesian coordinates

Greek symbols

α	thermal diffusivity (m^2s^{-1})
β	coefficient of thermal expansion (K^{-1})
θ	dimensionless fluid temperature
$\Delta\theta$	dimensionless temperature difference
ψ	stream function
ϕ	solid volume fraction

μ	dynamic viscosity of the fluid (m^2s^{-1})
ν	kinematic viscosity of the fluid (m^2s^{-1})
ρ	density of the fluid (kgm^{-3})
σ	fluid electrical conductivity ($\Omega^{-1}.m^{-1}$)

Subscripts

av	average
f	fluid
h	heated wall
i	inlet state
nf	nanofluid
s	solid nanoparticle

LIST OF TABLES

LIST OF FIGURES

CHAPTER 1

INTRODUCTION

Quite often we encounter fluid flow and heat transfer in cavities at different orientations. These classical problems have some analytical and huge numerical solutions. Heat transfer through channel is an important development and an area of very rapid growth in contemporary trend of heat transfer research. The flow of energy carrying fluids through channel is a rapidly growing branch of fluid mechanics and heat transfer. Mixed convection heat transfer in a channel with an open cavity in the presence of magnetic field is a new branch of thermo-fluid mechanics. To describe the heat transport phenomenon, strong background of the hydrodynamics, the convective heat transfer mechanism and the electromagnetic field are pre-requisite as they have a symbiotic relationship. On the other hand heat transfer properties of thermo fluid play an important role in the development of energy-efficient heat transfer equipment. Passive enhancement methods are commonly utilized in the electronics and transportation devices. But the working fluids such as ethylene glycol, water and engine oil have poor heat transfer properties. In that regard, various techniques have been proposed to enhance the heat transfer performance of fluids. Researchers have also tried to increase the thermal conductivity of base fluids by suspending micro- or larger-sized solid particles in fluids since the thermal conductivity of solid is typically higher than that of liquids. Therefore a new class of heat transfer fluids can be designed by suspending metallic nanoparticles in conventional heat transfer fluids. This chapter provides a general introduction to applied thermodynamics of nanofluids, which includes mixed convection heat transfer phenomena that occurs under different areas of applications in the field of engineering, such as Silicon mirror cooling, electronics cooling, vehicle cooling, transformer cooling, nuclear reactors, lakes and reservoirs, and solar applications etc.

The rest of this introductory chapter is as follows. Since the problem that we shall study in this thesis is MHD combined convection in a channel with cavity using nanofluids, we begin with a brief description on modes of heat transfer in section 1.1. Then reviews on fluid properties and some effective parameters have been given in sections 1.2 and 1.3 respectively. In section 1.4 mixed convection heat transfer in cavity is discussed shortly. For convenience of present investigation, Nano fluid properties are presented in section 1.5. Literature related to this study has been presented briefly in section 1.6. Then application, the motivation behind selection of the present problem and objective of the current study are described in sections 1.7 to 1.9. Finally, in section 1.10, a brief outline of the remainder of the thesis has been presented.

1.1 MODES OF HEAT TRANSFER

Heat transfer is the process of transportation of thermal energy from one region to another region as a result of temperature difference. The heat transfer takes places by the distinct mechanisms or modes: Conduction, Convection and Radiation. The heat transfer always takes place from higher temperature medium to lower temperature one and heat transfer stops when the two mediums reaches the same temperature.

Conduction is the transfer of energy from the higher energetic particle of a substance to adjacent lower energetic ones as a result of interactions between the particles. Conduction can take place in solids, liquids, or gases. In gases and liquids, conduction is due to the collisions and diffusion of the molecules during their random motion in solids it is due to the combination of vibrations of the molecules in a lattice and the energy transport by free electrons. The rate of heat conduction through a medium depends on the geometry of the medium, its thickness and the material of the medium, as well as the temperature difference across the medium.

Convection is the mechanism of heat transfer through a fluid in the presence of bulk fluid motion resulting from the temperature difference. The convection of heat transfer is of two types: natural convection and forced convection. If the fluid flow via convection occurs naturally, the convection is called natural (or free) convection. In this case fluid motion is set up by buoyancy effects resulting from the density variation caused by the temperature difference in the fluid and gravitational force. On the other hand, if the fluid motion is artificially created by means of external source like a blower or fan, the heat transfer mode is called forced convection.

Radiation is the energy emitted by matter in the form of electromagnetic waves (or photons) as a result of the changes in the electronic configuration of the atom or molecules. Unlike conduction and convection, the transfer of heat by radiation does not require the presence of an intervening medium. In fact, heat transfer by radiation is faster and suffers no reduction in a vacuum. This is how the energy of the sun reaches the earth. Radiation is a volumetric phenomenon, and all solids, liquids, and gases emit, absorb, or transmit radiation to varying degrees. However, radiation is usually considered to be a surface phenomenon for solids that are opaque to thermal radiation such as metals, wood and rocks

1.2 SOME DEFINITIONS

1.2.1 Viscosity

The viscosity of a fluid which is a strong function of temperature is a measure of its resistance to deformation. A friction force develops between two adjacent fluid layers while they move relative to each other and the slower layer tries to slow down the faster layer. This type of internal resistance to flow is quantified by the fluid property viscosity. All fluid flows involve viscous effects to some degree and therefore no fluid is of zero viscosity. As temperature increases, the viscosity of liquids decreases whereas the viscosity of gases increases with temperature.

1.2.2 Viscous Flow

Such flows are called viscous whose flow patterns are dominated by the viscous properties of the fluid. This arises in fluids where the velocity gradients are comparatively large. The flow close to the walls of the pipes can be treated as viscous flows.

1.2.3 Non-viscous Flow

The flow is defined as non-viscous or inviscid flow if the viscous properties are not dominant. These types of flows are common in the center region of flow in pipes and in gas flows.

1.2.4 Newton's Law of Viscosity

If the shearing stress, τ , increases by increasing the force *P*, the rate of shearing strain also increases in direct proportion to that; $\tau \ \alpha \ \frac{du}{dy}$ i.e., $\tau = \mu \frac{du}{dy}$, where μ is the dynamic viscosity of the fluid. This principle is known as the Newton's law of viscosity.

1.2.5 Newtonian Fluid

Newtonian fluids are those fluids for which the constant of proportionality i.e. the co-efficient of viscosity (μ) does not change with the rate of deformation. In other words, fluids that follow the Newton's law of viscosity are known as Newtonian fluids. Water, air and mercury are some examples of Newtonian fluids.

1.2.6 Non-Newtonian Fluid

Non-Newtonian fluids are those fluids for which the constant of proportionality i.e. the co-efficient of viscosity (μ) changes with the rate of deformation. In other words, fluids that do not follow the Newton's law of viscosity are known as non-Newtonian fluids. Blood, liquid plastic and polymer solutions are non-Newtonian fluids.

1.2.7 Compressibility

Compressibility is a property of fluid that measures the change in density and consequently, the change in the volume of a fluid during motion under the action of external forces. The compressibility is expressed in terms of Mach number (M) which is defined by $M = \frac{\text{speed of fluid}}{\text{speed of sound}} = \frac{u}{\alpha_0}$

1.2.8 Compressible Flow

A compressible flow is one in which the density varies in the different portion of the fluids. Thus the volume of every portion of fluid differs in compressible flow over the course of its motion.

1.2.9 Incompressible Flow

A flow is said to be incompressible if the density remains nearly constant throughout. Therefore, for incompressible flow the volume of every portion of fluid remains unchanged over the course of its motion. The density of liquids is basically constant and accordingly the flow of liquids is naturally referred to as incompressible.

1.2.10 Internal and External Flows

A fluid flow is classified into two categories; internal and external, depending on whether the fluid is forced to flow in a confined channel or over a surface. An internal flow is in a channel bounded on all sides by a solid surface except, possibly, for an inlet and exit. Flows through a pipe or in an air-conditioning duct are the examples of internal flow. Internal flows are dominated by the influence of viscosity throughout the flow field. The flow of an unbounded fluid over a surface is external flow.

1.2.11 Thermal Diffusivity

Thermal diffusivity represents how fast heat diffuses through a material and is defined as α = Heat conducted /Heat stored = $\frac{k}{\rho c_p}$

Here the thermal conductivity k represents how well a material conducts heat and the heat capacity ρCp represents how much energy a material stores per unit volume. Therefore, the thermal diffusivity of material can be viewed as the ratio of the heat conducted through the material to the heat stored per unit volume. A material that has a high thermal conductivity or a low heat capacity will obviously have a large thermal diffusivity. The large thermal diffusivity means that the propagation of heat into the medium is faster. A small value of thermal diffusivity means the heat is mostly absorbed by the material and a small amount of heat is conducted further.

1.2.12 Thermal Conductivity

Thermal conductivity is defined as the quantity of heat (Q) transmitted through a unit thickness (L) in a direction normal to a surface of unit area (A) due to a unit temperature gradient (ΔT) under steady state conditions and when the heat transfer is dependent only on the temperature gradient. In equation form this becomes the following:

Thermal Conductivity = heat × distance / (area × temperature gradient)

$$\lambda = Q \times L / (A \times \Delta T)$$

1.2.13 Magnetohydrodynamics

Magnetohydrodynamics (MHD) is that branch of science, which deals with the flow of electrically conducting fluids in electric and magnetic fields. The motion of the conducting fluid across the magnetic field generates electric currents which change the magnetic field and the action of the magnetic field on these currents give rise to

mechanical forces, which modify the fluid. However, MHD is usually regarded as a very contemporary subject. Probably the largest advance towards an understanding of such phenomena comes from the fields of astrophysics and geophysics. It has long been assumed that most of the matter in the universe is in the plasma or highly ionized state and much of the basic knowledge in the area of electromagnetic fluid dynamics evolved from these studies. Moreover MHD explains certain natural phenomena. The motions of the sea induce magnetic field that perturb the earth's magnetic field. Alternatively the electromagnetic force due to the interaction of currents and earth's magnetic field propels ocean movements. The MHD was originally applied to astrophysical and geophysical problems, where it is still very important. Engineers employ MHD principles in the design of heat exchanger, pumps and flow meters, in space vehicle propulsion, control and re-entry in creating novel power generating systems and developing confinement schemes for controlled fusion. Other potential applications for MHD include electromagnets with fluid conductors, various energy conversion or storage devices, and magnetically controlled lubrication by conducting fluids etc. Detailed discussion of the Magnetohydrodynamics (MHD) can be found in Shercliff (1965).

1.3 DIMENSIONLESS PARAMETERS

The dimensionless parameters can be considered as measures of the relative importance of certain aspects of the flow. Some dimensionless parameters related to the present study are discussed below:

1.3.1 Reynolds Number

The transition from laminar to turbulent flow depends on the surface geometry, surface roughness, flow velocity, surface temperature and type of fluid, among other things. In 1883 Osborn Reynolds discovered that the flow regime depends mainly on the ratio of the inertia forces to friction forces in the fluid. This ratio is called the Reynolds number, which is a dimensionless quantity, and is defined as

$$\mathrm{Re} = \frac{inertia\ \ Force}{Friction\ \ \ Force} = \frac{Mass \times Accelaretion}{Shering\ Stress \times Cross\,\mathrm{sec}tional\ Area}$$
$$= \frac{Volume \times Density \times (Velocity / Time)}{\mu \times (Velocity / Length) \times Cross\ Sectional\ Area}$$
$$= \frac{(Length)^3 \times Density \times (Length / Time)}{\mu \times (Length)^2}$$
$$= \frac{Length \times Density \times Velosity}{\mu} = \frac{L \times \rho \times V}{\mu} = \frac{LV}{\mu / \rho} = \frac{LV}{\nu}$$

Here *V, L, ρ and μ.* are characteristic values of reference velocity, characteristic length, density and coefficient of viscosity of the fluid flow respectively and $\nu = \frac{\mu}{\rho}$ is the kinematic viscosity.

1.3.2 Prandtl Number

The relative thickness of the velocity and the thermal boundary layers are best described by the dimensionless parameter Prandtl number, defined as

$$Pr = \frac{\nu}{\alpha} = \frac{\text{Viscous diffusion rate}}{\text{Thermal diffusion rate}} = \frac{c_p \mu}{k}$$

Where ν is the kinematic viscosity, $\nu = \frac{\mu}{\rho}$, α is the thermal diffusivity and $\alpha = \frac{k}{(\rho c_p)}$, μ is the dynamic viscosity, k is the thermal conductivity, c_p is the specific heat and ρ is the density. It is named after Ludwing Prandtl, who introduced the concept of boundary layer in 1904 and made significant contributions to boundary layer theory. The Prandtl number of fluids ranges from less than 0.01 for liquid metals to more than 100,000 for heavy oils.

1.3.3 Rayleigh Number

The Rayleigh number for a fluid is a dimensionless number associated with the heat transfer within the fluid. When the Rayleigh number is below the critical value for

that fluid, heat transfer is primary in the form of conduction; when it exceeds the critical value, heat transfer is primarily in the form of convection. The Rayleigh number is named after Lord Rayleigh and is defined as the product of the Grashof number, which describes the relationship between buoyancy and viscosity within a fluid, and the Prandtl number, which describes the relationship between momentum diffusivity and thermal diffusivity.

For free convection near a vertical wall, this number is

$$Ra_x = Gr_x \,\mathrm{Pr} = \frac{g\beta}{\nu\alpha}\left(T_s - T_\infty\right)x^3$$

where

Pr = Prandtl number

g = gravity

x = characteristic length (in this case, length of cavity)

T_s = Temperature of surface

T_∞ = Quiescent temperature

ν = kinematic viscosity

α = thermal diffusivity

β = thermal expansion coefficient

Fluid properties Pr, ν, α and β are evaluated at the field temperature, which is defined as $T_f = \frac{T_s + T_\infty}{2}$

For most engineering purposes, the Rayleigh number is large, somewhere around 10^6 and 10^8.

1.3.4 Hartmann Number

Hartmann number is the ratio of electromagnetic force to the viscous force first introduced by Hartmann. It is defined by $Ha = B_0 L\sqrt{\frac{\sigma}{\mu}}$

Where, B_0 is the magnetic field, L is the characteristic length scale, σ is the electric conductivity and μ is the viscosity. In addition, it is a dimensionless quantity characterizing flow of conducting fluid in a transvers magnetic field, being the product of the magnetic flux density, a representative length and the square root of the ratio of electric conductivity to viscosity.

1.3.5 Solid Volume Fraction

The Solid volume fraction ϕ_i is defined as the volume of a constituent V_i divided by the volume of all constituents of the mixture V prior to mixing $\phi_i = \frac{V_i}{\sum_j V_j}$

Being dimensionless, its unit is 1; it is expressed as a number. The volume fraction coincides with the volume concentration in ideal solutions where the volumes of the constituents are additive (the volume of the solution is equal to the sum of the volumes of its ingredients).The sum of all volume fractions of a mixture is equal to $1: \sum_i^N V_i = V;\ \sum_i^N \phi_i = 1$

The volume fraction (percentage by volume, vol%) is one way of expressing the composition of a mixture with a dimensionless quantity; mass fraction (percentage by weight, wt%) and mole fraction (percentage by moles, mol%) are others. Volume percent is a common expression of a solution's concentration. It is the volume fraction expressed with a denominator of 100, and thus is defined as:

$$Volume\ \ Percent = \frac{Volume\ of\ \ Solute}{Volume\ \ of\ \ Solution} \times 100\%$$

Volume percent is usually used when the solution is made by mixing two fluids, such as liquids or gases. However, percentages are only additive for ideal gases. The percentage by volume (vol%) is one way of expressing the composition of a mixture with a dimensionless quantity; mass fraction (percentage by weight, wt%) and mole fraction (percentage by moles, mol%) are others.

1.4 MIXED CONVECTION HEAT TRANSFER IN CAVITIES

Mixed convection in cavities is a topic of contemporary importance, because cavities filled with fluid are central components in a long list of engineering and geophysical systems. The flow and heat transfer induced in a cavity differs fundamentally from the external mixed convection boundary layer. Mixed convection in a cavity unlike the external mixed convection boundary layer that is caused by the heat transfer interaction between a single wall and a very large fluid reservoir is the result of the complex interaction between finite size fluid systems in thermal communication with all the walls that confine it. The complexity of this internal interaction is responsible for the diversity of flows that can exist inside cavity.

The phenomenon of mixed convection in cavities is varied by the geometry and the orientation of the cavity. Judging by the potential engineering applications, the cavity phenomena can loosely be organized into two classes.

1. Vented cavity and 2. Lid-driven cavity

In a vented cavity, where the interaction between the external forced stream provided by the inlet and the buoyancy driven flows induced by the heat source leads to the possibility of complex flows. Therefore it is important to understand the fluid flow and heat transfer characteristics of mixed convection in a vented cavity. On the other hand, the fluid flow and heat transfer in a lid-driven cavity where the flow is induced by a shear force resulting from the motion of a lid combined with the buoyancy force due to non-homogeneous temperature of the cavity wall, provides another problem, studied extensively by researchers to understand the interaction between buoyancy and shearing forces in such flow situation. The interaction between buoyancy driven and shear driven flows inside a closed cavity in a mixed convection regime is quite complex. Therefore it is also important to understand the fluid flow and heat transfer characteristics of mixed convection in a lid-driven cavity.

1.5 NANOFLUIDS

The addition of small particles into base fluid to improve base fluid's thermal conductivity has been in use since the establishment of Maxwell treatise. With the recent improvements in nanotechnology, the production of particles with sizes on the order of nanometers (nanoparticles) can be achieved with relative ease. Due to their small size, nanoparticles fluidize easily inside the base fluid, and as a consequence, blockage of channels and erosion in channel walls are no longer a problem. When it comes to the stability of the suspension, it was shown that sedimentation of particles can be prevented by utilizing proper dispersants. Many different particle materials are used for nanofluid preparation. Al_2O_3, CuO, TiO_2 SiC, TiC, Ag, Au, Cu, and Fe nanoparticles are frequently used in nanofluid research. Carbon nanotubes are also utilized due to their extremely high thermal conductivity in the longitudinal (axial) direction. Base fluids mostly used in the preparation of nanofluids are the common working fluids of heat transfer applications; such as, water, ethyleneglycol and engine oil. In order to improve the stability of nanoparticles inside the base fluid, some additives are added to the mixture in small amounts.

Nanoparticles used in nanofluid preparation usually have diameters below 100 nm. Particles as small as 10 nm have been used in nanofluid research. When particles are not spherical but rod or tube-shaped, the diameter is still below 100 nm, but the length of the particles may be on the order of micrometers. It should also be noted that due to the clustering phenomenon, particles may form clusters with sizes on the order of micrometers

1.5.1 Nanofluids Preparation

Rapid development in nanotechnology has made it possible to produce materials in nano dimension (nanoparticles). Nanoparticles are usually available in the form of powder and have higher thermal conductivity than fluid.

Being in nano scale, nanoparticles exhibits unique and enhanced physical and chemical characteristics compared to that of bulk materials (Murshed et al. 2008a; Yu et al. 2007). Nanofluids is not just a simple mixture of nanoparticles and base fluids. The nanofluids must be a stable and durable suspension, with no chemical reaction and minimum particles agglomeration (Wang and Mujumdar 2007). A stable nanoparticles suspension is a necessity to produce nanofluids with an optimum or enhanced thermal properties (Keblinski et al. 2005; Ghadimi et al. 2011).

Nanofluids can be produced through a two-step or single-step method. In two-step method, nanoparticle dry powders are produced either by physical or chemical synthesis. It will then be dispersed into the base fluid using ultrasonic disruptor (Murshed et al. 2005; Hwang et al. 2006; Duangthongsuk and Wongwises 2009) or high pressure homogenizer (Hwang et al. 2008). The limitations and disadvantages of this method are sedimentation, clustering and aggregation of nanoparticles with respect to length of time. Nanoparticles are prone of agglomeration due to the attractive force between them known as van der der waals attractive force aals attractive force. Typical transmission electron microscopy (TEM) images of nanoparticles in water base fluid

are shown in Figure 1.1.

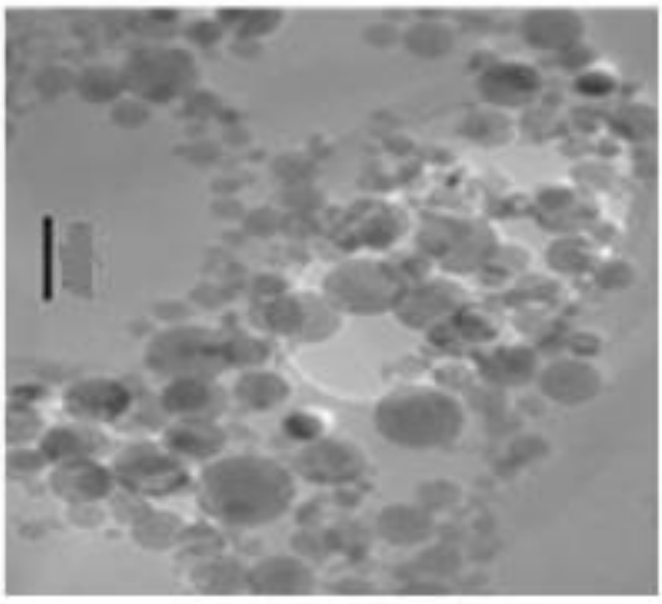

Figure 1.1 Typical Transmission of electron microscopy (TEM) image of Cu-water nanofluids.

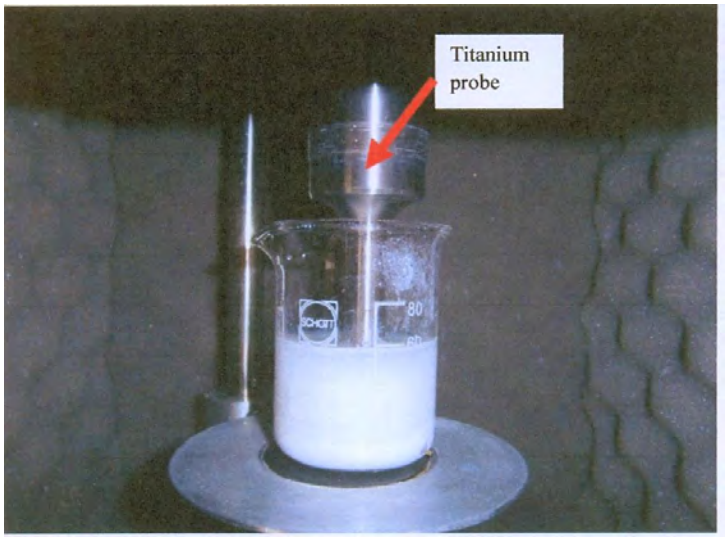

Figure 1.2 Ultrasonication process of nanofluids

From the figure, it is observed that there is slight particle agglomeration existent in the base fluid suspension. A stabilizer agent which is able to provide repulsive force is needed to overcome the attractive force. Aside from that, two-step method is preferable for oxide type nanoparticles compared to that of metallic type (Mahbubul et al. 2011; Ghadimi et al. 2011; Wang and Mujumdar, 2007; Sarit et al. 2008) emphasized that two-step method is not an effective approach for metal nanoparticles such as copper. Figure 1.2 shows typical nanofluids subjected to ultrasonication process.

Single-step method is a technique where fabrication of nanoparticles and nanofluids synthesis is done in a same single process. In this method, direct evaporation technique condenses the nanoparticles vapour directly to the lower vapour pressure base fluid in a vacuum chamber. Argonne laboratory used this method in preparing ethylene glycol based copper nanofluids (Eastman et al. 2001). Advantages of this method is the capability of reducting the nanoparticle aggolomeration (Murshed et al. 2008a), and prevention of nanoparticles oxidation (Yu et al. 2007). However, two-step method is preferred due to its low cost nature; therefore it is potential for bulk production. Table 1.2 summarizes synthesis used in nanofluid research. This can be concluded that two-step method is widely used in nanofluids research.

Table 1.1 Synthesis method in nanofluids formulation

Base fluid	Nanoparticles	Synthesis method	References
Water	Alumina (ϕ 15-50nm)	Two-steps	Zhu et al. (2009)
Ethylene glycol	Titanate nanotube (ϕ 10nm Length = ~100nm)	Two-steps	Chen et al. (2009)
Water	Alumina (ϕ <30 ± 5nm)	Two-steps	Do et al. (2010)
60%Ethylene glycol, 40% Water	Alumina, silicon dioxide, Copper(I) oxide	Two-steps	Vajjha et al. (2010)
Ethylene glycol	Copper	Two-steps	Yu et al. (2010)
Ethylene glycol	Diamond	Two-steps	Yu et al. (2011)
De-ionized water	Alumina (10-30nm)	Two-steps	Lin et al. (2011)
Water	Silver	Single-step	Paul et al. (2012)
De-ionized water	Alumina (43nm); Copper oxide (30nm)	Two-steps	Suresh et al. (2012)
De-ionized water	Alumina, titanium dioxide, zinc oxide	Two-steps	Putra et al. (2012)
Ethylene glycol	Copper	Single-step	De Roberties et al. (2012)

1.5.2 Tharmal Conductivity of Nanofluids

Nanofluids thermal conductivity represents the ability of the heat to flow. It is the most important characteristic used to justify the suitability of nanofluids as a heat transfer fluid. Substantial studies have been conducted to investigate the factors affecting the thermal conductivity of nanofluids. Summary of nanofluids thermal conductivity related studies is depicted in Table 1.2.

Table 1.2 Nanofluids thermal conductivity related studies

References	Base fluid	Particle	Study related to				
			Temp	Shape /size	Vol.% /Wt.%	Surfactant /pH	Particle
Eastman et al. (2011)	Ethylene glycol	Cu			√	√	
Murshed et al. (2005)	De-ionized water	TiO_2		√	√		
Liu et al. (2006)	Water	Cu		√	√		
Yoo et al. (2007)	Water, ethylene glycol	TiO_2,Al_2O_3, Fe,WO_3		√	√		√
Zhang et al. (2007)	Toluene, water	Au, Al_2O_3, TiO_2,CuO, CNT	√	√	√		√
Beck et al. (2007)	Ethylene glycol	Al_2O_3	√		√		
Lee et al. (2008)	De-ionized water	Al_2O_3			√		
Li et al. (2008)	Water	Cu			√	√	
Duangthongsuk and Wongwises, (2009)	Water	TiO_2	√		√		
Mintsa et al. (2009)	Distilled water	CuO,TiO_2	√	√	√		√
Zhu et al. (2009)	Water	Al_2O_3			√	√	
Yu et al. (2009)	Ethylene glycol	ZnO	√		√		
Chandrasekar et al. (2010)	Water	Al_2O_3			√		
Yu et al. (2010)	Ethylene glycol	Cu	√		√	√	
Teng et al. (2010)	Water	Al_2O_3	√	√	√		
Lee et al. (2011)	De-ionized water	SiO			√	√	
Lin et al. (2011)	De-ionized water	Al_2O_3	√			√	

1.5.3 Effect of Particle Volume Fractions

The distinguished research of Eastman et al. (2001) which draws great interest and attention of thermal scientists and engineers reported that thermal conductivity of ethylene glycol based copper (<10nm) nanofluids with 0.3 vol.% was enhanced up to 40% compared to that of base fluid. Study found that the metallic-based nanofluids provide higher thermal conductivity than oxide type of nanofluids. This is attributed to higher intrinsic thermal conductivity of Cu nanoparticle compared to that of Al_2O_3 and CuO. Another reason is that the Cu particle used in this study was four times smaller than oxide particle. Same type of nanofluids was investigated by Yu et al. (2010). In contrast to the Eastman's result, only 11% enhancement was obtained for the same particle loading. This discrepancy may be due to different synthesis methods of nanofluid preparation and type of dispersant used in both studies. In another research, Liu et al. (2006) found that water containing only 0.1% vol. of Cu nanoparticles exhibited 23.8% improvement in thermal conductivity. The nanofluids in their study were produced through one step chemical reduction method.

Up to now, most of the studies implied that the thermal conductivity increases with respect to particles volume fractions. Some researchers indicated that a linear relationship was discovered. However, there are researchers that observed a non-linear thermal conductivity trend. Chandrasekar et al. (2010) studied thermal conductivity of water based Al_2O_3 nanofluids and concluded linear dependency on the particle volume fractions. For the lower range of Al_2O_3 volume fractions (0.01 to 0.3 vol. %) Lee et al. (2008) showed that thermal conductivity increased linearly with particle volume fractions. However, in other researches, non-linear relationship was observed for nanofluids thermal conductivity with low concentration. Murshed et al. (2005) experiment found that, thermal conductivity of TiO_2 nanofluids showed non- linear relationship for volume fractions less than 2%. This could be due to the addition of CTAB surfactant into the base fluid in their study.

Non linear relationship was also discovered for nanofluids containing up to 5 vol. % of ZnO particle (Yu et al. 2009). The slope of the thermal conductivity enhancement with respect to particle volume fraction was higher at lower volume fractions (about 0.2 to 0.7 vol. %) compared to the slope at higher volume fractions (1 to 5 vol. %). Authors explained that this was due to the larger increase of nanofluids viscosity compared to thermal conductivity enhancement.

Two types of nanofluids that are commonly used in researches are Al_2O_3 and TiO_2 nanofluids. Murshed et al. (2005) experimentally showed that thermal conductivity of water based TiO_2 nanofluids correlates with particle volume fractions. With only 5 vol. %, of TiO_2 nanoparticles, 29.7% and 32.8% thermal conductivity enhancement were observed for nanofluids with TiO_2 ϕ 15nm and ϕ 10nm × 40nm, respectively. Comparison between water based Al_2O_3 and TiO_2 nanofluids were carried out by Yoo et al. (2007). Study revealed that by adding 1% nanoparticle volume fraction, thermal conductivity enhancement of Al_2O_3 (4% enhancement) was lower than TiO_2 (14.4% enhancement) although it is known that Al_2O_3 has higher bulk thermal conductivity than TiO_2. This shows that particle's thermal conductivity is not the major factor to improve nanofluids thermal conductivity. The same study also found that ceramic type nanofluids have lower thermal conductivity than metallic type nanofluids under the same concentration. Beck et al. (2007) demonstrated the dependence of Al_2O_3 nanofluids thermal conductivity on particle volume fractions. Duangthongsuk and Wongwises (2009) performed research on TiO_2/ water nanofluids with respect to volume fraction up to 2%.

Another study done by Mintsa et al. (2009) covered a larger range of nanoparticle volume fraction (up to 18%). Similar to the previous studies, these authors experimentally pointed out that the nanofluids (Al_2O_3, CuO) thermal conductivity was relatively higher than base fluid. The drawback of the addition of higher particle volume fractions is the stability issue. Wu et al. (2009) revealed nanoparticles tend to agglomerate at higher volume component. There are also studies which focused on nanofluids containing carbon Nanotube.

Hwang et al. (2006) highlighted that 11.3% enhancement was achieved with addition of 1% of MWCNT into water. It has the highest thermal conductivity improvement compared to that of CuO /water, SiO_2/water, and CuO/EG nanofluids. Thermal conductivity of water containing 3wt. % MWCNT enhanced about 13% is higher than predicted value from Maxwell correlation (Lee et al. 2011).

1.5.4 Effect of Particle Size and Shape

Most of the researchers found that thermal conductivity of nanofluids with smaller nanoparticles sizes tend to produce higher values compared to larger particles. Chon and Kihm (2005) investigate the thermal conductivity of three different sizes of Al_2O_3 nanofluids. Thermal conductivity of nanofluids with 11nm Al_2O_3 particles was the highest compared to 47 and 150nm alumina nanofluids. Smaller nanoparticle increases the surface area and number of particles interactions. Sarit et al. (2008) added that the heat transfer process happens on the surface of the particles thus higher thermal conductivity of nanoluids is observed.

Another researcher, Yoo et al. (2007) revealed that particle size is the main factor in affecting thermal conductivity compared to particle thermal conductivity. Smaller particle sizes provide larger surface to volume ratios which facilitates nanofluids heat transfer process. In their study, it was indentified that nanofluids with smaller TiO_2 exhibited higher thermal conductivity than the bigger Al_2O_3 nanoparticles. Vajjha and Das (2009) noted that effective thermal conductivity for ethylene glycol/water mixture based ZnO (29nm) was 3% higher than nanofluids with ZnO (77nm) for 2% volume fraction concentration. However, Mintsa et al. (2009) reported that particle sizes of nanofluids have substantial effect on thermal conductivity only at high operating temperatures. At ambient temperature, particle sizes have limited influence on thermal conductivity. Murshed et al. (2005) found that thermal conductivity of nanofluids with cylindrical particles is higher than spherical shape particle.

1.5.5 Effect of Temperature

Beck et al. (2007) measured the thermal conductivity of ethylene glycol based Al_2O_3 nanofluids at 298K to 411K. It was argued that, the thermal conductivity characteristics of nanofluids at higher temperatures are almost similar to the base fluid. This concludes that effect of Brownian motion only plays a minor role in nanofluids thermal conductivity enhancement.

In contrast to the previous research, Murshel et al. (2008b) highlighted the importance of Brownian motion of nanoparticles on nanofluids thermal conductivity. Higher operating temperature will intensify the effect of Brownian motion of nanoparticles which eventually contributes to formation of micro convection in the base fluid. Subsequently, thermal conductivity enhancement is observed. The selected nanofluids used in their study were Al_2O_3 nanoparticles with three different types of base fluids (ethylene glycol, water and engine oil).

Duangthongsuk and Wongwises (2009) tested TiO_2/water-based nanofluids thermal conductivity at three different temperatures, 15^0C, 25^0C, 35^0C. It is conclusively found that thermal conductivity is a function of temperature. Yu et al. (2009) reiterated that thermal conductivity of ethylene glycol based ZnO nanofluids increases with temperature. The enhancement ratio is almost constant when the temperature increases. Similar conclusion is deduced by Lin et al. (2011) who investigated the water based Al_2O_3 nanofluids. However, Colango et al. (2011) revealed that temperature has no effect on the diathermic oil nanofluids thermal conductivity.

1.5.6 Theoretical Model of Nanofluid's Thermal Conductivity

The models used to predict the nanofluids thermal conductivity are classified into two (2) categories. They are static and dynamic models. Typical static models are Maxwell and Hamilton Crosser models as depicted in Equation (1.1) and (1.2), respectively.

$$\frac{k_{eff}}{k_f} = \frac{k_p + 2k_f + 2\phi\left(k_p - k_f\right)}{k_p + 2k_f - \phi\left(k_p - k_f\right)} \tag{1.1}$$

$$\frac{k_{eff}}{k_f} = \frac{k_p + (n-1)k_f - (n-1)\phi - \left(k_f - k_p\right)}{k_p + (n-1)k_f + \phi\left(k_f - k_p\right)} \tag{1.2}$$

Maxwell model is based on the concept of conduction heat transfer through a stagnant suspension of the spherical particles (Khanafer and Vafai 2011). Both models are function of particle volume fractions and thermal conductivity of particle base fluid. However, Maxwell model is only valid for spherical particles. Hamilton Crosser model is applicable for both spherical and cylindrical particles due to the introduction of shape factor, *n* is the model.

Several researchers have further improved these classical models by incorporating the effect of interfacial layer (Yu and Choi 2003 Yu and Choi 2004; Leong et al. 2006). It is presumed that each particle is surrounded by an ordered layer. Inclusion of ordered layer increases the volume fraction of nanoparticles. Yu and Choi (2004) improved the Hamilton Crosser model to accommodate the non-spherical nanoparticles. In this model, the interface is described as a confocal ellipsoid with a solid particle.

Thermal conductivity model which incorporates particles Brownian motion is started by Jang and Choi (2004). Authors proposed that Brownian motion is an important factor for heat transport of nanoparticles suspended in a base fluid. This contradiction with the classical approach which assumes the discrete particles are stagnant and motionless. The proposed model is developed based on several mechanisms such as collision between base fluid molecules, thermal diffusion of collision between nanoparticles due to Brownian motion and thermal interaction of dynamic nanoparticles with base fluid molecule.

Another well-known model based on Brownian motion is developed by Prasher et al. (2006). The proposed model considers the effect of interfacial thermal resistance between the nanoparticles and liquid.

Authors proposed that the thermal conductivity enhancement of nanofluids is due to localized convection by nanoparticles' Brownian moion. The proposed model is a combination of Maxwell-Garnett (MG) conduction and convection models. Although numerous models have been developed, at present there are no model available to predict the nanofluids thermal conductivity accurately (Khanafer and Vafai 2011). Thus, Corcione (2011) and Khanafer and Vafai (2011) developed empirical models based on the experimental data available in the literatures. For instance, the model constructed by Khanafer and Vafai is valid and suitable for water based Al_2O_3 and CuO based nanofluids.

1.5.7 Theoretical Model of Nanofluids' Viscosity

Viscosity of nanofluids is influenced by several factors. The main factors are particle volume fraction and operating temperature and theology behavior of nanofluid. There are a few analytical models available to estimate the viscosity behavior of nanofluids. It is interesting to find that most of the models are originated from Einstein's pioneering work. His model is based on the linearly viscous fluid containing dilute spherical particles (δ<2%). The proposed formulation is shown in Equation (1.3)

$$\frac{\mu_{nf}}{\mu_f} = \left(1 + 2.5\phi\right) \tag{1.3}$$

The limitation of this formula are: it only considers non-interacting particle and negligible inertia force in the fluid. Since then, many researchers have introduced new models to overcome the mentioned limitations of Einstein's model. An extended Einstein's model for higher particle volume concentrations was developed by Brinkman (1952) as shown in Equation (1.4)

$$\mu_{nf} = \frac{1}{\left(1-\phi\right)^{2.5}}\mu_f \tag{1.4}$$

Another researcher, Batchelor (1977) focused on the hydrodynamic and Brownian effect of spherical particle as shown in Equation (1.5)

$$\frac{\mu_{nf}}{\mu_f} = \left(1 + 2.5\phi + 6.2\phi^2\right) \tag{1.5}$$

Lundgren (1972) developed a Taylor series formulation as shown in Equation (1.6)

$$\frac{\mu_{eff}}{\mu_f} = \frac{1}{\left(1 - 2.5\phi\right)} = \left(1 + 2.5\phi + 6.25\phi^2 + ...\right) \tag{1.6}$$

Nguyen et al. (2007) presented viscosity correlation for water based copper oxide (CuO) and alumina (Al_2O_3) nanofluid as shown in Equations (1.7 - 1.9)

$$\frac{\mu_{nf}}{\mu_f} = \left(1.475 - 0.319\phi + 0.051\phi^2 + 0.009\phi^3\right) \text{ for CuO} \tag{1.7}$$

$$\frac{\mu_{nf}}{\mu_f} = \left(1 + 0.025\phi + 0.015\phi^2\right) \text{for 36nm } Al_2O_3 \tag{1.8}$$

$$\frac{\mu_{nf}}{\mu_f} = \left(0.904\ e^{0.1483\phi}\right) \text{ for 47nm } Al_2O_3 \tag{1.9}$$

1.5.8 Density and Specific Heat of Nanofluids

To the best of the author's knowledge, most researchers used single formulation to determine the density of nanofluids. The density formulation is shown in Equation (1.10).

$$\rho_{nf} = \left(1 - \phi\right)\rho_f + \phi\rho_p \tag{1.10}$$

Similar formulation has also been used by other researchers (Namburu et al. 2007 and Kulkarni et al. 2009). From the formulation, it seems that the density of nanofluids tends to increase with the increase of particle volume fraction.

The common formulation for specific heat used by researchers is shown in Equation (1.11). Specific heat tends o reduce with particle volume fraction.

$$C_{p,nf} = \frac{(1-\phi)\rho_f C_{p,f} + \phi \rho_p C_{p,p}}{\rho_{nf}} \tag{1.11}$$

1.6 LITERATURE REVIEW

Simultaneous convection of buoyancy and forced convection is called as combined or mixed convection, which is of great interest in engineering applications such as nuclear reactors, lakes and reservoirs, cooling process of electronic devices, solar applications, combustion chambers, food processing and float glass production in industry. Various researchers investigated the effects of mixed convective flows in cavities, channels by using analytical, experimental and numerical methods. Mixed convection heat transfers in channels with open cavities have been reported by Abu-Mulaweh (2003). Mixed convection in an open cavity with a heated wall bounded by a horizontally insulated plate is studied numerically by Manca et al. (2003). Aminossadati and Ghasemib (2009) performed a numerical study on the mixed convection in a horizontal channel with a discrete heat source in an open cavity. They considered three different heating modes and found noticeable differences among the indicated three heating modes. Mixed convection heat transfer in open-ended enclosures has been studied numerically for three different flow angles of attack by Khanafer et al. (2002). The obtained results show that thermal insulation of the cavity can be achieved through the use of high horizontal velocity flow. Leong et al. (2005) performed a numerical study on the mixed convection from an open cavity in a horizontal channel. Authors found that the heat transfer rate was reduced, and the flow became unstable in the mixed convection regime. A numerical analysis of laminar mixed convection in a channel with an open cavity and a heated wall bounded by a horizontally insulted plate was presented in Manca et al. (2003), where they considered three heating modes: assisting flow, opposing flow and heating from below. Later on, similar problem for the case of assisting forced flow configuration was tested experimentally by Manca et al. (2006).

Omri and Nasrallah (1999) performed numerical analysis by a control volume finite element method on mixed convection in a rectangular enclosure with differentially heated vertical sidewalls. Very recently, Oztop (2011) studied the influence of exit opening location on mixed convection in a channel with volumetric heat sources using finite volume method. It was found that both the Richardson number and the locations of exit openings have strong effects on flow and temperature distribution in the presence of volumetric heat sources. The highest heat transfer was formed when the outlet port is located onto top of vertical wall. Singh and Sharif (2003) extended Omri and Nasrallah's (1999) works by considering six placement configurations of the inlet and outlet of a differentially heated rectangular enclosure whereas the previous work was limited to only two different configurations of inlet and outlet. Billah et al. (2011) analyzed mixed convection inside a ventilated cavity along with a centered heat conducting horizontal circular cylinder. Steady laminar mixed convection inside a lid-driven square cavity filled with water is studied numerically by Chamkha and Ismael (2014). They have shown the results that there are critical values for the partial slip parameter at which the convection is declined. Chang and Shiau (2005) numerically investigated the effects of a horizontal baffle on the heat transfer characteristics of pulsating opposing mixed convection in a parallel vertical open channel. Gau and Sharif (2004) performed mixed convection heat transfer in a two-dimensional rectangular enclosure with constant heat flux from partially heated bottom wall while the isothermal sidewalls were moving in the vertical direction. A numerical investigation of unsteady laminar mixed convection heat transfer in a lid driven cavity using an externally excited sliding lids executed by Khanafer et al. (2007). Their results reveal that the Reynolds number and Grashof number would either enhance or retard the energy transport process and drag force behavior depending on the conduct of the velocity cycle.

Moreover, relatively small lid oscillation values are found to constrain the lid associated motion to a shallow depth from the sliding lid plane. A numerical study of mixed convection heat transfer in two dimensional open-ended enclosures were investigated by Khanafer et al. (2002) for three different forced flow angle of attack. Mamun et al. (2010), studied numerically on the effect of a heated hollow cylinder on mixed convection in a ventilated cavity. They observed that the cylinder diameter has significant effect on both the flow and thermal fields but the solid-fluid thermal conductivity ratio has significant effect only on the thermal field.

Unsteady mixed convection in a horizontal channel containing heated blocks on its lower wall was studied numerically by Najam et al. (2003). The fully developed forced flow is found to reduce considerably the heat transfer through the cold surface of the channel at relatively large Re. Pantokratoras (2004) considered the steady laminar opposing mixed convection along vertical isothermal moving plates and cylinders. The bodies were moving upwards while their temperature was lower than the ambient atmosphere. The results were obtained with the direct numerical solution of the boundary layer equations. He found that the velocity profiles took some interesting shapes that would not been observed before. Rahman et al. (2007) studied numerically the opposing mixed convection in a vented enclosure. They found that with the increase of Reynolds and Richardson numbers the convective heat transfer becomes predominant over the conduction heat transfer and the rate of heat transfer from the heated wall is significantly depended on the position of the inlet port. After few days Rahman et al. (2008a) studied mixed convection in a square cavity with a heat conducting square cylinder at different locations. The results indicate that the flow field and temperature distributions inside the cavity are strongly dependent on the Richardson numbers and the position of the inner cylinder. At the same time Rahman et al. (2008b) studied mixed convection in a vented square cavity with a heat conducting horizontal solid circular cylinder. They found that the streamlines, isotherms, average Nusselt number at the heated surface, average temperature of the fluid in the cavity and dimensionless temperature at the cylinder center strongly depend on the Richardson number as well as the diameter of the cylinder.

Rahman et al. (2009) again analyzed mixed convection in a rectangular cavity with a heat conducting horizontal circular cylinder by using finite element method. The results indicate that both the heat transfer rate from the heated wall and the dimensionless temperature in the cavity strongly depend on the governing parameters and configurations of the system studied, such as size, location, thermal conductivity of the cylinder and the location of the inflow and outflow opening. Again Rahman et al. (2011) performed the effect of Reynolds and Prandtl numbers on mixed convection in an obstructed vented cavity. They found that the flow and thermal field strongly depend on the Reynolds number, Prandtl number as well as Richardson number. As the Reynolds number and Prandtl number increase, the heat transfer rate increases but average fluid temperature in the cavity and temperature at the cylinder center decrease at the three convective regimes. Then after Rahman et al. (2013) investigated mixed convection inside a square ventilated cavity with a heat generating solid body located at the center. It was observed that heat transfer had a strong relation with conductivity ratio between solid and fluid as well as the diameter of the heat generating body. They found that the flow and temperature field is strongly dependent on the parameters D, K, and Q. for the ranges considered. A parametric study on flow behavior and heat transfer in an inclined triangular cavity subjected to a moving lid and temperature differential is investigated by Chen and Chung (2015). The study also reveals that the good thermal performance within a local region can generate higher friction force on the neighboring boundary and this friction force may reduce the strength of the vortex. Multiple fluid flow and heat transfer solutions in a two-sided lid-driven cavity is studied by Luo and Yang (2007). A thumb-shaped boundary line is established which identifies a restricted region defined in terms of the Grashof and Reynolds numbers within which a stable flow state exists. A Numerical study on the effect of a heated hollow cylinder on mixed convection in a ventilated cavity investigated by Mamun et al. (2010).They observed that the cylinder diameter has significant effect on both the flow and thermal fields but the solid-fluid thermal conductivity ratio has significant effect only on the thermal field.

Yapici et al. (2015) investigated laminar mixed convection in a lid-driven square cavity considering different shapes of hot bottom wall. It was found that at low Ri, rectangular wave shaped bottom wall produced maximum heat transfer. Satish et al. (2015) investigated the mixed convective transport within a ventilated square cavity in presence of a heat conducting circular cylinder. They found that the Richardson number has significant influences on the fluid flow and heat transfer characteristics in the cavity. A two-dimensional numerical study is undertaken to investigate the influences of cross buoyancy on the vortex shedding phenomena behind a long heated equilateral triangular cylinder for the low-Reynolds-number laminar regime by Dipankar and Bittagopal (2015). The study of two-dimensional mixed convection from a heated square solid cylinder located at the center of a vented cavity filled with air (Pr = 0.71) is performed.by Chamkha et al. (2011).The results shown that the average Nusselt number along the heated surface of the inner square values increases with increasing values of the Reynolds and Richardson numbers. The effect of the locations of the inner square cylinder and aspect ratio is found to play a significant role in the streamline and isotherm patterns. A channel with a cavity heated from below is numerically investigated for the mixed convection case for a range of Richardson numbers (Ri = 0.1, 1, 5, 10, 15 and 20) and Reynolds numbers (Re = 400, 500, 600, 700 and 800) in the laminar flow regime is investigated by Fatih (2013). Mixed convection flows in a lid-driven square cavity filled with porous medium are studied numerically using penalty finite element analysis for uniformly heated bottom wall, linearly heated side walls or cooled right wall by Tanmay basak et al. (2010). They found that the isotherms are generally symmetric at smaller Pr irrespective of Da and Re at Gr = 10^5 for linearly heated side walls. The isotherms are also almost symmetric at small Re with higher Gr (Gr = 10^5) and Da (Da = 10^{-3}) and natural convection is found to be dominant whereas the isotherms are compressed near the left and bottom walls at higher Re for linearly heated side walls.

A combined free and forced convection flow of an electrically conducting fluid in a cavity or in a channel in the presence of magnetic field is of special technical significance because of its frequent occurrence in many industrial applications such as geothermal reservoirs, cooling of nuclear reactors, thermal insulations and petroleum reservoirs. A study of magnetohydrodynamic (MHD) mixed convection around a heat conducting horizontal circular cylinder placed at the center of a rectangular cavity along with joule heating has been carried out.by Rahman et al. (2009). It was found that the streamlines, isotherms, average Nusselt number, average fluid temperature and dimensionless temperature at the cylinder center strongly depend on the Richardson number, Hartmann number and the cavity aspect ratio. After a few years a finite element analysis is performed by Rahman et al. (2011a) on the conjugated effect of joule heating and magneto-hydrodynamic on double-diffusive mixed convection in a horizontal channel with an open cavity. The results represented that the parameters like as Richardson number, Hartmann number, joule heating, buoyancy ratio and Lewis number have noticeable effect on the flow pattern and heat and mass transfer. On the same time, the development of magnetic field effect on mixed convective flow in a horizontal channel with a bottom heated open enclosure has been numerically studied again by Rahman et al. (2011b). The results indicate that the parameters like as Rayleigh number, Reynolds number and Hartmann number strongly affect the flow phenomenon and temperature field inside the cavity whereas in the channel these effects are less significant. A numerical study is presented by Sarris et al. (2005) of unsteady two-dimensional natural convection of an electrically conducting fluid in a laterally and volumetrically heated square cavity under the influence of a magnetic field. They got that the usual damping effect of increasing Hartmann number is not found to be straightforward connected with the resulting flow patterns in the present flow configuration. The fully developed flow of an electrically conducting, internally heated fluid in a vertical square duct under the influence of buoyancy and magnetohydrodynamic forces is studied by Sposito and Ciofalo (2008).

Magneto-hydrodynamic mixed convection in a lid driven cavity along with a heated circular hollow cylinder positioned at the centre of the cavity is studied numerically by Farid et al. (2013). The results are shown that Hartmann number and Richardson number have noticeable effect on the flow pattern and heat transfer characteristics inside the cavity. Magnetohydrodynamic (MHD) mixed-convection flow and heat transfer characteristics inside a square double-lid driven enclosure have been investigated by Rahman et al. (2012). They obtained that the flow and thermal fields are influenced by the Hartmann number, heat-generating parameter, and Richardson number. The fluid flows and heat transfer induced by the combined effects of mechanically driven lid and buoyancy force within a rectangular cavity is investigated numerically by Rahman et al. (2010). The results indicated that both the streamlines and isotherms strongly depend on the Reynolds number and Prandtl number. Sharif et al. (2012) investigated steady MHD mixed convection heat transfer characteristics within a ventilated square cavity. The results demonstrate that the flow and thermal fields strongly influenced by the governing parameter. A boundary layer analysis has been presented by Swati Mukhopadhyay et al. (2007) for combined convection flow of an electrically conducting liquid due to a porous vertical stretching plate with a power law stretching velocity in the presence of a transverse magnetic field. They found the skin friction decreases and heat transfer rate increases due to the suction parameter. With the increase of magnetic field intensity, the fluid velocity decreases, but the temperature increases. In the absence of magnetic field intensity and suction, the streetwise velocity displays a velocity maximum within the boundary layer when the stretching velocity power law exponent is negative. The problem of laminar mixed convection flow of non-Newtonian power-law fluids from a constantly rotating isothermal cone or disk in the presence of a uniform magnetic field is investigated by Abo-Eldahaband Salem (2004). The governing partial-differential equations are transformed into ordinary differential equations using similarity transformations.

The transformed equations, on the assumption of a small magnetic Reynolds number, are solved numerically by employing the shooting method. Emmanuel et al (2008) is concerned with the effect of combined viscous dissipation and Joule heating on unsteady mixed convention magnetohydrodynamics (MHD) flow on a rotating cone in an electrically conducting rotating fluid in the presence of Hall and ion-slip currents. A numerical study is presented by Ahmad and Salam (2015) for mixed convection flow of air (Pr = 0.71) within a parallel motion two sided lid-driven parallelogrammic cavity in the presence of magnetic field. They found that as the Hartmann number increases the circulation of the rotating vortices is reduced and the conduction mode of heat transfer is dominant. Also, it is found that both Richardson number and direction of two sided lid-driven sidewalls affect the heat transfer and fluid flow in the parallelogrammic cavity. The group transformation method is applied for solving the combined convection problem in an unsteady, two-dimensional, laminar, boundary-layer flow of a viscous, incompressible and electrically-conducting fluid along a vertical continuous moving plate saturated porous medium in the presence of a uniform transverse magnetic field by EL-Kabeir et al. (2007). The problem of mixed convection flow in the presence of magnetic field in a lid-driven square cavity with internal heat generation or absorption and uniform heating of bottom wall were investigated numerically by Liean et al. (2015). The significant reduction in the average Nusselt numbers were produced as the strength of the applied magnetic field was increased. In addition, heat generation predicted to decrease the average Nusselt number whereas heat absorption increases it. MHD Combined convection in an open channel with a square cavity which has a partially or fully heated on left side to simulate assisting flow is carried out numerically by Rahman et al. (2013) using finite element method. They observed that length of heater becomes insignificant on flow field for higher values of Hartmann number. On the contrary, higher heat transfer is formed for partial heater at the higher values of Rayleigh number.

Heat transfer has been given a enormous importance now a day as many engineering and modern science and technology system involves the problem of heat transfer. In most of the case it has been observed that traditional fluid cannot meet the demand of the desired thermo physical property which is needed for the desired level of heat transfer. As a result scientists and researcher are now a day trying different fluid to increase the heat transfer rate. The thermal conductivities of several nanofluids (dispersions of alumina nanoparticles in ethylene glycol) were measured at temperatures ranging from 298 to 411 K using a liquid metal transient hot wire apparatus is investigated by Beck et al. (2007). Their results confirm that additional temperature contributions inherent in Brownian motion models are not necessary to describe the temperature dependence of the thermal conductivity of nanofluids. Experimental investigations and theoretical determination of effective thermal conductivity and viscosity of Al_2O_3/H_2O nanofluids are reported by Chandrasekar et al. (2010). The thermal conductivity and viscosity of nanofluids are measured and it is found that the viscosity increase is substantially higher than the increase in thermal conductivity. Both the thermal conductivity and viscosity of nanofluids increase with the nanoparticle volume concentration. Also they found that the proposed models show reasonably good agreement with their experimental results. Experiments are carried out by Chen et al. (2009) on the rheological behavior of ethylene glycol (EG) based titanate nanotubes (TNT) nanofluids containing 0.5, 1.0, 2.0, 4.0 and 8.0 wt. % TNT at 20–60 °C. Their results show a very strong shear thinning behavior of the TNT nanofluids and big influences of particle concentration and temperature on the zero shear viscosity (ZSV) and high shear viscosity (HSV), for which the conventional form of Brenner & Condiff equation fails to predict. Choi (2009) investigated Nanofluids: From vision to reality through research. He highlights recent advances in this new field of research and shows future directions in nanofluids research through which the vision of nanofluids can be turned into reality

Very recently a numerical investigation of mixed convection due to a copper–water nanofluid in a Lid –Driven square enclosure is presented.by Nayak et al. (2015). They obtained the enhancement rate in heat transfer and entropy generation in nanofluid for a wide range of parameter values. The experimental results from a study on diathermic oil based nanofluids are executed by Colangelo et al. (2011). The results showed that the heat transfer performance of diathermic oil enhances more than water with the same nanoparticles. Two empirical correlations for predicting the effective thermal conductivity and dynamic viscosity of nanofluids, based on a high number of experimental data available in the literature, are proposed and discussed by Corcione (2011). They found that, given the nanoparticle material and the base fluid, the ratio between the thermal conductivities of the nanofluid and the pure base liquid increases as the nanoparticle volume fraction and the temperature are increased, and the nanoparticle diameter is decreased. Additionally, also the ratio between the dynamic viscosities of the nanofluid and the pure base liquid increases as the nanoparticle volume fraction is increased, and the nanoparticle diameter is decreased, being practically independent of temperature. The heat transfer features of buoyancy-driven nanofluids inside rectangular enclosures differentially heated at the vertical walls are investigated theoretically by Corcione (2010). They observed that for any assigned combination of solid and liquid phases, the optimal volume fraction is found to increase slightly with decreasing the nanoparticle size, and to increase much more remarkably with increasing both the nanofluid average temperature and the slenderness of the enclosure. The numerical modeling of steady laminar mixed convection flow in a lid-driven cavity with a wavy wall filled with a water–CuO nanofluid is focused by Nada and Chamkha (2014). They found that the presence of nanoparticles causes significant heat transfer augmentation for all values of Richardson numbers and bottom wall geometry ratios. A numerical study is carried out by Hasib et al. (2014) to investigate the transition from laminar to chaos in mixed convection heat transfer inside a lid-driven trapezoidal enclosure. It is found that both the flow and the temperature profiles are influenced by the combined effect of Reynolds and Grashof numbers to a great extent.

The profiles also vary with the presence of nanofluids. A numerical study is carried out by Garoosi et al. (2014) concerning natural and mixed convection heat transfer of nanofluids (Al_2O_3–water) in a laterally-heated square cavity. The simulation results indicate that there is an optimal volume fraction of the nanoparticles at each Rayleigh and Richardson number for which the maximum heat transfer rate can be obtained. It is also observed that at low Rayleigh numbers and high Richardson numbers, the particle distribution is fairly non-uniform while at high Ra and low Ri values particle distribution remains almost uniform for free and mixed convection cases, respectively. The problem of natural and mixed convection in an adiabatic enclosure containing several pairs of hot and cold cylinders is studied numerically by Garoosi and Hoseininejad (2016). The results indicate that heat transfer rate may increase or decrease by changing rotation direction of the hot and cold cylinders. Moreover, it is found that by changing the location of the heat source/sink from bottom – top to top – bottom configuration the heat transfer rate decreases significantly. Finally, the results show that by changing the position of the cold cylinder from vertical to horizontal mode, the average Nusselt number reduces dramatically. A numerical study ofmixed convection flowand heat transfer inside a square cavity with inlet and outlet ports is performed by Ganji et al. (2014). It is observed that the average Nusselt number is an increasing function of Reynolds number, Richardson number and nanoparticle volume fraction. The pressure drop coefficient is also increased in the presence of nanoparticles. Moreover the performance of the nanoparticle utilization on the enhancement of heat transfer at higher Richardson numbers is less than that at lower Richardson numbers.

1.7 APPLICATIONS

Mixed convection heat transfer has always been of great interest because of its wide applications in different areas such as the cooling systems of electronic components, building and thermal insulation systems, the built-in-storage solar collectors, the nuclear reactor systems, the food storage industry and the geophysical fluid mechanics and chemical processing equipment.

Moreover mixed convection heat transfer enhancements of nanofluids with magnetic effects in a channel with cavity are expansively used in various sizes of electrical and electronic devices. Also nanofluids are now being developed for medical applications, including cancer therapy and safer surgery by cooling. However, Nanofluids technology can help to develop better oils and lubricants.

1.8 MOTIVATION

From the literature review it is clear that very little numerical study on the MHD mixed convection heat transfer in a channel with cavity have been carried out. The study of mixed convection in a channel with cavity is important for numerous engineering applications. To implement a system as an effective heat transfer devices such as in designing nuclear reactors, solar collectors, electrical, microelectronic equipment and in many other design problems mixed convection heat transfer is prominent. Thus the analysis of the effect of mixed convection for different boundary conditions and shapes are necessary to ensure efficient performance of heat transfer equipment. On the other hand, the majority of the mixed convection studies were carried out in channel or cavity. Numerous studies on nanofluids are being conducted by talented thermal scientists and engineers all over the world, and they have made the scientific breakthrough not only in discovering unexpected thermal properties of nanofluids, but also in proposing new mechanisms behind the enhanced thermal properties of nanofluids and thus identifying unusual opportunities to develop them as next generation coolants for computers and safe coolants for nuclear reactors. Researchers have started showing interest in the study of heat transfer characteristics of these nanofluids in recent years. The study of mixed convection effects in cavities using nanofluids is very important in numerous engineering applications. The literature survey indicates a little attention has been paid to investigate the heat transfer characteristics of the nanofluids contained in a channel with cavity using magnetic effect. Numerical studies are therefore essential to observe the variation in fluid flow and heat transfer due to the above physical and properties changes, which forms the basis for the motivation behind the present study.

1.9 OBJECTIVES OF THE PRESENT STUDY

A review of earlier studies indicates that, the MHD combined convection in a channel with cavity using nanofluids has not been analyzed yet. The study will be carried out numerically with an accurate numerical procedure, and the related results will be shown using streamlines, isotherms, and related graphs and charts.

The specific objectives of the present research work are:

- To modify the developed mathematical model on MHD mixed convection flow in a channel with a cavity using nanofluids.
- To investigate the effect of governing parameters namely, Reynolds number Re, Hartmann number Ha, solid volume fraction ϕ and the physical parameter cavity aspect ratio for the three values of mixed convective parameter on the flow and thermal field in the cavity.
- To make an optimum combination of the aforesaid parameters.
- To compare the present results with other published works.

It is expected that the present numerical investigation will contribute to the search for finding more efficient and better renewable energy equipment. The challenge of augmentation of heat transfer in solar thermal collectors can be met with this model.

1.10 OUTLINE OF THE THESIS

This dissertation contains four chapters. In chapter 1, a brief introduction is presented with aim and objective. This chapter also consists a literature review of the past studies on fluid flow and heat transfer in cavities or channels. In this state-of-the art review, different aspects of the previous studies have been mentioned categorically. This is followed by the post-mortem of a recent historical event for the illustration of fluid flow and heat transfer effects in cavities or channels.

Chapter 2 presents the computational procedure of the problem for viscuss incompressible flow. Basically finite element method is employed in this study and explained elaborately. We have investigated the effects of MHD in mixed convection flow in a channel with cavity utilizing copper–water nanofluids

In Chapter 3 a detailed parametric study on MHD combined convection in a channel with cavity using nanofluids is conducted. Effects of the major parameters such as Reynolds number, Hartmann number, solid volume fraction and the physical parameter such as cavity aspect ratio for the three values of Rayleigh number on the flow and thermal field in the channel with cavity have been presented.

Finally, in Chapter 4 the dissertation is rounded off with the conclusions and comparison. Lastly, recommendations for further study of the present problem are outlined.

CHAPTER 2

MATHEMATICAL MODELLING

The mathematical model of physical phenomena may be ordinary or partial differential equations, which have been the subject of numerical and analytical investigations. The governing partial differential equations of fluid mechanics and heat transfer are solvable for only a limited number of flows. To determine an approximate solution numerically, we have to use a discretization method which approximated the differential equations by a system of algebraic equations, which can then be solved on a computer. The approximations are used to small domains in space and /or time so the numerical solution provides results at discrete locations in space and time. Much as the accuracy of experimental data depends on the quality of the tools used, the accuracy of numerical solutions is dependent on the quality of discretizations used.

Computational fluid dynamics (CFD) computation involves the formation of a set numbers that constitutes a practical approximation of a real life system. The outcome of computation process improves the understanding of the performance of a system. Thereby, engineers need CFD codes that can make physically realistic results with good quality accuracy in simulations with finite grids. Contained within the broad field of computational fluid dynamics are activities that cover the range from the automation of well-established engineering design methods to the use of detailed solutions of the Navier-Stokes equations as substitutes for experimental research into the nature of complex flows. CFD have been used for solving wide range of fluid dynamics problem. It is more frequently used in fields of engineering where the geometry is complicated or some important feature that cannot be dealt with standard methods.

The analysis of flow and heat transfer in thermodynamics can be performed either theoretically or experimentally.

Experimental study of such problem could not gain that much popularity in the field of thermodynamics because of their limited flexibility and applications. For every change of geometry and boundary conditions, it needs separate investigation, involving separate experimental requirement/ arrangement, which, in turn makes it unattractive, especially, from the time involved and economical point of views.

The remainder of this chapter is as follows. In section 2.1, the physical configurations of the current research interest is shown. Then the appropriate mathematical model (both governing equations and boundary conditions) is considered in section 2.2. After that a numerical scheme that is employed in this study are described in the section 2.3.

2.1 PHYSICAL MODEL

Considered model is presented in figure. 2.1. In this figure, channel includes a cavity and magnetic field affects in –x direction and gravity acts in the vertical direction. Flow enters to channel via inlet port at a uniform velocity, u_i, temperature, T_i and exit the channel via outlet port. The length and height of the cavity are defined by L and H respectively, the length of channel is chosen as H + L, bottom side of cavity is heated under constant temperature, T_h, remaining solid walls are adiabatic. In case 1, case 2, case 3 and case 4 AR = 2, 1.5, 1 and 0.5 are considered respectively.

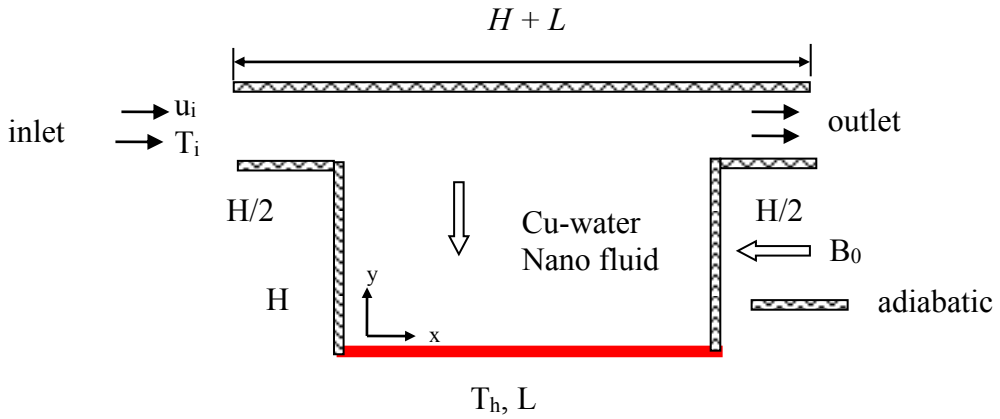

Figure 2.1. Physical model under consideration

2.2 GOVERNING EQUATIONS ALONG WITH BOUNDARY CONDITIONS

The fundamental laws used to solve the fluid flow problems are the law of conservation of mass or continuity equations, conservation of momentums, and conservation of energy, which constitute a set of coupled, nonlinear, partial differential equations. The nanofluids in the enclosure are Newtonian, incompressible and laminar. The nanoparticles are assumed to have uniform shape and size. It is considered that thermal equilibrium exists between water and nanoparticles (Cu nanoparticles), and no slip occurs between the two media. It should be stated that, in a practical situation, most nanofluids used for augmentation of heat transfer are made up of extremely fine particles, usually under 40 nm diameter. The thermo-physical properties of cu-water nanofluids of [Mansour et al. (2010)] are listed in Table 2.1.

Table 2.1. Thermophysical properties of water and copper [Mansour et al (2010)]

Property	Fluid phase (water)	Solid phase (copper)
c_p (J Kg^{-1} K^{-1})	4179	385
ρ (Kg m^{-3})	997.1	8933
k (W m^{-1} K^{-1})	0.613	401
β (K^{-1})	2.1×10^{-4}	1.67×10^{-5}

The physical properties of the nanofluids are considered to be constant except the density variation in the body force term of the momentum equation which is satisfied by the Boussinesq's approximation. The effects of radiation and viscous dissipation are neglected. Under the above assumptions, the system of equations governing the two-dimensional motion of nanofluids is as follows:

Continuity Equation

$$\frac{\partial u}{\partial x}+\frac{\partial v}{\partial y}=0 \tag{2.1}$$

Momentum Equations

$$\rho_{nf}\left(u\frac{\partial u}{\partial x}+v\frac{\partial u}{\partial y}\right)=-\frac{\partial p}{\partial x}+\mu_{nf}\left(\frac{\partial^2 u}{\partial x^2}+\frac{\partial^2 u}{\partial y^2}\right) \tag{2.2}$$

$$\rho_{nf}\left(u\frac{\partial v}{\partial x}+v\frac{\partial v}{\partial y}\right)=-\frac{\partial p}{\partial y}+\mu_{nf}\left(\frac{\partial^2 v}{\partial x^2}+\frac{\partial^2 v}{\partial y^2}\right)+\left(\rho\beta\right)_{nf}\left(T-T_i\right)g-\sigma_{nf}\beta_0^2 v \tag{2.3}$$

Energy Equations

$$u\frac{\partial T}{\partial x}+v\frac{\partial T}{\partial y}=\alpha_{nf}\left(\frac{\partial^2 T}{\partial x^2}+\frac{\partial^2 T}{\partial y^2}\right) \tag{2.4}$$

where the effective density ρ_{nf} of a fluid containing suspended particles at a reference temperature is given by

$$\rho_{nf}=\left(1-\phi\right)\rho_f+\phi\rho_s \tag{2.5}$$

where ϕ is the solid volume fraction of nanoparticles. In addition, the thermal diffusivity α_{nf} of the nanofluids can be expressed as:

$$\alpha_{nf}=\frac{k_{nf}}{\left(\rho c_p\right)_{nf}} \tag{2.6}$$

The heat capacitance of nanofluids can be defined as

$$\left(\rho c_p\right)_{nf}=\left(1-\phi\right)\left(\rho c_p\right)_f+\phi\left(\rho c_p\right)_s \tag{2.7}$$

Additionally, the thermal expansion coefficient of the nanofluids $\left(\rho\beta\right)_{nf}$ is expressed as:

$$\left(\rho\beta\right)_{nf}=\left(1-\phi\right)\left(\rho\beta\right)_f+\phi\left(\rho\beta\right)_s \tag{2.8}$$

The viscosity of the nanofluids can be estimated with the existing relations for the two-phase mixture.

The equation given by Brinkman (1952) has been used as the relation for dynamic viscosity of the nanofluids in this problem, as given

$$\mu_{nf} = \frac{\mu_f}{(1-\phi)^{2.5}} \tag{2.9}$$

For particle–fluid mixtures, several theoretical studies have been conducted dating back to the classical work of Maxwell (1881).

The effective electrical conductivity of nanofluid is given:

$$\sigma_{nf} = \sigma_f + \frac{3(\gamma-1)\sigma_f\phi}{(\gamma+2)-(\gamma-1)\phi},\ where\ \gamma = \frac{\sigma_s}{\sigma_f} \tag{2.10}$$

The Maxwell model for thermal conductivity for solid–liquid mixtures of relatively large particles (micro-/minisize) is good for low solid concentrations.

The effective thermal conductivity of nanofluids, k_{nf}, is given by

$$k_{nf} = \frac{k_s + 2k_f - 2\phi(k_f - k_s)}{k_s + 2k_f + \phi(k_f - k_s)} k_f \tag{2.11}$$

where, k_s is the thermal conductivity of the nanoparticles and k_f is the thermal conductivity of base fluid and ϕ is the particle volume fraction of the suspension. Maxwell's formula shows that the effective thermal conductivity of nanofluids relies on the thermal conductivity of the spherical particle, the base fluid and the volume fraction of the solid particles.

2.2.1 Boundary Conditions

The boundary conditions for the present problem are specified as follows:

At the inlet: $u = u_i, v = 0,\ T = T_i$

At the outlet: $\frac{\partial u}{\partial x} = 0, v = 0, \frac{\partial T}{\partial x} = 0$

at all solid boundaries other than bottom wall: $u = v = \frac{\partial T}{\partial n} = 0$

At the heated wall: $u = v = 0, T = T_h$

where *n* is the non-dimensional distances either along *x* or *y* direction acting normal to the surface.

Such local values have been further averaged over the entire heated surface to obtain the surface averaged or overall mean Nusselt number

$$Nu_{av} = -\frac{1}{L}\int_0^L \frac{\partial T}{\partial N} ds$$

where L is the length of the heated wall. The average Nusselt number can be used in process engineering design calculations to estimate the rate transfer from the heated surface.

2.2.2 Dimensional Analysis

The non-dimensional parameters that are used for making the governing equations (2.1−2.4) into dimensionless form are stated as follows:

$$X = \frac{x}{H},\ Y = \frac{y}{H},\ U = \frac{u}{u_i},\ V = \frac{v}{u_i},\ AR = \frac{L}{H}, P = \frac{(p+\rho g y)H^2}{\rho_{nf}\, {u_i}^2} \text{ and } \theta = \frac{(T-T_i)}{(T_h - T_i)}$$

where X and Y are the coordinates varying along horizontal and vertical directions, respectively, U and V are, the velocity components in the X and Y directions, respectively, θ is the dimensionless temperature and P is the dimensionless pressure. After substitution the dimensionless variables into the equations (2.1-2.4), we get the following dimensionless equations as

Continuity Equation

$$\frac{\partial U}{\partial X} + \frac{\partial V}{\partial Y} = 0 \tag{2.12}$$

Momentum Equations

$$U\frac{\partial U}{\partial X} + V\frac{\partial U}{\partial Y} = -\frac{\partial P}{\partial X} + \frac{\mu_{nf}}{\rho_{nf}\nu_f}\frac{1}{Re}\left(\frac{\partial^2 U}{\partial X^2} + \frac{\partial^2 U}{\partial Y^2}\right) \tag{2.13}$$

$$U\frac{\partial V}{\partial X}+V\frac{\partial V}{\partial Y}=-\frac{\partial P}{\partial Y}+\frac{\mu_{nf}}{\rho_{nf}\nu_f}\frac{1}{Re}\left(\frac{\partial^2 V}{\partial X^2}+\frac{\partial^2 V}{\partial Y^2}\right)+\frac{(\rho\beta)_{nf}}{\rho_{nf}\beta_f}\frac{Ra}{Re^2\,Pr}\theta-\frac{\rho_f\sigma_{nf}}{\rho_{nf}\sigma_f}\frac{Ha^2}{\mathrm{Re}}V \tag{2.14}$$

Energy Equations

$$U\frac{\partial \theta}{\partial X}+V\frac{\partial \theta}{\partial Y}=\frac{\alpha_{nf}}{\alpha_f}\frac{1}{Re\,Pr}\left(\frac{\partial^2 \theta}{\partial X^2}+\frac{\partial^2 \theta}{\partial Y^2}\right) \tag{2.15}$$

The nondimensional numbers that appear in equations (2.13)-(2.15) are as follows:

Reynolds number $Re=u_iH/\upsilon_f$, Prandtl number $Pr=\nu_f/\alpha_f$, Rayleigh number $Ra=\dfrac{\beta_f g\left(T_h-T_i\right)H^3}{\upsilon_f{}^2}$ and Hartmann number $Ha=\beta_0 H\sqrt{\dfrac{\sigma_f}{\mu_f}}$.

2.2.3 Boundary Conditions (non-dimensional)

The dimensionless boundary conditions under consideration can be written as:

At the inlet: $U=1,\ V=0,\ \theta=0$

At the outlet: $\dfrac{\partial U}{\partial X}=0, V=0, \dfrac{\partial \theta}{\partial X}=0$

At the bottom wall: $U=V=0,\ \theta=1$

At all solid boundaries other than heated wall: $U=0, V=0, \dfrac{\partial \theta}{\partial N}=0$

Where N is the non-dimensional distances either X or Y direction acting normal to the surface.

The average Nusselt number at the heated wall of the cavity based on the conduction contribution may be expressed as $Nu_{av}=-\dfrac{k_{nf}}{k_f}\int_0^{L/H}\dfrac{\partial \theta}{\partial Y}dX$ (2.16)

and an index of cooling effectiveness is the bulk average temperature defined as $\theta_{av}=\int\theta\, d\,\overline{A}/\overline{A}$ (2.17)

where $\overline{A}$ is the area of the considered domain. The fluid motion is displayed using the stream function (ψ) obtained from velocity components U and V. The relationships between stream function and velocity components for two dimensional flows can be expressed as:

$$U = \frac{\partial \psi}{\partial Y},\ V = -\frac{\partial \psi}{\partial X} \tag{2.18}$$

2.3 NUMERICAL ANALYSIS

The governing equations along with the boundary conditions are solved numerically, employing Galerkin weighted residual finite element techniques discussed below.

2.3.1 Finite Element Formulation and Computational Procedure

To derive the finite element equations, the method of weighted residuals [Zienkiewicz and Taylor (1991)] is applied to the equations (2.12) – (2.15) as

$$\int_A N_\alpha \left(\frac{\partial U}{\partial X} + \frac{\partial V}{\partial Y} \right) dA = 0 \tag{2.19}$$

$$\int_A N_\alpha \left(U \frac{\partial U}{\partial X} + V \frac{\partial U}{\partial Y} \right) dA = -\int_A H_\lambda \left(\frac{\partial P}{\partial X} \right) dA + \frac{\mu_{nf}}{\rho_{nf} \nu_f} \frac{1}{Re} \int_A N_\alpha \left(\frac{\partial^2 U}{\partial X^2} + \frac{\partial^2 U}{\partial Y^2} \right) dA \tag{2.20}$$

$$\int_A N_\alpha \left(U \frac{\partial V}{\partial X} + V \frac{\partial V}{\partial Y} \right) dA = -\int_A H_\lambda \left(\frac{\partial P}{\partial Y} \right) dA + \frac{\mu_{nf}}{\rho_{nf} \nu_f} \frac{1}{Re} \int_A N_\alpha \left(\frac{\partial^2 V}{\partial X^2} + \frac{\partial^2 V}{\partial Y^2} \right) dA + \frac{(\rho\beta)_{nf}}{\rho_{nf} \beta_f} \frac{Ra}{\mathrm{Re}^2 \,\mathrm{Pr}} \int_A N_\alpha \theta dA - \frac{\rho_f \sigma_{nf}}{\rho_{nf} \sigma_f} \frac{Ha^2}{\mathrm{Re}} \int_A N_\alpha V dA \tag{2.21}$$

$$\int_A N_\alpha \left(U \frac{\partial \theta}{\partial X} + V \frac{\partial \theta}{\partial Y} \right) dA = \frac{\alpha_{nf}}{\alpha_f} \frac{1}{Re\, Pr} \int_A N_\alpha \left(\frac{\partial^2 \theta}{\partial X^2} + \frac{\partial^2 \theta}{\partial Y^2} \right) dA \tag{2.22}$$

where A is the element area, N_α (α = 1, 2, … … , 6) are the element interpolation functions for the velocity components and the temperature and H_λ (λ = 1, 2, 3) are the element interpolation functions for the pressure.

Then apply Gauss's theorem into equations (2.20)-(2.22) to generate the boundary integral terms associated with the surface tractions and heat flux. After that the equations (2.20)-(2.22) become

$$\int_A N_\alpha \left(U\frac{\partial U}{\partial X} + V\frac{\partial U}{\partial Y} \right) dA + \int_A H_\lambda \left(\frac{\partial P}{\partial X} \right) dA + \frac{\mu_{nf}}{\rho_{nf}\nu_f}\frac{1}{Re}\int_A \left(\frac{\partial N_\alpha}{\partial X}\frac{\partial U}{\partial X} + \frac{\partial N_\alpha}{\partial Y}\frac{\partial U}{\partial Y} \right) dA = \int_{S_0} N_\alpha S_x dS_0 \tag{2.23}$$

$$\int_A N_\alpha \left(U\frac{\partial V}{\partial X} + V\frac{\partial V}{\partial Y} \right) dA + \int_A H_\lambda \left(\frac{\partial P}{\partial Y} \right) dA + \frac{\mu_{nf}}{\rho_{nf}\nu_f}\frac{1}{Re}\int_A \left(\frac{\partial N_\alpha}{\partial X}\frac{\partial V}{\partial X} + \frac{\partial N_\alpha}{\partial Y}\frac{\partial V}{\partial Y} \right) dA - \frac{(\rho\beta)_{nf}}{\rho_{nf}\beta_f}\frac{Ra}{\mathrm{Re}^2\,\mathrm{Pr}}\int_A N_\alpha \theta\, dA + \frac{\rho_f\sigma_{nf}}{\rho_{nf}\sigma_f}\frac{Ha^2}{\mathrm{Re}}\int_A N_\alpha V dA = \int_{S_0} N_\alpha S_y dS_0 \tag{2.24}$$

$$\int_A N_\alpha \left(U\frac{\partial \theta}{\partial X} + V\frac{\partial \theta}{\partial Y} \right) dA + \frac{\alpha_{nf}}{\alpha_f}\frac{1}{Re\,Pr}\int_A \left(\frac{\partial N_\alpha}{\partial X}\frac{\partial \theta}{\partial X} + \frac{\partial N_\alpha}{\partial Y}\frac{\partial \theta}{\partial Y} \right) dA = \int_{S_w} N_\alpha\, q_{1w}\, dS_w \tag{2.25}$$

The equations (2.23)-(2.24) specify surface tractions (S_x, S_y) along outflow boundary S_0 and (2.25) specifying velocity components and fluid temperature or heat flux (q_w) that flows into or out from domain along wall boundary S_w.

The basic unknowns for the above differential equations are the velocity components U, V the temperature, θ and the pressure, P. The six node triangular element is used in this work for the development of the finite element equations. All six nodes are associated with velocities as well as temperature; only the corner nodes are associated with pressure. This means that a lower order polynomial is chosen for pressure and which is satisfied through continuity equation.

The velocity component and the temperature distributions and linear interpolation for the pressure distribution according to their highest derivative orders in the differential equations (2.12)-(2.15) as

$$U(X,Y) = N_\beta U_\beta \tag{2.26}$$

$$V(X,Y) = N_\beta V_\beta \tag{2.27}$$

$$\theta(X,Y) = N_\beta \theta_\beta \tag{2.28}$$

$$P(X,Y) = H_\lambda P_\lambda \tag{2.29}$$

where $\beta = 1, 2, \ldots \ldots, 6$; $\lambda = 1, 2, 3$.

Substituting the element velocity component distributions, the temperature distribution, and the pressure distribution from equations (2.26)-(2.29), we get the following equations:

$$\int_A N_\alpha \left(N_{\beta,x} U_\beta + N_{\beta,y} V_\beta \right) dA = 0 \tag{2.30}$$

$$\begin{aligned} &\int_A N_\alpha \left[\left(N_\beta U_\beta \right)\left(N_{\gamma,x} U_\gamma \right) + \left(N_\beta V_\beta \right)\left(N_{\gamma,y} U_\gamma \right) \right] dA + \int_A H_\lambda H_{\mu,x} P_\mu \, dA + \\ &\frac{\mu_{nf}}{\rho_{nf} \nu_f} \frac{1}{Re} \int_A \left(N_{\alpha,x} N_{\beta,x} U_\beta + N_{\alpha,y} N_{\beta,y} U_\beta \right) dA = \int_{S_0} N_\alpha S_x \, dS_0 \end{aligned} \tag{2.31}$$

$$\begin{aligned} &\int_A N_\alpha \left[\left(N_\beta U_\beta \right)\left(N_{\gamma,x} V_\gamma \right) + \left(N_\beta V_\beta \right)\left(N_{\gamma,y} V_\gamma \right) \right] dA + \int_A H_\lambda H_{\mu,y} P_\mu \, dA + \\ &\frac{\mu_{nf}}{\rho_{nf} \nu_f} \frac{1}{Re} \int_A \left(N_{\alpha,x} N_{\beta,x} V_\beta + N_{\alpha,y} N_{\beta,y} V_\beta \right) dA \\ &- \frac{(\rho\beta)_{nf}}{\rho_{nf} \beta_f} \frac{Ra}{\mathrm{Re}^2 \, \mathrm{Pr}} \int_A N_\alpha N_\beta \theta_\beta \, dA + \\ &\frac{\rho_f \sigma_{nf}}{\rho_{nf} \sigma_f} \frac{Ha^2}{\mathrm{Re}} \int_A N_\alpha N_\beta V_\beta dA = \int_{S_0} N_\alpha S_y \, dS_0 \end{aligned} \tag{2.32}$$

$$\begin{aligned} &\int_A N_\alpha \left[\left(N_\beta U_\beta \right)\left(N_{\gamma,x} \theta_\gamma \right) + \left(N_\beta V_\beta \right)\left(N_{\gamma,y} \theta_\gamma \right) \right] dA \\ &+ \frac{\alpha_{nf}}{\alpha_f} \frac{1}{Re \, Pr} \int_A \left(N_{\alpha,x} N_{\beta,x} \theta_\beta + N_{\alpha,y} N_{\beta,y} \theta_\beta \right) dA = \int_{S_w} N_\alpha \, q_w \, dS_w \end{aligned} \tag{2.33}$$

Then the finite element equations can be written in the form

$$K_{\alpha\beta^x}U_\beta + K_{\alpha\beta^y}V_\beta = 0 \tag{2.34}$$

$$K_{\alpha\beta\gamma^x}U_\beta U_\gamma + K_{\alpha\beta\gamma^y}V_\beta U_\gamma + M_{\lambda\mu^x}P_\mu + \left(\frac{\mu_{nf}}{\rho_{nf}\nu_f}\frac{1}{Re}\right)\left(S_{\alpha\beta^{xx}} + S_{\alpha\beta^{yy}}\right)U_\beta = Q_{\alpha^u} \tag{2.35}$$

$$\begin{aligned} &K_{\alpha\beta\gamma^x}U_\beta V_\gamma + K_{\alpha\beta\gamma^y}V_\gamma V_\gamma + M_{\alpha\mu^y}P_\mu + \left(\frac{\mu_{nf}}{\rho_{nf}\nu_f}\frac{1}{Re}\right)\left(S_{\alpha\beta^{xx}} + S_{\alpha\beta^{yy}}\right)V_\beta \\ &-\frac{(\rho\beta)_{nf}}{\rho_{nf}\beta_f}\frac{Ra}{\mathrm{Re}^2\,\mathrm{Pr}}K_{\alpha\beta}\theta_\beta + \frac{\rho_f\sigma_{nf}}{\rho_{nf}\sigma_f}\frac{Ha^2}{Re}K_{\alpha\beta}V_\beta = Q_{\alpha^v} \end{aligned} \tag{2.36}$$

$$K_{\alpha\beta\gamma^x}U_\beta\,\theta_\gamma + K_{\alpha\beta\gamma^y}V_\beta\,\theta_\gamma + \frac{\alpha_{nf}}{\alpha_f}\frac{1}{Re\,Pr}\left(S_{\alpha\beta^{xx}} + S_{\alpha\beta^{yy}}\right)\theta_\beta = Q_{\alpha^\theta} \tag{2.37}$$

where the coefficients in element matrices are in the form of the integrals over the element area and along the element edges S_0 and S_w as

$$K_{\alpha\beta^x} = \int_A N_\alpha N_{\beta,x}dA \tag{2.38a}$$

$$K_{\alpha\beta^y} = \int_A N_\alpha N_{\beta,y}dA \tag{2.38b}$$

$$K_{\alpha\beta\gamma^x} = \int_A N_\alpha N_\beta N_{\gamma,x}dA \tag{2.38c}$$

$$K_{\alpha\beta\gamma^y} = \int_A N_\alpha N_\beta N_{\gamma,y}dA \tag{2.38d}$$

$$K_{\alpha\beta} = \int_A N_\alpha N_\beta dA \tag{2.38e}$$

$$S_{\alpha\beta^{xx}} = \int_A N_{\alpha,x}N_{\beta,x}dA \tag{2.38f}$$

$$S_{\alpha\beta^{yy}} = \int_A N_{\alpha,y}N_{\beta,y}dA \tag{2.38g}$$

$$M_{\lambda\mu^x} = \int_A H_\lambda H_{\mu,x}dA \tag{2.38h}$$

$$M_{\alpha\mu^y} = \int_A H_\alpha H_{\mu,y} dA \tag{2.38i}$$

$$Q_{\alpha^u} = \int_{S_0} N_\alpha S_x dS_0 \tag{2.38j}$$

$$Q_{\alpha^v} = \int_{S_0} N_\alpha S_y dS_0 \tag{2.38k}$$

$$Q_{\alpha\theta} = \int_{S_w} N_\alpha \, q_w dS_w \tag{2.38*l*}$$

These element matrices are evaluated in closed form ready for numerical simulation. Details of the derivation for these element matrices are omitted herein.

For numerical simulation, these element matrices are evaluated in closed-form. Details of the derivation for these element matrices are omitted herein for briefness.

The resultant finite element equations (2.34)-(2.37), are nonlinear. These nonlinear algebraic equations are solved employing the Newton-Raphson iteration technique by first writing the unbalanced values from the set of the finite element equations (2.34)-(2.37) as,

$$F_{\alpha^p} = K_{\alpha\beta^x} U_\beta + K_{\alpha\beta^y} V_\beta \tag{2.39a}$$

$$\begin{aligned} F_{\alpha^u} &= K_{\alpha\beta\gamma^x} U_\beta U_\gamma + K_{\alpha\beta\gamma^y} V_\gamma U_\gamma + M_{\alpha\mu^x} P_\mu \\ &+ \left(\frac{\mu_{nf}}{\rho_{nf} \nu_f} \frac{1}{Re} \right) (S_{\alpha\beta^{xx}} + S_{\alpha\beta^{yy}}) U_\beta - Q_{\alpha^u} \end{aligned} \tag{2.39b}$$

$$\begin{aligned} F_{\alpha^v} &= K_{\alpha\beta\gamma^x} U_\beta V_\gamma + K_{\alpha\beta\gamma^y} V_\gamma V_\gamma + M_{\alpha\mu^y} P_\mu + \left(\frac{\mu_{nf}}{\rho_{nf} \nu_f} \frac{1}{Re} \right) (S_{\alpha\beta^{xx}} + S_{\alpha\beta^{yy}}) V_\beta \\ &- \frac{(\rho\beta)_{nf}}{\rho_{nf} \beta_f} \frac{Ra}{\mathrm{Re}^2 \, \mathrm{Pr}} K_{\alpha\beta} \theta_\beta + \frac{\rho_f \sigma_{nf}}{\rho_{nf} \sigma_f} \frac{Ha^2}{Re} K_{\alpha\beta} V_\beta - Q_{\alpha^v} \end{aligned} \tag{2.39c}$$

$$F_{\alpha\theta} = K_{\alpha\beta\gamma^x} U_\beta \theta_\gamma + K_{\alpha\beta\gamma^y} V_\beta \theta_\gamma + \frac{\alpha_{nf}}{\alpha_f} \frac{1}{Re \, Pr} \left(S_{\alpha\beta^{xx}} + S_{\alpha\beta^{yy}} \right) \theta_\beta - Q_{\alpha\theta} \tag{2.39d}$$

This leads to a set of algebraic equations with the incremental unknowns of the element nodal velocity components, temperatures, and pressures in the form,

$$\begin{bmatrix} K_{uu} & K_{uv} & K_{u\theta} & K_{up} \\ K_{vu} & K_{vv} & K_{v\theta} & K_{vp} \\ K_{\theta u} & K_{\theta v} & K_{\theta\theta} & 0 \\ K_{pu} & K_{pv} & 0 & 0 \end{bmatrix} \begin{bmatrix} \Delta u \\ \Delta v \\ \Delta\theta \\ \Delta p \end{bmatrix} = \begin{bmatrix} F_{\alpha^u} \\ F_{\alpha^v} \\ F_{\alpha^\theta} \\ F_{\alpha^p} \end{bmatrix} \tag{2.40}$$

where $K_{uu} = K_{\alpha\beta\gamma^x} U_\beta + K_{\alpha\beta\gamma^x} U_\gamma + K_{\alpha\beta\gamma^y} V_\beta + \left(\frac{\mu_{nf}}{\rho_{nf} \nu_f} \frac{1}{Re} \right) \left(S_{\alpha\beta^{xx}} + S_{\alpha\beta^{yy}} \right)$

$K_{uv} = K_{\alpha\beta\gamma^y} U\gamma$

$K_{u\theta} = 0$

$K_{up} = M_{\alpha\mu^x}$

$K_{vu} = K_{\alpha\beta\gamma^x} V\gamma$

$K_{vv} = K_{\alpha\beta\gamma^x} U_\beta + K_{\alpha\gamma\beta^y} V_\gamma + K_{\alpha\beta\gamma^y} V_\gamma + \left(\frac{\mu_{nf}}{\rho_{nf} \nu_f} \frac{1}{Re} \right) \left(S_{\alpha\beta^{xx}} + S_{\alpha\beta^{yy}} \right)$

$K_{v\theta} = -\frac{(\rho\beta)_{nf}}{\rho_{nf} \beta_f} \frac{Ra}{\mathrm{Re}^2 \,\mathrm{Pr}} K_{\alpha\beta}$

$K_{vp} = M_{\alpha\mu^y}$

$K_{\theta u} = K_{\alpha\beta\gamma^x} \theta\gamma$

$K_{\theta v} = K_{\alpha\beta\gamma^y} \theta\gamma$

$K_{\theta\theta} = K_{\alpha\beta\gamma^x} U_\beta + K_{\alpha\beta\gamma^y} V_\beta + \frac{\alpha_{nf}}{\alpha_f} \frac{1}{Re\, Pr} (S_{\alpha\beta^{xx}} + S_{\alpha\beta^{yy}})$

$$K_{pu} = M_{\alpha\mu^x}$$

$$K_{pv} = M_{\alpha\mu^y}$$

and $K_{\theta p} = K_{p\theta} = K_{pp} = 0$

The iteration process is terminated if the percentage of the overall change compared to the previous iteration is less than the specified value.

To solve the sets of the global nonlinear algebraic equations in the form of matrix, the Newton-Raphson iteration technique has been adapted through PDE solver with MATLAB interface. The convergence of solutions is assumed when the relative error for each variable between consecutive iterations is recorded below the convergence criterion ε such that

$\left|\Psi^{n+1} - \Psi^{n}\right| < \varepsilon$, where n is number of iteration and $\Psi = U, V, \theta$ .The convergence criterion was set to 10^{-5}.

2.3.2 Grid Size Sensitivity Test

A grid independence study was executed to make sure the correctness of the numerical results for a square cavity (AR = 1) at the representative value of Ra = 10^5, Ha = 5, Re = 100, Pr = 6.2 and ϕ = 4%. Non-uniform triangular element grid system is employed in the present study. The extreme value of Nu_{av} is used as a sensitivity measure of the accuracy of the solution and is selected as the monitoring variable considering both the accuracy of numerical value and computational time. This is described in Table 2.2 and Figure 2.2. It is observed that the magnitude of the average Nusselt number for 6248 elements shows a very little difference with the results obtained for the other higher elements. The element 6248 is chosen for further calculation of the case AR = 1. This grid resolution is therefore used for all consequent calculations for AR < 1 and AR > 1.

Table 2.2: Grid Sensitivity Check at Ra = 10^5, Ha = 5, Re = 100, Pr = 6.2 and ϕ = 4%

Elements	2742	3536	5120	6248	8106
Nu_{av}	3.32416	4.91563	5.64745	5.74165	5.74166
Time(s)	258.436	342.746	417.842	496.784	678.357

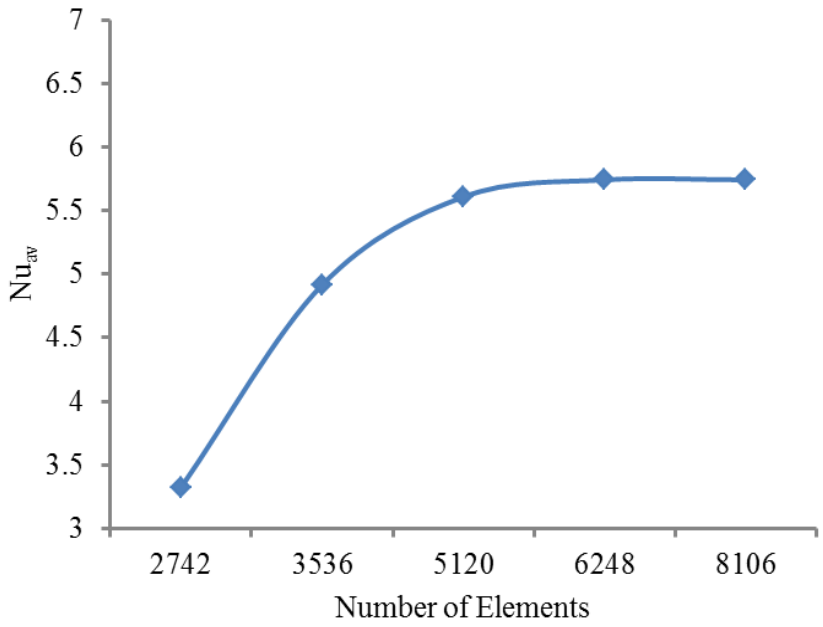

Figure 2.2. Grid independency study for different elements while Re = 100, Ra = 10^5, ϕ = 0.04, Ha = 5 and Pr = 6.2.

2.3.3 Validation of the Numerical Scheme

In order to verify the accuracy of the numerical results and the validity of the mathematical model obtained throughout the present study, comparisons with the previously published results are essential. But due to the lack of availability of experimental data on the particular problems along with its associated boundary conditions investigated in this study, validation of the predictions could not be done against experiment.

However, the outcome of the present numerical code is benchmarked against the numerical result of Nasrin et al. (2013) which was reported for numerical investigation of nanofluid of forced convection in a channel with an open cavity having porous medium. The streamlines and isotherms for the solid volume fraction ($\phi = 0.05$), the Reynolds number Re = 100 are presented in the Figure 2.3 that is an excellent agreement with Nasrin et al. (2013). As a result the validation boosts the confidence in our numerical code to carry on with the above stated objective of the current investigation.

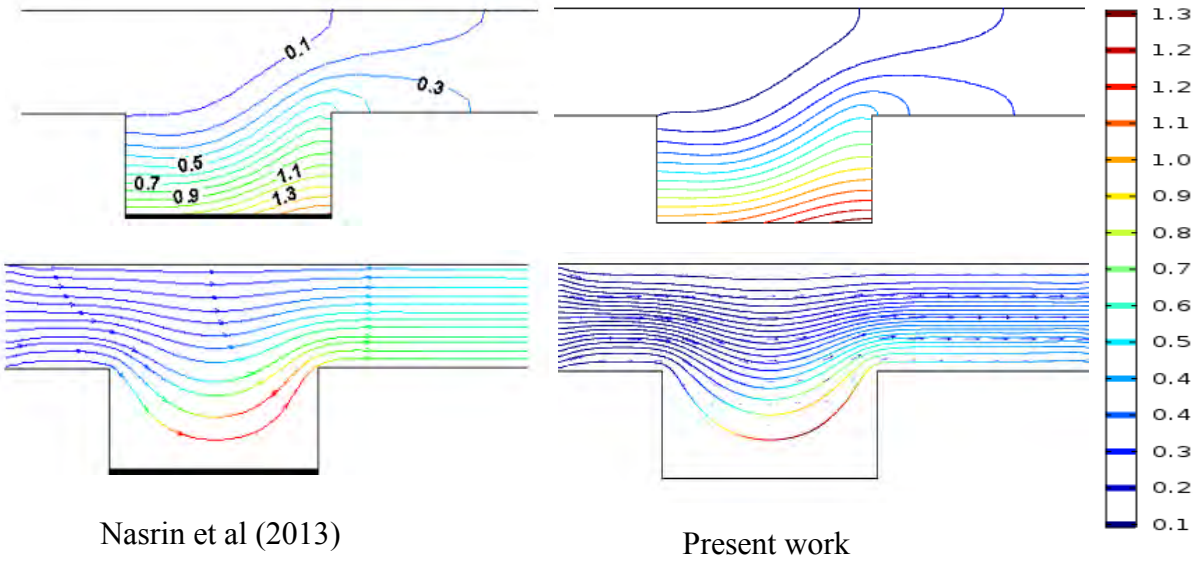

Figure 2.3. Comparison of present work with Nasrin et al. (2013) while $\phi = 0.05$ and Re = 100 for Streamlines (bottom) and Isotherms (top).

CHAPTER 3

RESULTS AND DISCUSSION

The present numerical study is carried out for copper-water nanofluids with the help of finite-element method. The current investigation is to explore the conjugate effects of nanofluids on laminar mixed convection heat transfer in an open channel with a cavity in the presence of a magnetic field. Numerical results are presented in order to determine the effects of the considered parameters. The dimensionless parameters specified for the system are Hartmann number (Ha), Reynolds number (Re), solid volume fraction (ϕ), Rayleigh number (Ra) and physical parameter for the system is the cavity aspect ratio (AR). Results are presented through streamline and isotherm contours along with necessary plots at the four different AR = 2, 1.5, 1 and 0.5 along with Ra = 10^4 to 10^6, Ha = 0 to 20 for different values of ϕ = 0% to 15%. Furthermore, the heat transfer rate of the heated surface is displayed in terms of average Nusselt number (Nu_{av}) and the dimensionless average fluid temperature θ_{av} are displayed.

3.1 CASE 1 (AR = 2)

3.1.1 Effect of Hartmann number

The effects of Hartmann number Ha (= 0.0, 5.0, 10.0, 20.0) on streamlines as well as isotherms for the present configuration at Ra=10^4, ϕ = 0.04 and Re = 100 has been demonstrated in figure 3.1(a)–(b). From figure 3.1 (a) it is seen that the flow velocity creates a small non uniform curvature shape at the right bottom part of the cavity at Ha = 0 due to the buoyancy force. This non uniform curvature shape is disappeared with increasing Hartmann number and creates parabolic shape in the cavity. It is also observed from the figure that the magnetic field affects only the flow inside the cavity whereas in the channel it remains almost similar. On the other hand temperature field shows that the convection is almost suppressed, and the isotherms are almost parallel to the horizontal wall inside the cavity but in the channel it forms twist shape, indicating that a quasi-convection regime is reached.

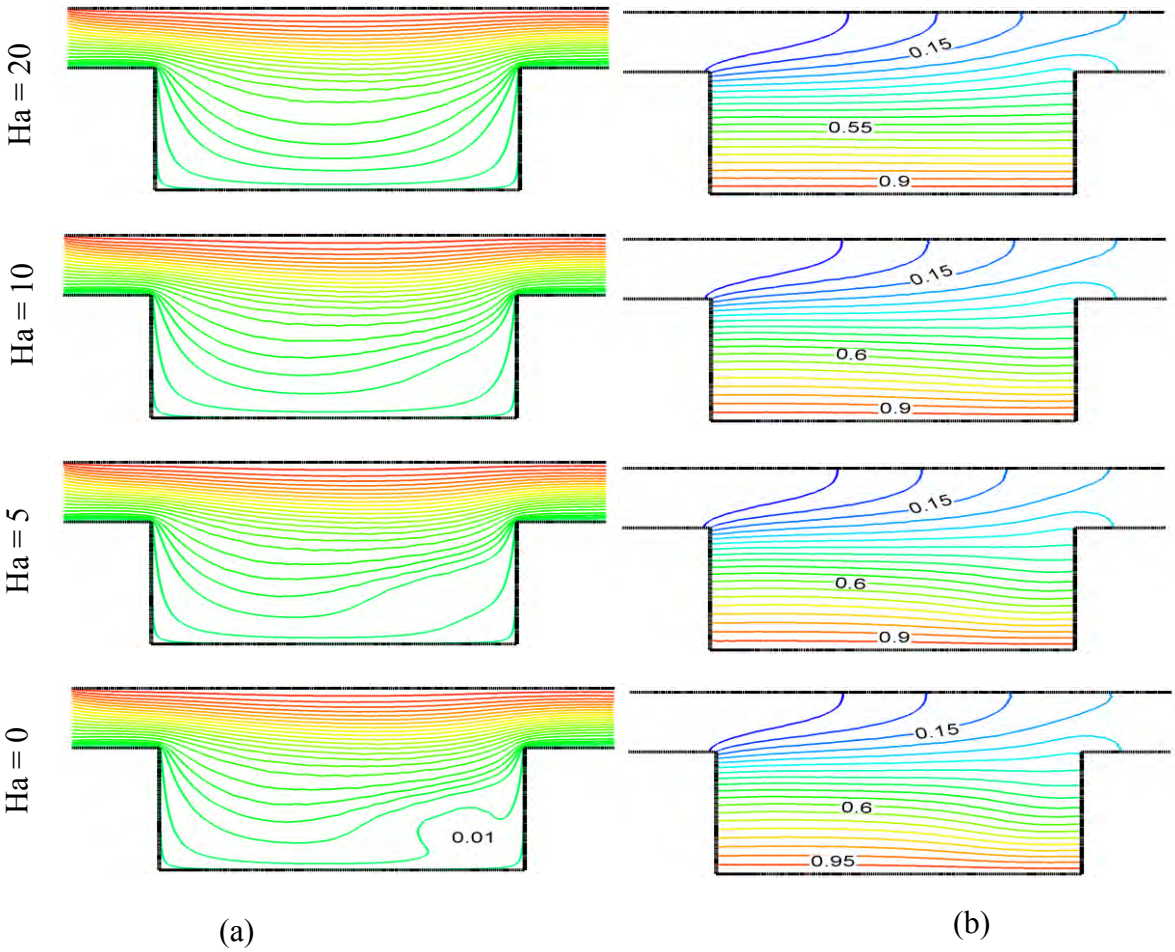

Figure 3.1: Effect of Hartmann number on (a) streamlines and (b) isotherms for AR = 2 and Ra = 10^4, while ϕ = 0.04, Re = 100.

The influence of Hartmann number Ha (= 0, 5, 10, 20) on streamlines and isotherms are presented at Ra = 10^5 for ϕ = 0.04 and Re = 100 in figure 3.2 (a)–(b). The flow with Ha = 0 creates a small vortex at the right bottom part of the cavity due to the buoyancy force. This vortex is disappeared with increasing Hartmann number as shown in figure 3.2(a). It is also observed from the figure that the magnetic field affects only the flow inside the cavity whereas in the channel it remains almost similar. The isothermal lines become almost similar pattern in figure 3.1(b).

The effect of Hartmann number on the flow field and temperature fields has been shown in figure 3.3 at Ra = 10^6, ϕ = 0.04 and Re = 100. An interesting result is found that three circulating cells are formed by the flow field.

Near the right and left vertical wall clockwise circulation cell is appeared whereas anticlockwise circulation cell is appeared at the middle position and near the hot bottom wall. It is also seen that the strength of these circulation cells become gradually weaker for increasing of Hartmann number. For higher value of Hartmann number (Ha = 20) left and middle circulation cells disappeared. Isotherms line formed wave shaped in cavity and wayness of the lines decrease very slowly for increasing of Hartmann number. But isotherms in the channel formed twist shape. It is clear that convection is dominant for lower value of Hartmann number.

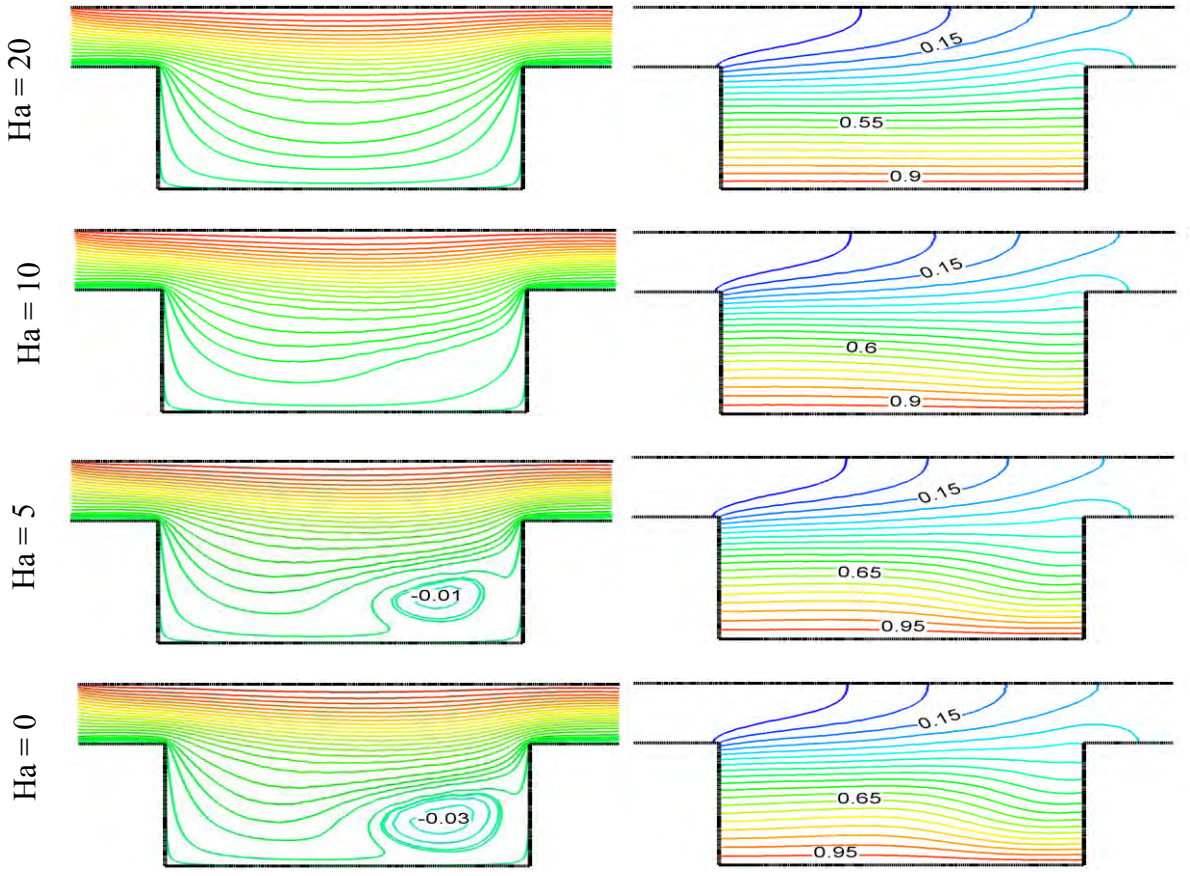

Figure 3.2 Effect of Hartmann number on (a) streamlines and (b) isotherms for AR = 2 and Ra = 10^5 while ϕ = 0.04, Re = 100.

From the figure 3.1 to 3.3, it is observed that the strength of flow field in the cavity is increasing for higher values of Rayleigh numbers. It is because of convection is dominant in the cavity for higher value of Rayleigh numbers.

On the other hand, flow pattern is almost similar in the channel. Isotherms are similar for Ra = 10^4 and 10^5 but for 10^6 isotherms is formed twist shape in the cavity as well as in the channel.

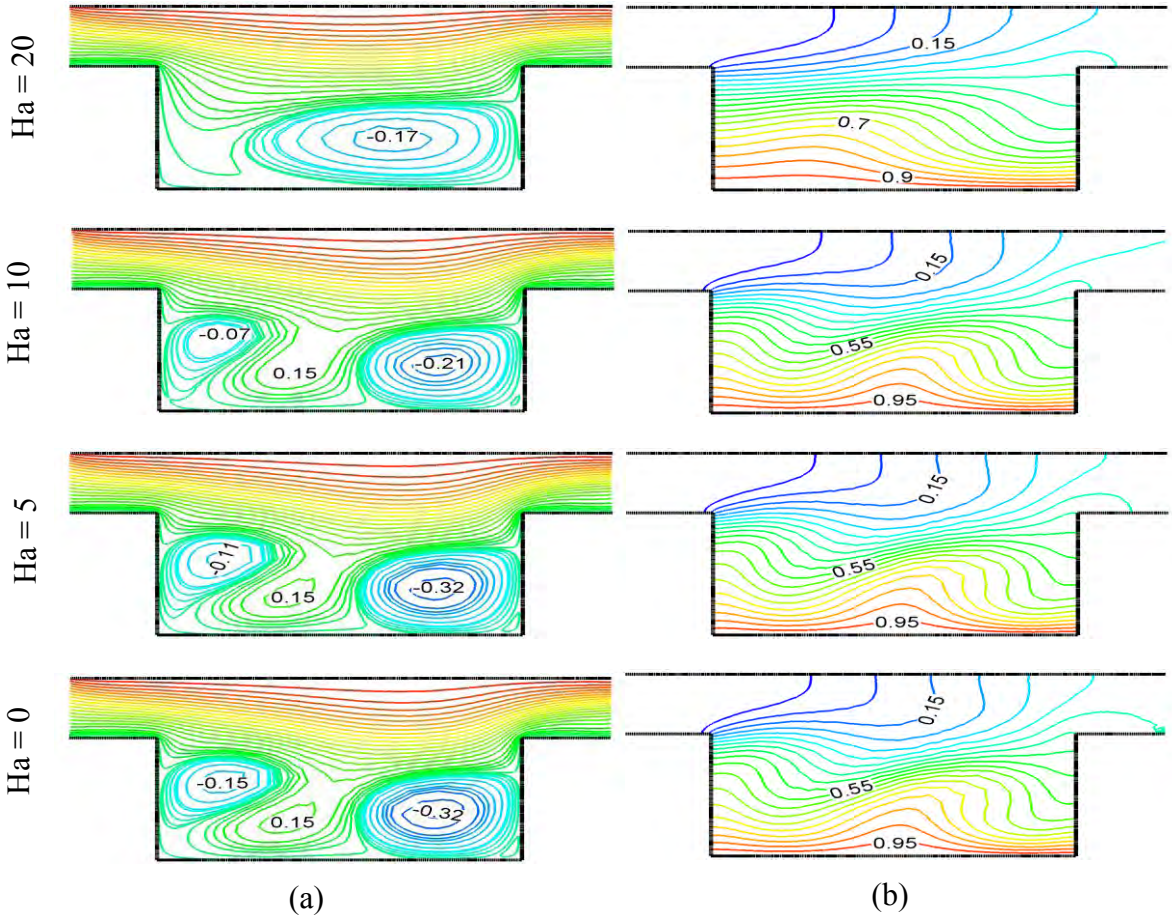

Figure 3.3 Effect of Hartmann number on (a) streamlines and (b) isotherms for AR = 2 and Ra = 10^6, while ϕ = 0.04, Re = 100.

Figure 3.4(a) and (b) illustrates the average Nusselt number and average fluid temperature respectively. The figures are given for different Rayleigh numbers and different cases at selected values of Hartmann numbers. Both heat transfer rate and average fluid temperature decrease with increasing of Hartmann numbers. Heat transfer rate and average fluid temperature become almost constant for Ra = 10^3 and 10^4 but it drastically increase for higher value of Ra = 10^6 due to increasing of buoyancy driven force.

Heat transfer rate and average temperature increase with increasing of Rayleigh number for all values of Hartmann number. It means that the magnetic field can be used to control the heat transfer phenomena.

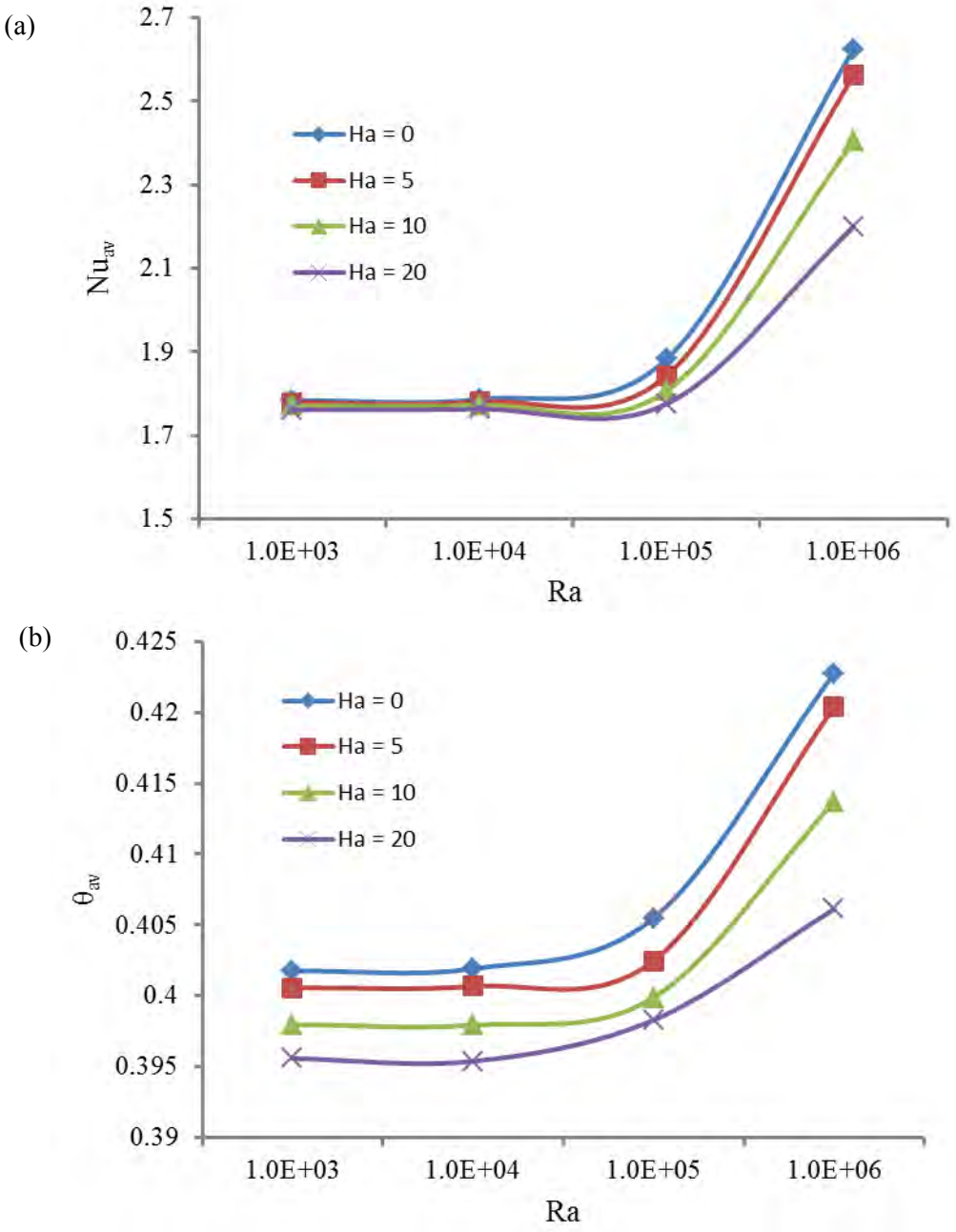

Figure 3.4 Effect of Hartman number on (a) average Nusselt number and (b) average fluid temperature for different values of Ra and AR = 2, while Re = 100 and $\phi = 0.04$.

3.1.2 Effects of solid volume fraction

In this investigation, our attention is taken into account to investigate the effects of controlling parameters namely the solid volume fraction (ϕ) and Rayleigh numbers (Ra). Here, the effect of the solid volume fractions is investigated in the range of 0% – 15% whiles the Re and Ha are kept fixed at 100 and 5, respectively. Figure 3.5-3.7 shows the streamlines and isotherms in a channel with cavity for various values of the solid volume fractions (ϕ = 0, 0.05, 0.1, and 0.15) for different Ra (= 10^4, 10^5 and 10^6).

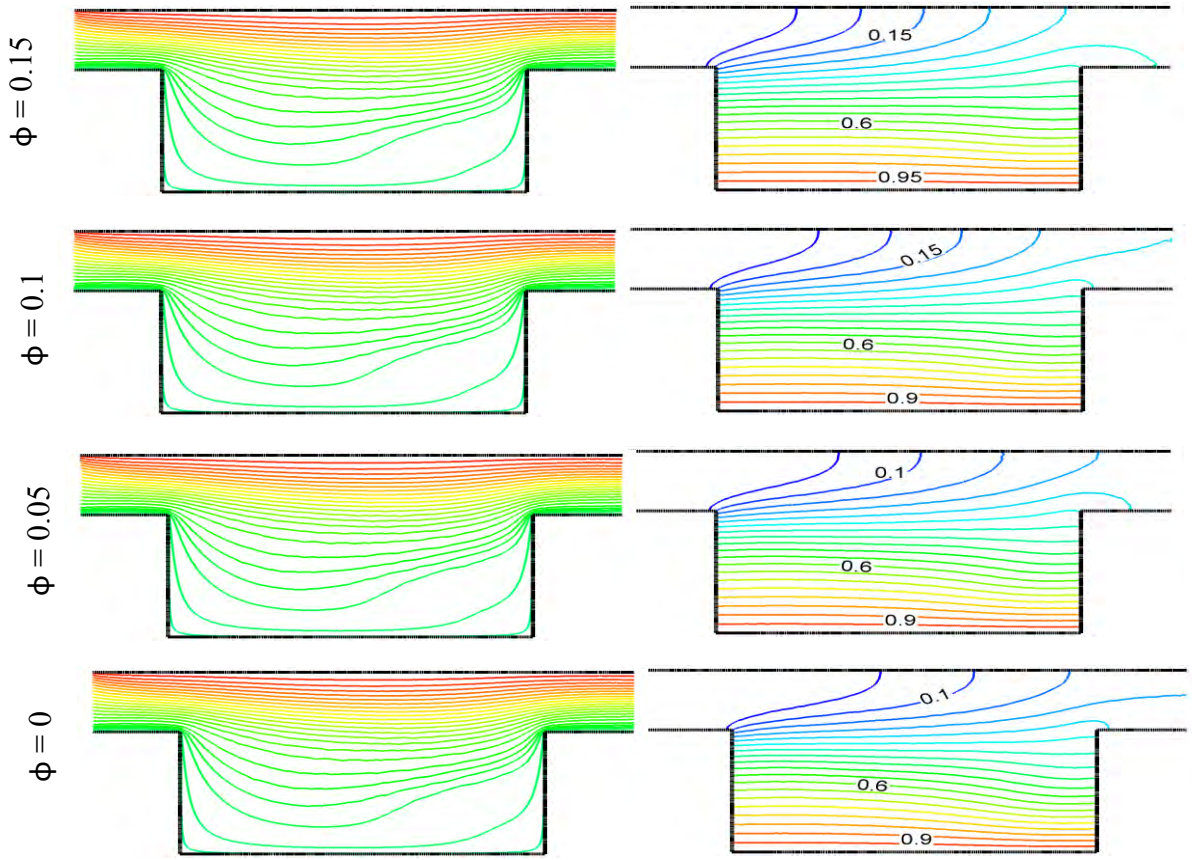

Figure 3.5 Effect of solid volume fraction on (a) streamlines and (b) isotherms for AR = 2 and Ra = 10^4 while Ha = 5, Re = 100.

It can easily be seen from the left column of figure 3.5(a) that the streamlines formed are almost parabolic shape in the cavity for all values of ϕ but in the channel it is parallel to the horizontal wall.

Isotherms in the cavity has no significant change for different values of ϕ presented in figure 3.5 (b). It is seen that the temperature lines through the horizontal pipe with an open cavity dense near the inlet for increasing ϕ. But initially (ϕ = 0%) these lines try to gather near the heated walls of the cavity corresponding to physical changes of the working fluid.

The effects of solid volume fraction on stream lines and isotherms for Ra = 10^5 while Ha = 5 and Re = 100 is presented in figure 3.6 (a) – (b). Flow pattern with ϕ = 0.0 creates a small vortex at the right bottom part of the cavity due to base fluid goes very fast than the nanofluid. This vortex is disappeared with increasing solid volume concentraton as shown in figure 3.6(a). It is also observed from the figure that the solid volume concentration affects only the flow inside the cavity whereas in the channel it remains almost similar. On the other hand temperature field shows similar pattern with the figure 3.5(b).

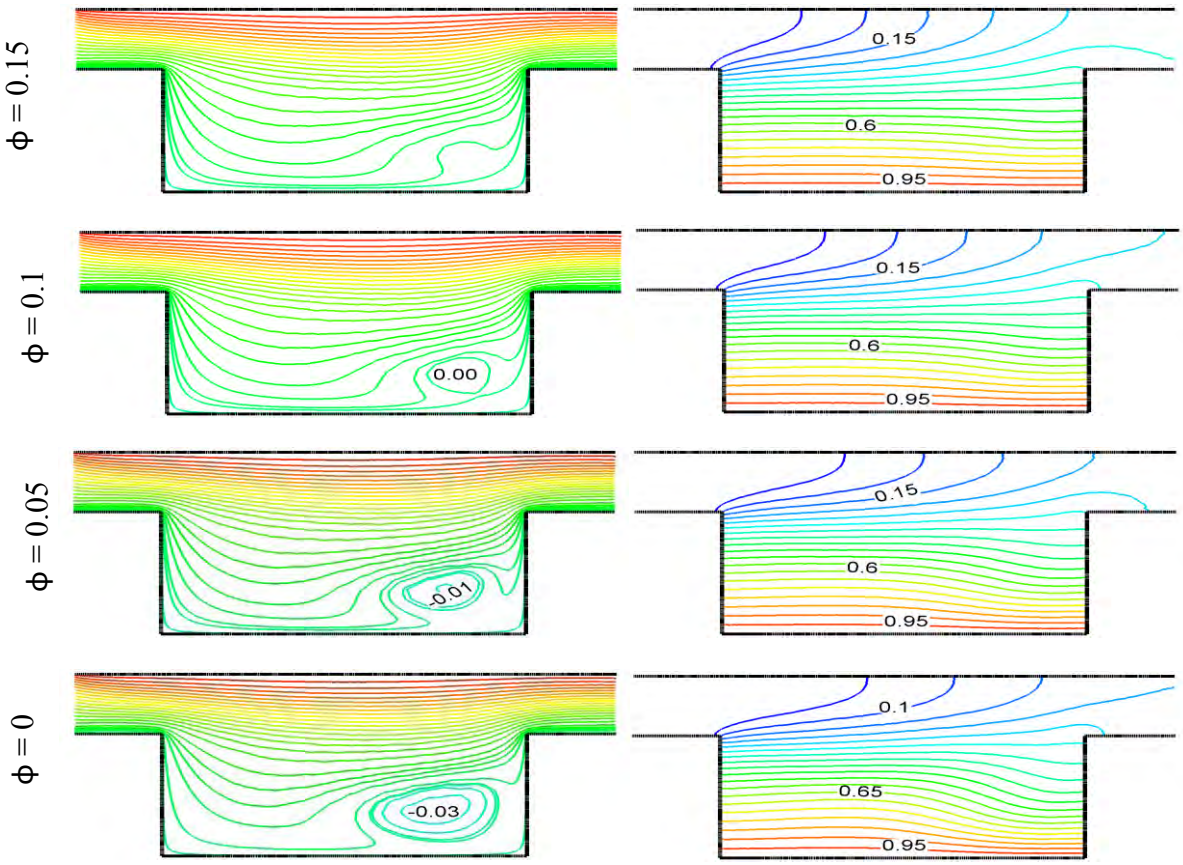

Figure 3.6 Effect of solid volume fraction on (a) streamlines and (b) isotherms for AR = 2 and Ra = 10^5, while Ha = 5, Re = 100.

Figure 3.7(a) and (b) shows the streamlines and isotherms for different values of solid volume fraction for AR = 2 at Ra = 10^6, Ha = 5 and Re = 100. As seen from the left column of this figure, an amount of fluid near the right, left vertical wall and heating wall of the cavity are activated so as to create buoyancy-induced clockwise and anticlockwise rotating cell for the lowest value of ϕ = 0 respectively. As the solid volume fraction increases the strength of the rotating cells are reduced. For escalating ϕ, through flow in the channel gains its strength and try to occupy the whole of the cavity as well as the channel indicating the establishment of conduction mode of heat transfer. The corresponding isotherms for the lowest value of ϕ = 0 shows the usual convective twist inside the cavity. The distortion of isothermal lines appears due to the high convective current inside the cavity. Distortions of isothermal lines start to disappear with increasing solid volume fraction. As solid volume fraction increases, isothermal lines inside the cavity as well as the channel approaches more and more towards the conduction like distribution pattern of isothermal lines. For large solid volume fraction ϕ = 0.15, the convection is almost suppressed, and the isotherms are almost parallel to the horizontal wall, indicating that a quasi-conduction regime is reached.

From the figure 3.5 to 3.7 it is seen that fluid flow is stronger in the cavity for higher values of Rayleigh number beside this in the channel the flow pattern has no significant change for different values of Rayleigh numbers. But for the lower values of solid volume fraction (ϕ = 0, 0.05) at higher value of Rayleigh number isotherms formed more curvy shaped than the lower values of Rayleigh number. At the same temperature field has no significant change for higher values of solid volume fraction with the Rayleigh number.

The average Nusselt number (Nu_{av}) at the hot surface, which is a measure of the overall heat transfer rate for the abovementioned values of the solid volume fractions (ϕ) is shown in figure 3.8(a). This figure shows a linear variation of the average Nusselt number with the solid volume fraction for Rayleigh number Ra = 10^3 to 10^5 but it increases promptly for Rayleigh number 10^6.As clearly be seen that the heat transfer increases with increasing ϕ. When the solid volume fraction increases from 0% to 15% the heat transfer increases very commonly. However, the values

of Nu_{av} are always maximum for the highest value of Rayleigh number Ra = 10^6.The effect of the solid volume fractions (ϕ) on average fluid temperature (θ_{av}) in the enclosure is depicted in figure 3.8(b). It is observed that θ_{av} increases significantly with the increasing of solid volume fractions. It is clearly being seen that θ_{av} is maximum for the highest value of Rayleigh number for all values of solid volume fraction except $Ra = 10^6$, θ_{av} is almost constant and at 10^6 increases uniformly.

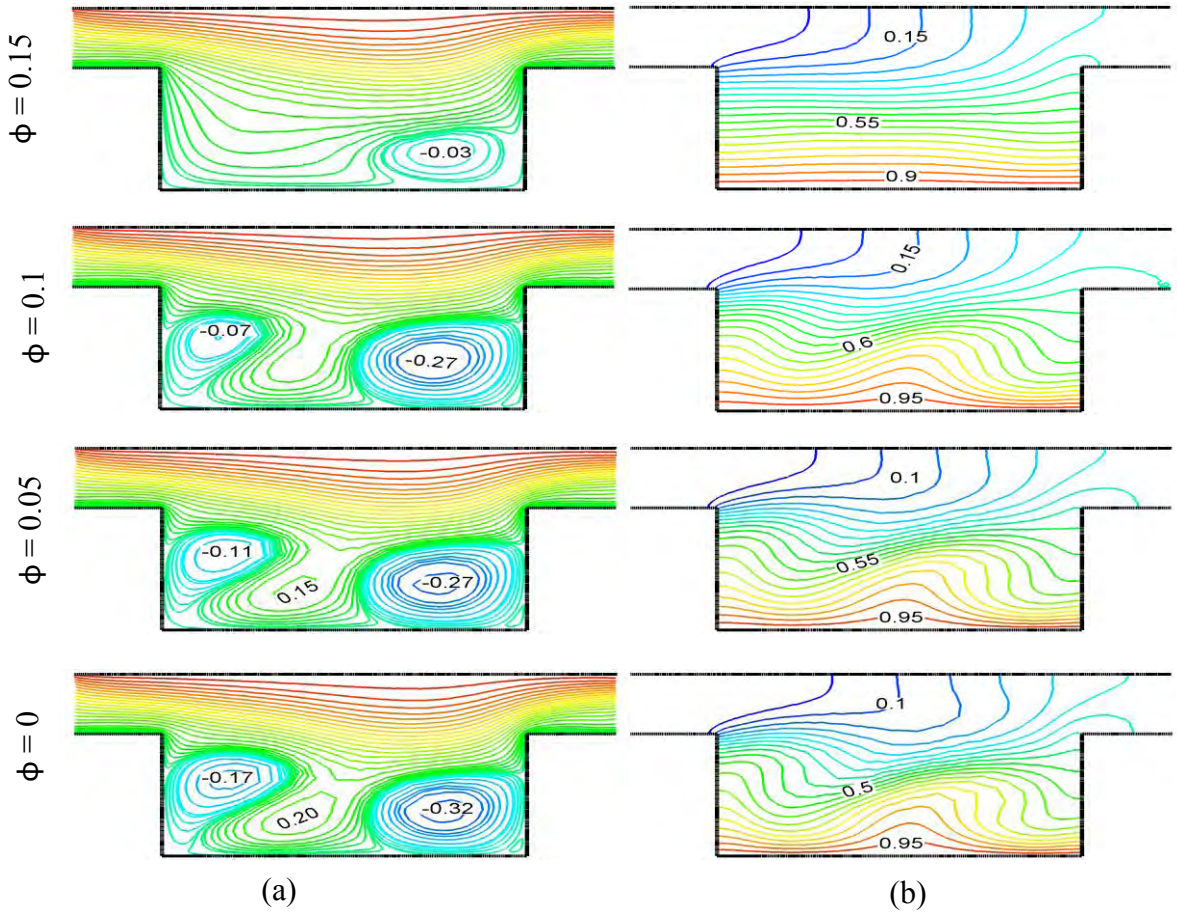

Figure 3.7 Effect of solid volume fraction on (a) streamlines and (b) isotherms for AR = 2 and Ra = 10^6, while Ha = 5, Re = 100.

3.1.3 Effects of Reynolds Number

The effect of Reynolds Number Re and Rayleigh number Ra on the fluid flow and temperature distribution in the channel with cavity are illustrated in the figures 3.9 to 3.11 by plotting the streamlines and isotherms for Re = 100, 200, 400 and 500 and various Ra (10^4 to10^6), while ϕ = 0.04 and Ha = 5.

The basic flow structure in the absence of natural convection effect is presented in the left bottom corner of figure 3.9 at Re = 100.

(a)

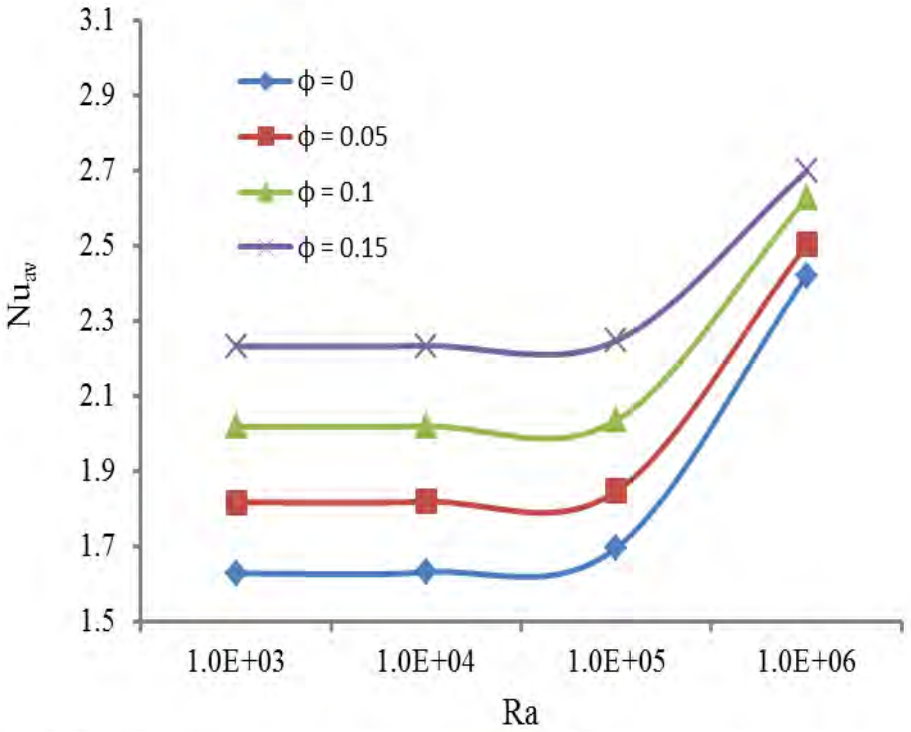

(b)

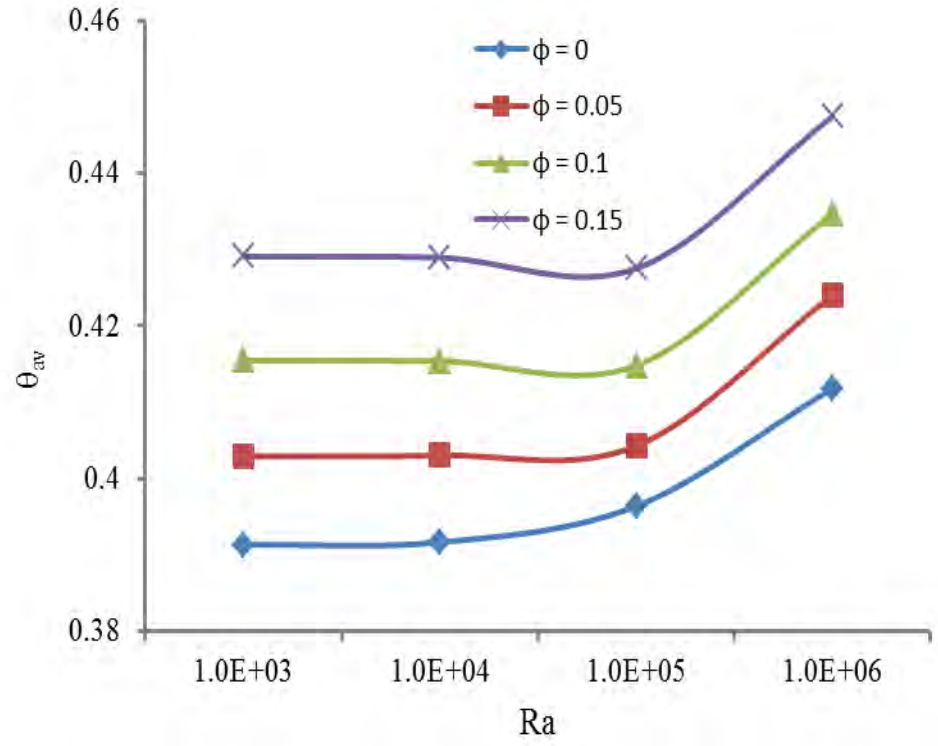

Figure 3.8 Effect of solid volume fraction on (a) average Nusselt number and (b) average fluid temperature for different values of Ra and AR = 2, while Re = 100 and Ha = 5.

It is seen clearly that for Ra = 10^4 and low Reynolds number (Re = 100), the forced convection plays a dominant role, and the recirculation flow is mostly generated only by the moving lid. The fluid flow in a two dimensional horizontal channel with cavity is characterized and a weaker anticlockwise rotating cell close to the right bottom corner. In the figure 3.9(a) it is found that rotating cell is formed for highest value of Reynolds number near the right and bottom wall of the cavity and gradually disappear for lower values of Reynolds number. But in the channel streamlines are parallel to channel. The isotherm patterns for different Reynolds number at Ra = 10^4 are described in figure 3.9(b). It is seen that the isotherms formed a thin thermal spot on the right side of the bottom wall for highest value of Reynolds number and it reduces very slowly for decreasing of Reynolds number.

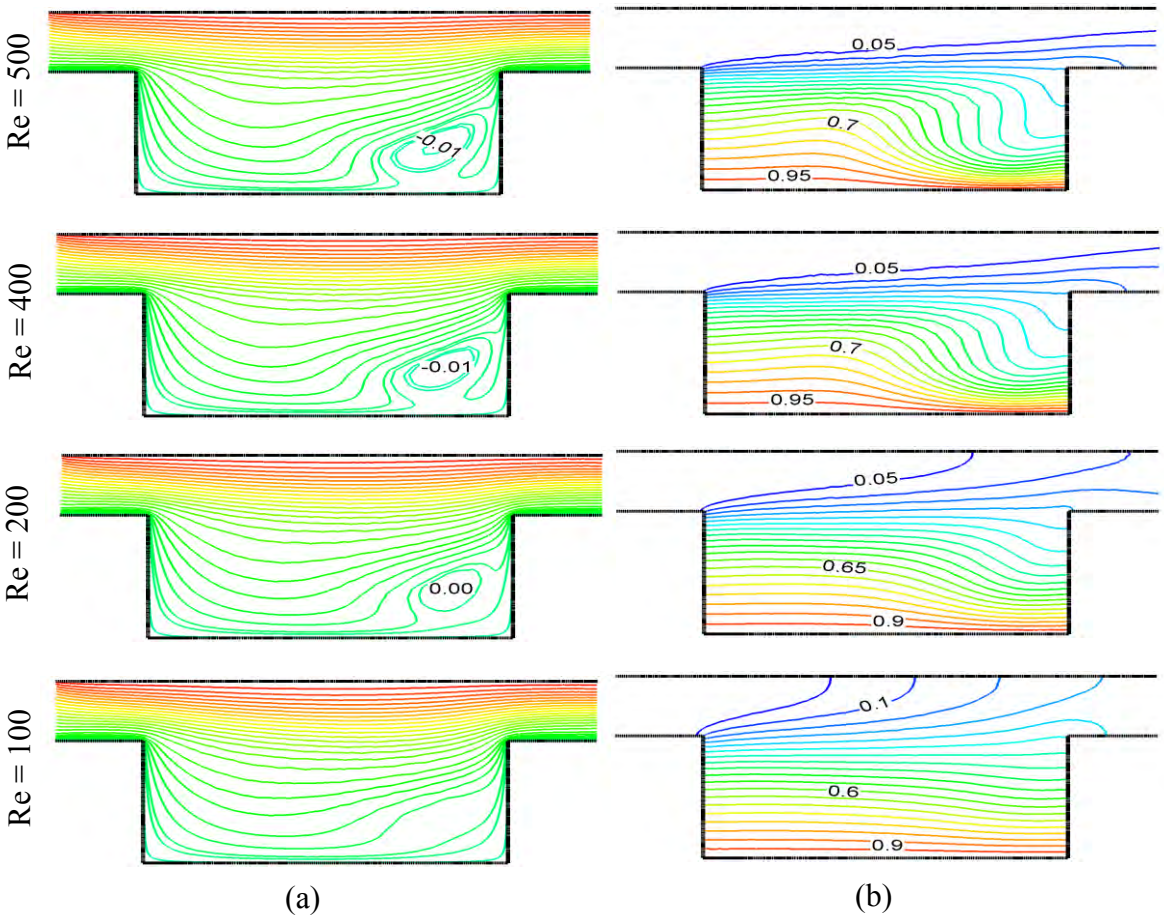

Figure 3.9 Effect of Reynolds number on (a) streamlines and (b) isotherms for AR = 2 and Ra = 10^4, while Ha = 5 and ϕ = 0.04.

Also seen that temperature profile created curvature shape for higher values of Re and gradually become parallel shape for lower value of Ra. The effects of Reynolds number on streamlines and isotherms for Ra = 10^5, Ha = 5 and ϕ = 0.04 is described in the figure 3.10. It is observed that the streamlines formed a tiny vortex along right bottom corner of the cavity and it became weaker for lower values of Reynolds number but flow field in the channel has no significant change with the figure 3.9. Corresponding temperature field shows that for the grater values of Reynolds number the isothermal lines form a thin thermal boundary layer near the hot bottom wall along the right side of the cavity which are radically changed with decreasing of Reynolds number and at lowest value of Ra = 100 it is totally disappeared. There is a little bit of change for the temperature field in the channel due to decreasing of Reynolds numbers.

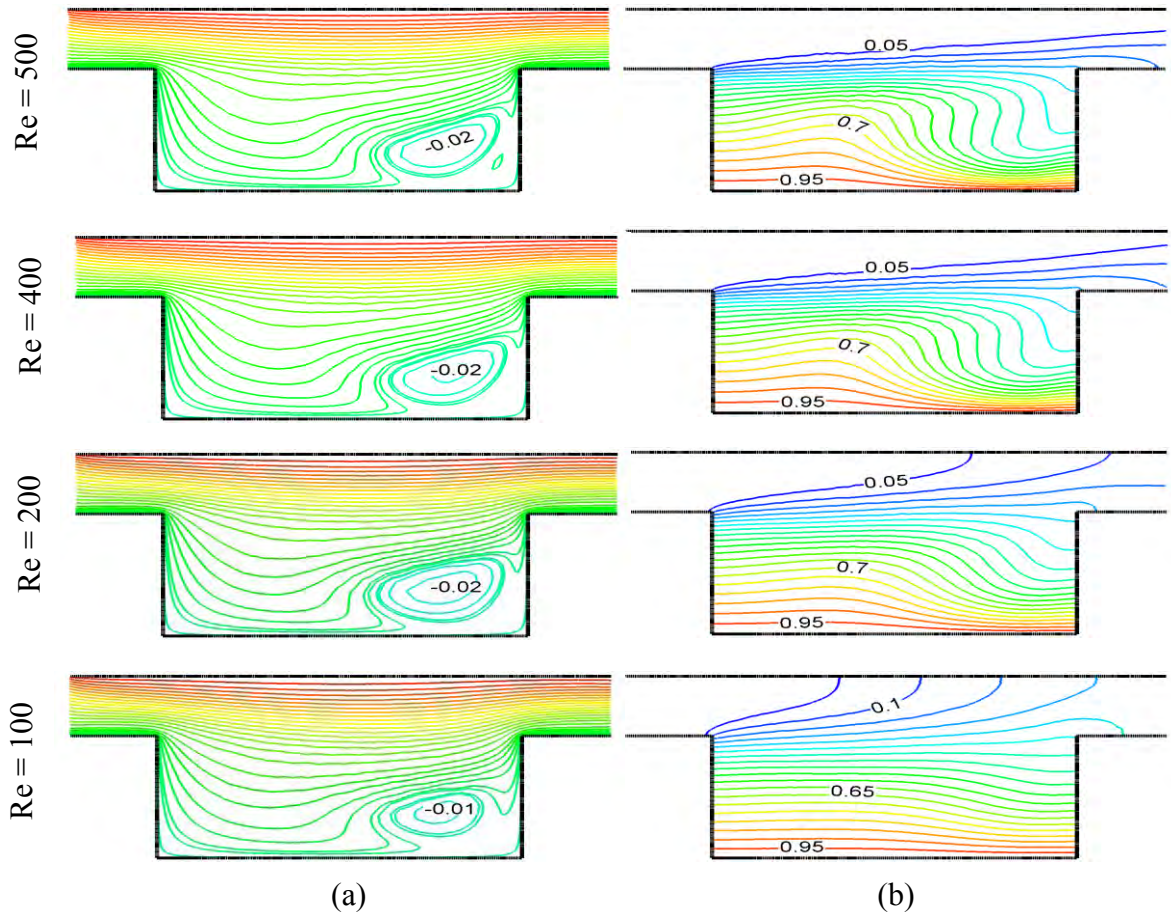

Figure 3.10 Effect of Reynolds number on (a) streamlines and (b) isotherms for AR = 2 and Ra = 10^5, while Ha = 5 and ϕ = 0.04.

The figure 3.11 shows the effects of Reynolds number on streamlines and isotherms for Ra = 10^6, at Ha = 5 and ϕ = 0.04. Streamlines designed two clockwise rotating cells near the right and left vertical wall at the same time it creates an anticlockwise shape at the middle of clockwise cell for Reynolds number Re = 100. These rotating cells became weaker for higher values of Re and left and middle rotating cell totally vanish for Re = 400 and 500. On the other hand, temperature field shows that stronger thermal boundary layer near the hot bottom wall along the right side of the cavity and depth of boundary layer slightly decrased with decreasing of Reynolds number. Higher tempareture gradient is observed near the hot wall as well as for higher values of Re. Because increasing Re causes more flow of the working nanofluids then the average heat transfer enhances.

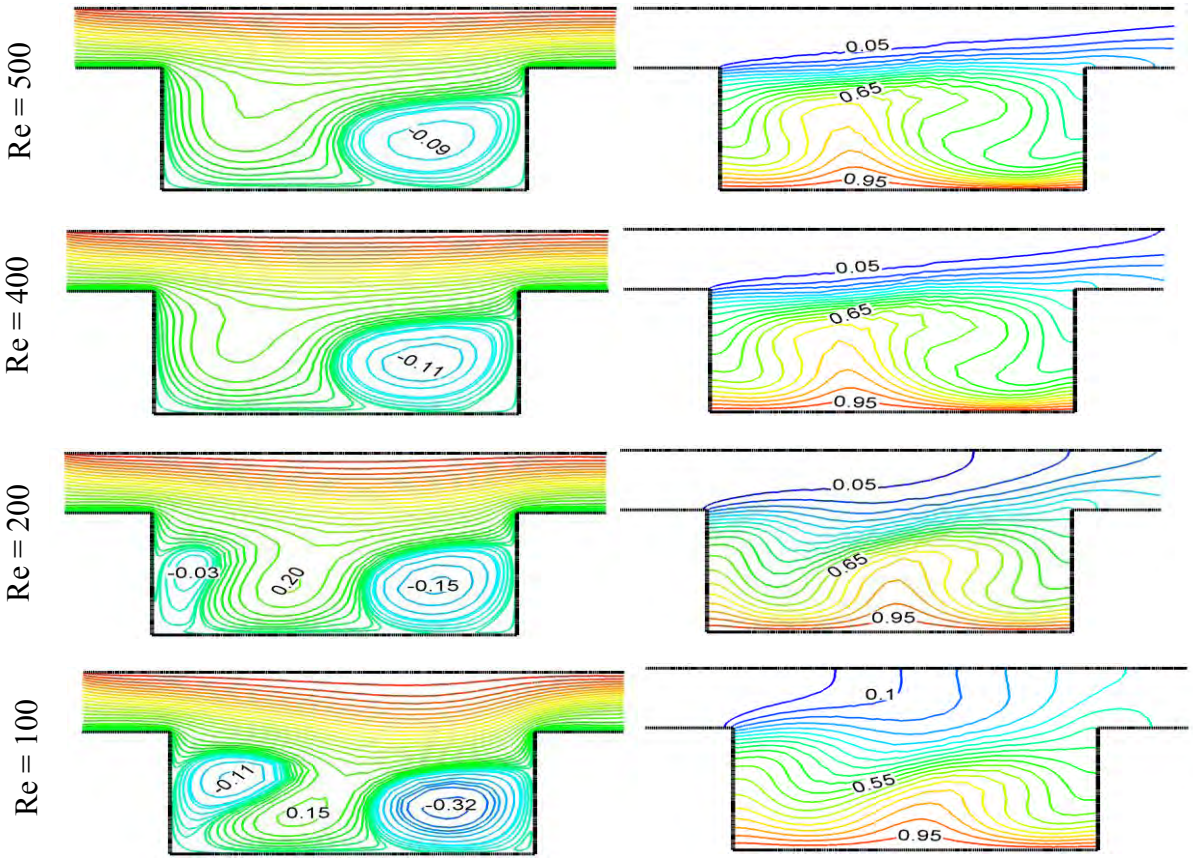

Figure 3.11 Effect of Reynolds number on (a) streamlines and (b) isotherms for AR = 2 and Ra = 10^6, while Ha = 5 and ϕ = 0.04.

From the figures 3.9 to 3.11 it is clearly seen that flow field is dominant due to increasing the Rayleigh number. It is because of force convection gain the strength due to increasing of Reynolds number. Similarly temperature field is dominant in the cavity as well as in the channel for increasing the Rayleigh number.

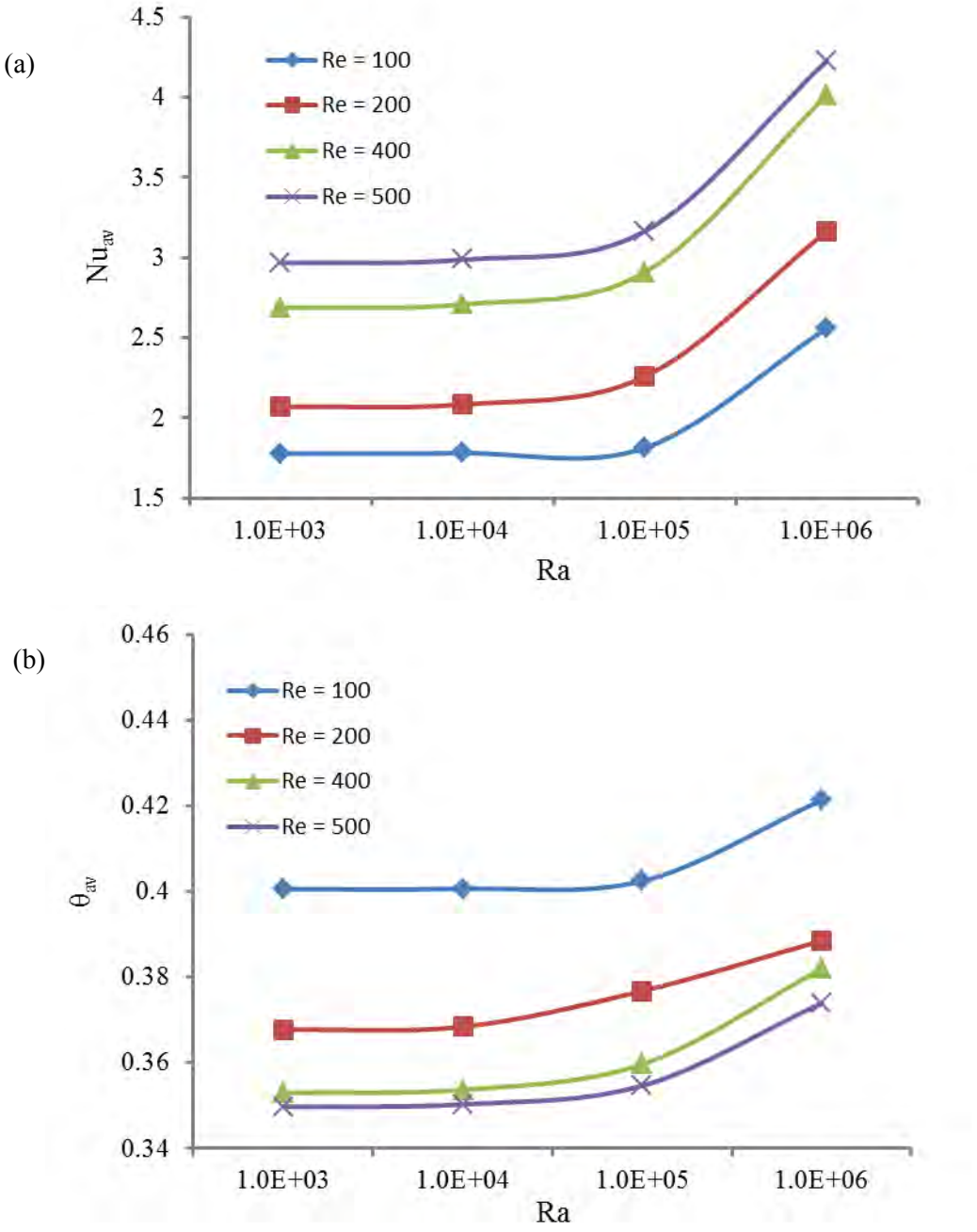

Figure 3.12 Effect of Reynolds number on (a) average Nusselt number and (b) average fluid temperature for different values of Ra, while $\phi = 0.04$ and Ha = 5.

The average Nusselt number at the heat source is plotted as a function of Rayleigh number for a particular Reynolds number is shown in figure 3.12(a). Figure 3.12(a) presents a very illustrative picture of how the heat is transferred in accordance with Re and Ra. Average Nusselt number is almost constant for Ra = 10^3 to 10^5 but increases gradually at Ra = 10^6 for all values of Reynolds number. Also, the average Nusselt number at the heated surface is found to increase as Re increases at fixed Ra. These results are expected because nanoparticles increases heat absorbing capacity of the base fluid. Therefore, it can be concluded that more heat transfer rate is expected in the case of larger value of Re as well as Ra. Nevertheless, the values of Nu_{av} are always maximum for the higher value of Re (= 500). The effect of Reynolds number Re on average fluid temperature θ_{av} in the cavity is revealed in the figure 3.12(b). From this figure, it can clearly be seen that the value of θ_{av} decreases regularly with the raise of Re for all considered Rayleigh numbers. On the other hand average fluid temperature almost constant for the range of Ra = 10^3-10^4 at all selected values of Re but it is little bit of increase after Ra = 10^4.

3.2 CASE 2 (AR = 1.5)

3.2.1 Effect of Hartmann number

The Influence of Hartman number on the streamlines and isotherms for different values of Ha (= 0, 5, 10, and 20) at Ra (= 10^4, 10^5 and 10^6) while the values of ϕ and Re kept fixed at 0.04 and 100 respectively are shown in figures 3.13, 3.14 and 3.15.

As seen from the figure 3.13(a) when Ra = 10^4 ,the values of ϕ and Re kept fixed at 0.04 and 100 respectively, a buoyancy-induced anti-clockwise rotating cell is formed by streamlines in absence of magnetic field and this cell totally vanished in presence of higher values of magnetic field. A uniform parabolic curvature shape is formed by flow field in the cavity for higher values of Hartmann number and in the cavity it is parallel to the horizontal wall with no noteworthy change for variation of Hartmann number. From the figure 3.13(b) it is clear that isotherms in the cavity are parallel to the heated surface and variation of magnetic effect has no important value. But temperature profile in the channel makes curl shape.

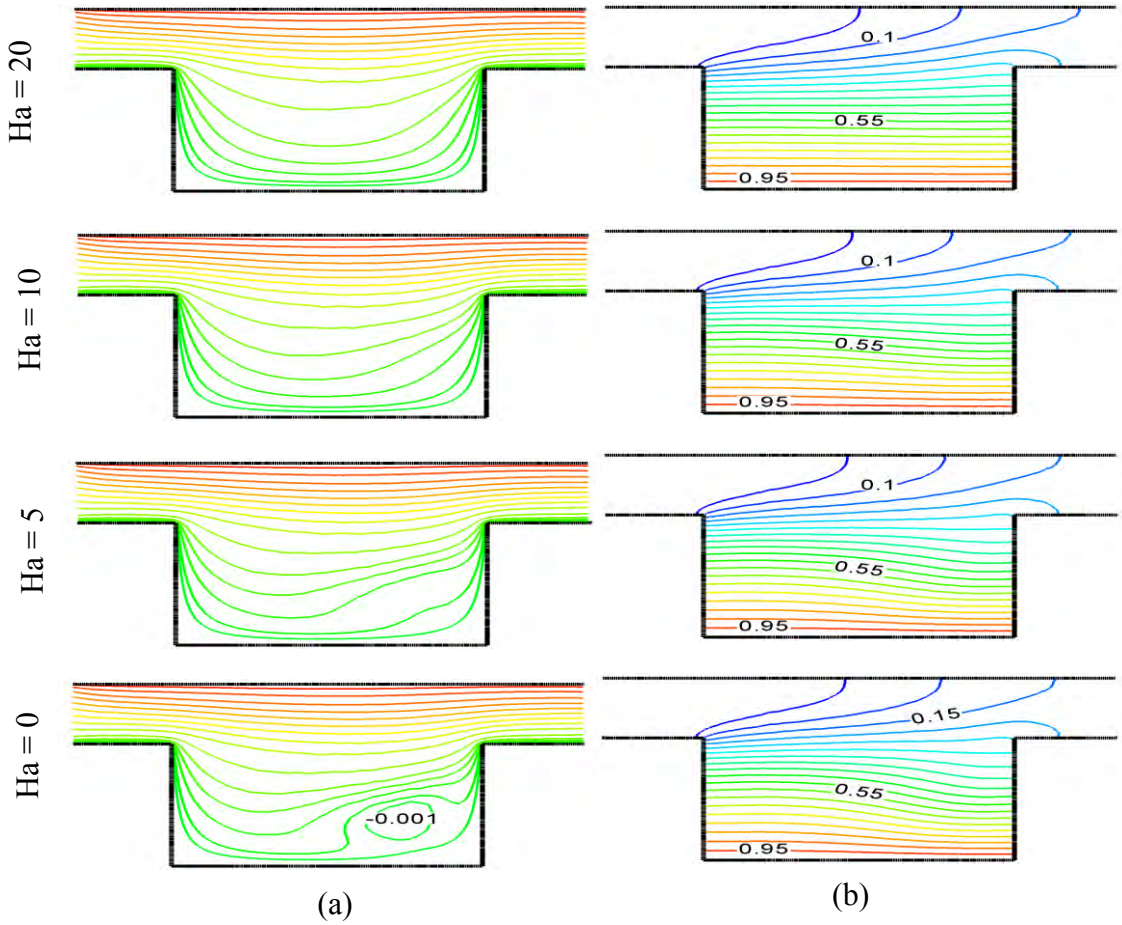

Figure 3.13 Effect of Hartmann number on (a) streamlines and (b) isotherms for AR = 1.5 and Ra = 10^4, while ϕ = 0.04, Re = 100.

From the figure 3.14 at Ra = 10^5 it is seen that a buoyancy-induced anti-clockwise rotating cell is formed by isotherms in absence of magnetic field and this cell totally vanishes in presence of magnetic field. The velocity profile is becoming weaker for higher values of Hartmann number. On the same way from the figure 13.14(b) it is seen that temperature profile is quite stronger for lower values of Hartmann number and becoming weaker for increasing of Hartmann number.

The effect of Hartmann number at Ra = 10^6 is shown in figure 13.15. A uniform parabolic curvature shape is formed by flow field in the cavity for higher values of Hartmann number and in the cavity it is parallel to the horizontal wall with no noteworthy change for variation of Hartmann number.

A buoyancy-induced anti-clockwise rotating cell is formed in the cavity near the right bottom corner and gradually weak for higher values of Hartmann number. This rotating cell totally disappears for Ha = 20. On the other hand temperature field is stronger for lower values of Hartmann number and formed curvature shape. But this curvature shape becomes parallel to the bottom wall of the cavity for Ha = 20. It means that temperature field is obstructed by the magnetic field.

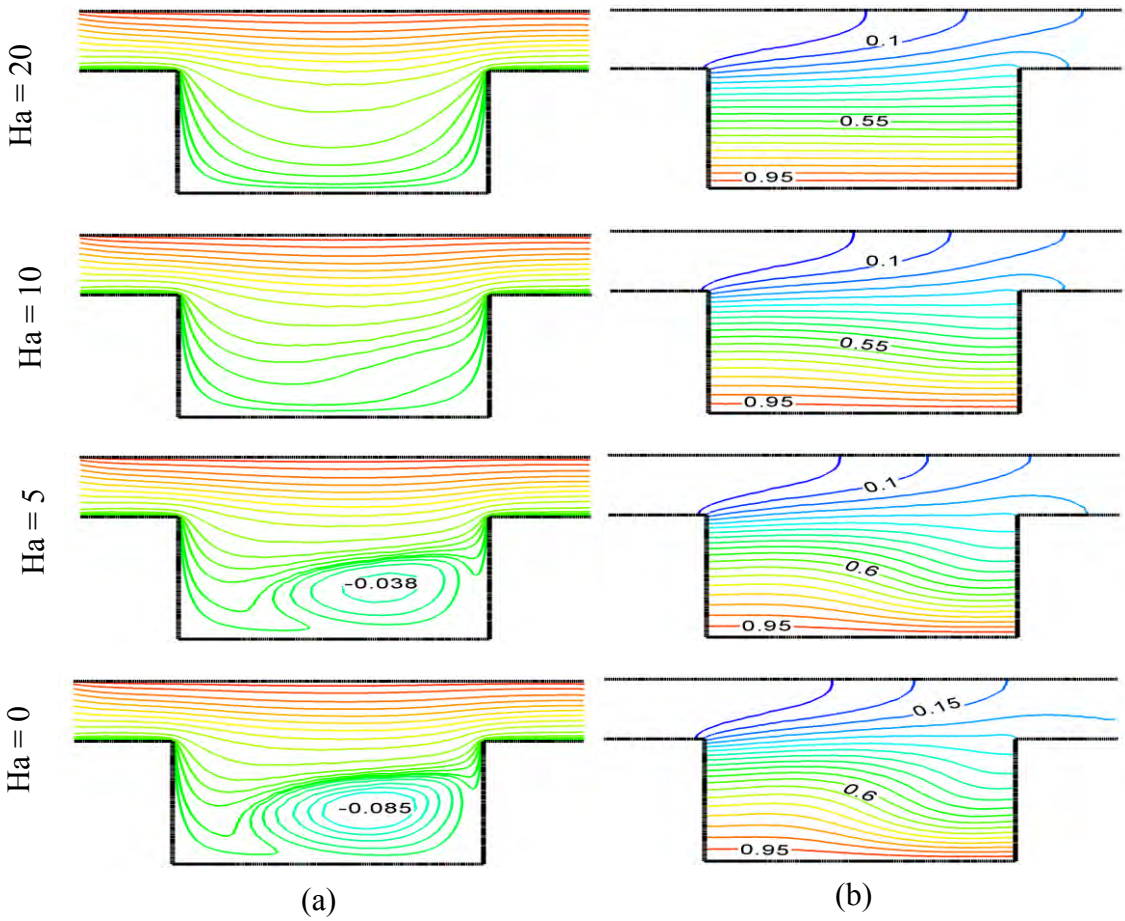

Figure 3.14 Effect of Hartmann number on (a) streamlines and (b) isotherms for AR = 1.5 and Ra = 10^5, while ϕ = 0.04, Re = 100.

It is observed that the strength of flow field in the cavity is increasing for higher values of Rayleigh numbers and it is more noticeable in absence of magnetic field. It is because of convection is dominant in the cavity for higher value of Rayleigh numbers.

On the other hand, flow pattern is almost similar in the channel. Isotherms are similar for Ra = 10^4 and 10^5 but for 10^6 isotherms take twist shape in the cavity as well as in the channel for lower values of Hartmann number.

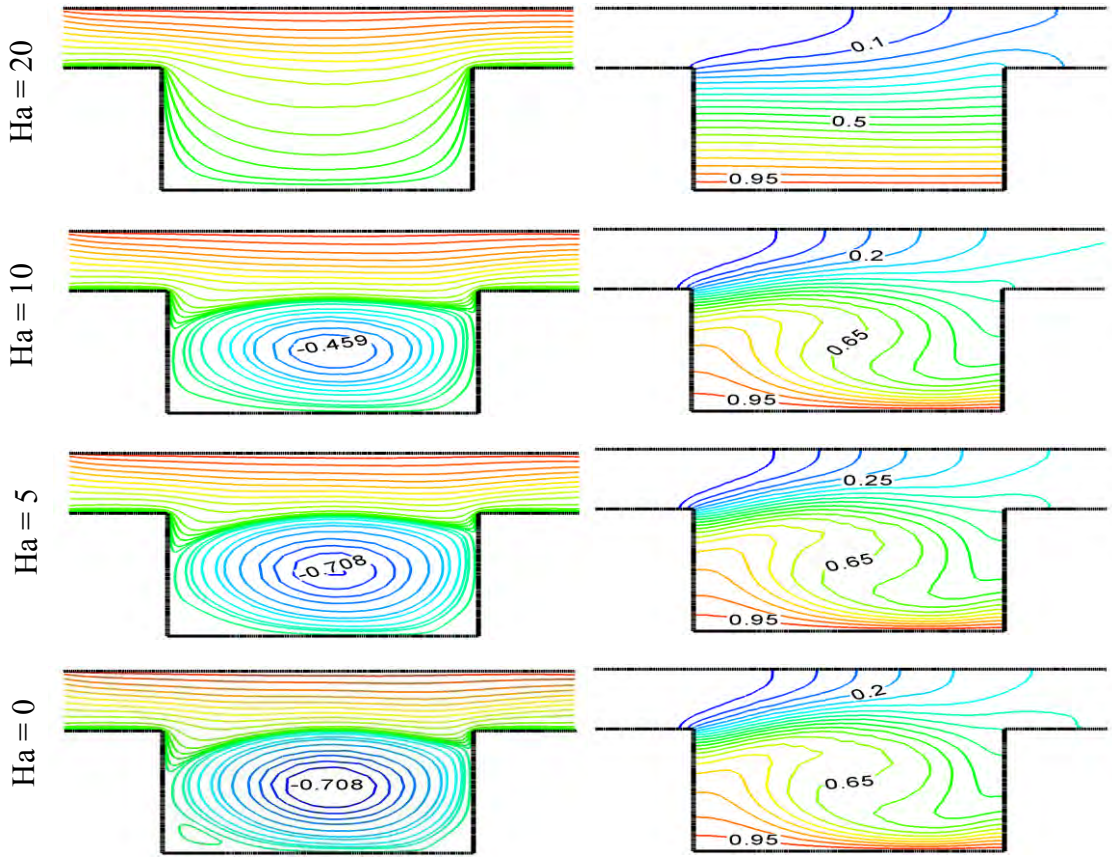

Figure 3.15 Effect of Hartmann number on (a) streamlines and (b) isotherms for AR = 1.5 and Ra = 10^6, while ϕ = 0.04, Re = 100.

Figure 3.16(a) and (b) depict the average Nusselt number (Nu_{av}) and average fluid temperature respectively with the variation of Ha (Ha = 0, 5, 10, 20). In these figures we consider heat transfer rate as well as average fluid temperature as a function of Rayleigh number. From Nu_{av} - Ra and θ_{av} – Ra profiles for Hartmann number Ha it is clearly shown that escalating Ra both heat transfer rate and average fluid temperature decrease with increasing of Hartmann numbers.

Heat transfer rate and average fluid temperature become almost constant for Ra = 10^3 and 10^4 but it drastically increase for higher value of Ra = 10^6 due to higher values of buoyancy force. Heat transfer rate and average fluid temperature decrase with increasing of Hartmann number. It means that the magnetic field can be used to control the heat transfer phenomena.

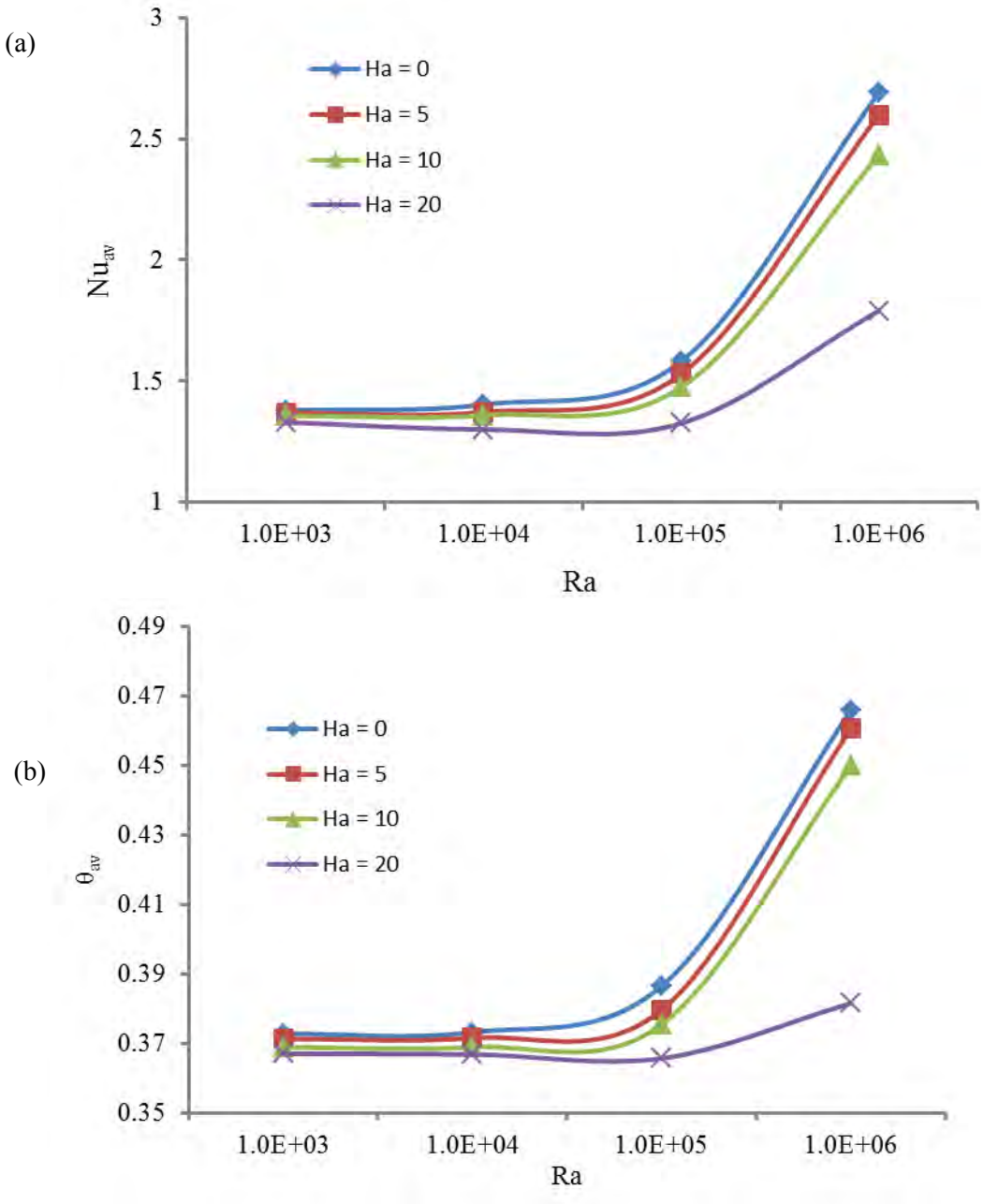

Figure 3.16 Effect of Hartman number on (a) average Nusselt number and (b) average fluid temperature for different values of Ra and AR = 1.5, while Re = 100 and ϕ = 0.04.

3.2.2 Effects of solid volume fraction

The effect of the solid volume fractions is investigated in the range of 0% – 15% while the Re and Ha are kept fixed at 100 and 5, respectively. Figures 3.17-3.19 show the streamlines and isotherms in a channel with cavity for various values of the solid volume fractions (ϕ = 0, 0.05, 0.1 and 0.15) for different Ra (= 10^4, 10^5 and 10^6).

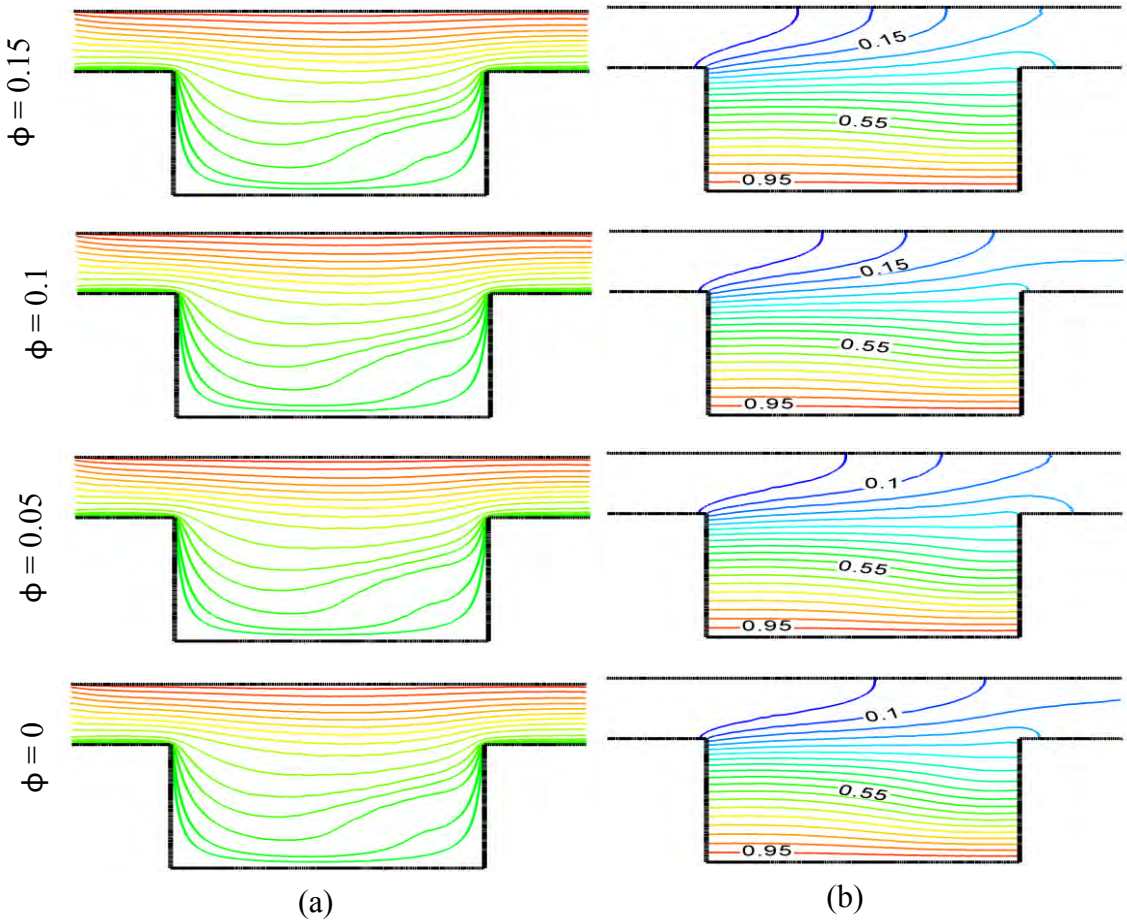

Figure 3.17 Effect of solid volume fraction on (a) streamlines and (b) isotherms for AR = 1.5 and Ra = 10^4, while Ha = 5, Re = 100.

From the figure 3.17(a) it is observed that there is no significant change in the streamlines except the middle part of the channel. The streamlines are very similar to those reported in figure 3.5(a) because the solid volume effect is not functional over the size of domain.

The streamlines have very low velocity in the zone adjacent the bottom heated wall. Figure 3.17(b) shows the influences of solid volume fraction (ϕ) on the temperature profile. The strength of the thermal current activities is mentionable activated with escalating ϕ from 0% (clear water) to 15%. The temperature lines through the horizontal pipe with an open cavity dense near the inlet for increasing ϕ. But initially (ϕ = 0%) these lines try to gather near the heated walls of the cavity corresponding to physical changes of the working fluid. Increasing solid volume fraction enhance thermal conductivity of the nanofluids. Due to rising values of ϕ, the temperature distributions become distorted resulting in an increase in the overall heat transfer. This result can be attributed to the performance of the solid volume fraction.

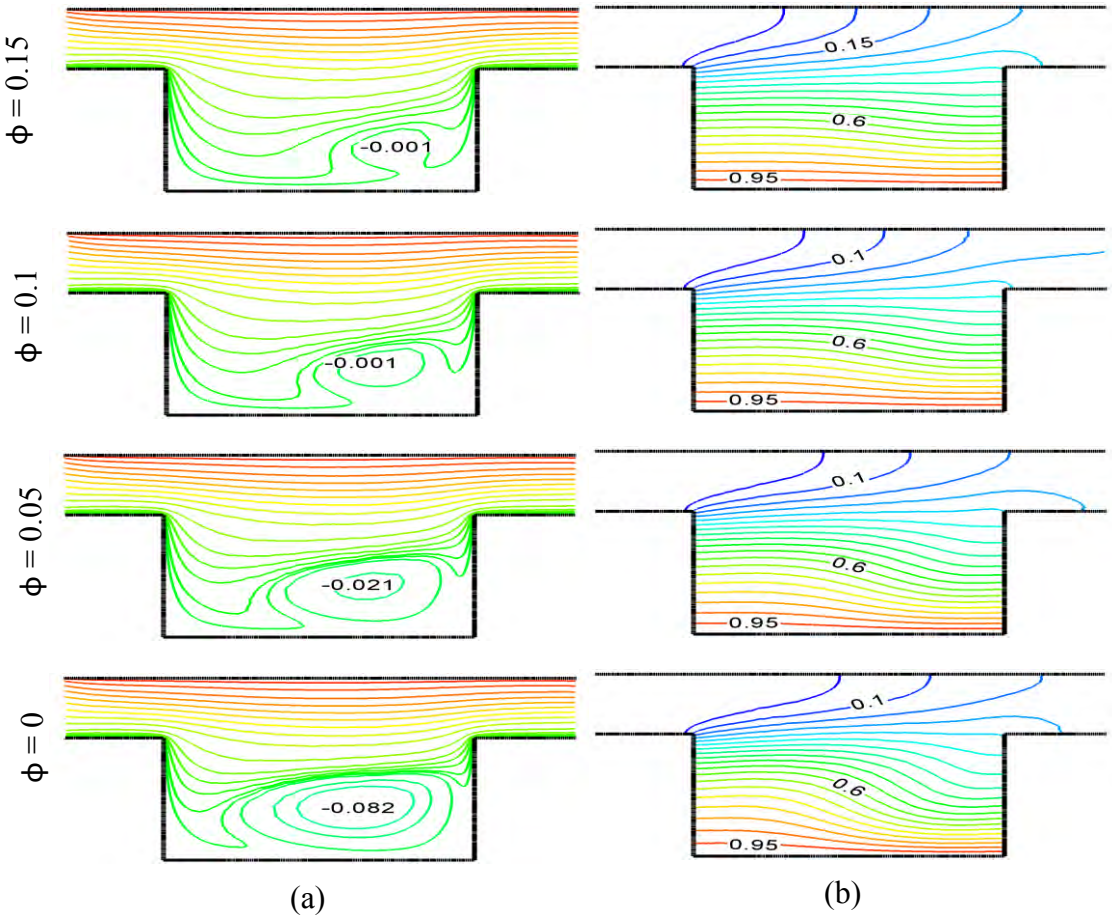

Figure 3.18 Effect of solid volume fraction on (a) streamlines and (b) isotherms for AR = 1.5 and Ra = 10^5, while Ha = 5, Re = 100.

The effects of solid volume fraction on stream lines and isotherms for Ra = 10^5 while Ha = 5 and Re = 100 is presented in figure 3.18 (a) – (b). Flow pattern creates a small vortex at the right bottom corner of the cavity due to the buoyancy force. This vortex gradually weak with increasing of solid volume fraction as shown in figure 3.18(a). It is also observed from the figure that the solid volume concentration affects only the flow inside the cavity whereas in the channel it remains almost similar. On the other hand temperature field shows similar pattern with the figure 3.17(b) for higher values of ϕ. But initially (ϕ = 0%) temperature field is stronger than those of higher values of ϕ and becomes weak gradually

Figure 3.19 (a) and (b) shows the influences of solid volume fraction (ϕ) on the velocity temperature profile while Ra = 10^6, Ha = 5 and Re = 100. As seen from the left column of this figure, an amount of fluid near the right, left vertical wall and heating wall of the cavity are activated so as to create buoyancy-induced anticlockwise rotating cell As the solid volume fraction increases the strength of the rotating cells are reduced. This is due to the fact that ba2se fluid (ϕ = 0%) moves rapidly than solid concentrated copper-water nanofluids. The temperature lines through the horizontal pipe with an open cavity dense near the inlet for increasing ϕ. Initially (ϕ = 0%) these lines try to gather near the heated bottom wall of the cavity corresponding to physical changes of the working fluid. Increasing solid volume fraction causes the enhancement of thermal conductivity of the nanofluids. Due to rising values of ϕ the temperature distributions become distorted resulting in an increase in the overall heat transfer. This result can be attributed to the performance of the solid volume fraction. It is worth noting that as the ϕ increases, the thickness of the thermal boundary layer near the input opening enhances which indicates a steep temperature gradient and, hence, an increase in the overall heat transfer through the channel with an open cavity.

From the figure 3.17 to 3.19 it is seen that fluid flow is stronger in the cavity for higher values of Rayleigh numbers beside this in the channel the flow pattern has no significant change for different values of Rayleigh numbers. But for the lower values of solid volume fraction (ϕ = 0, 0.05) at higher value of Rayleigh number isotherms formed more curvy shaped than the lower values of Rayleigh number. Due to rising values of Ra the temperature distributions and velocity become distorted resulting in an increase in the overall heat transfer and fluid velocity.

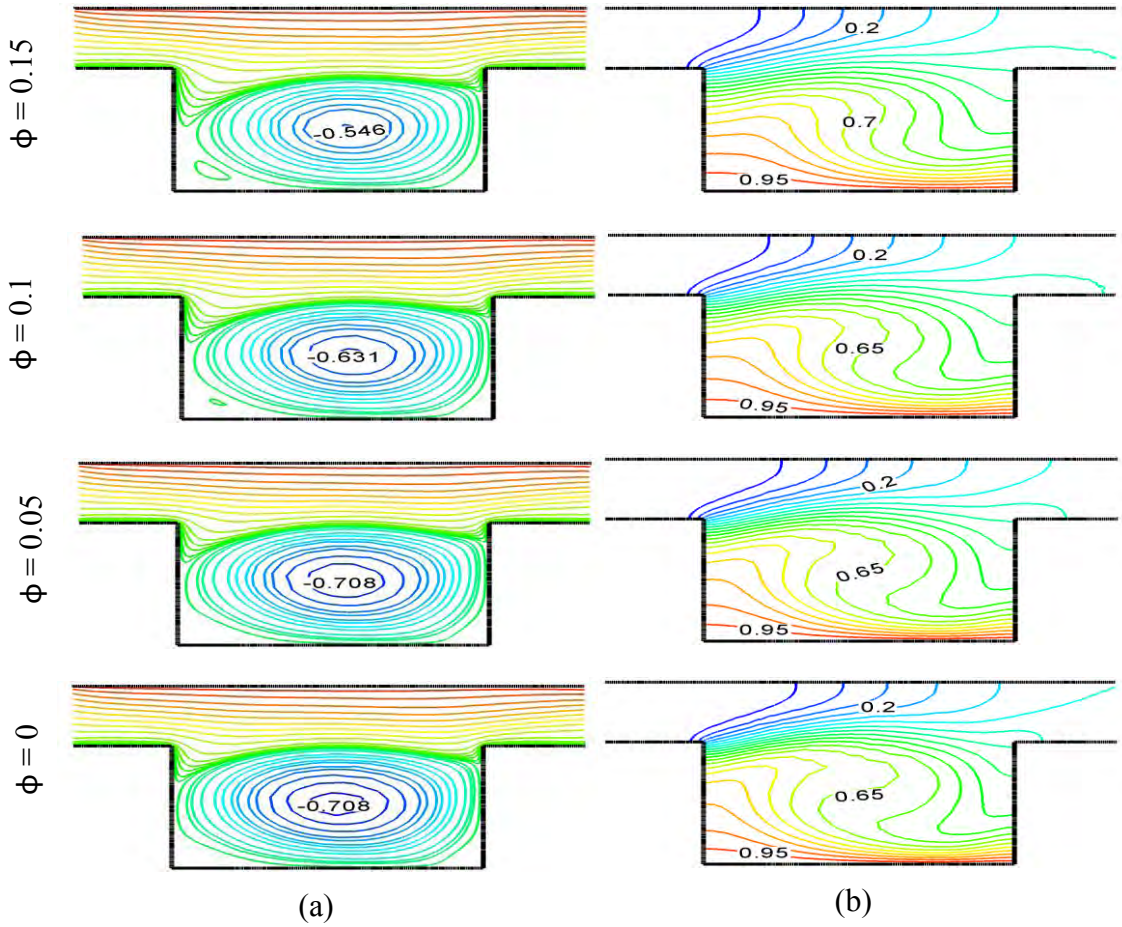

Figure 3.19 Effect of solid volume fraction on (a) streamlines and (b) isotherms for AR = 1.5 and Ra = 10^6, while Ha = 5, Re = 100.

Figure 3.20(a) and (b) depict the average Nusselt number (Nu_{av}) and average fluid temperature respectively with the variation of ϕ (ϕ = 0, 0.05, o.1 and 0.15). In these figure we consider heat transfer rate as well as average fluid temperature as a function of Rayleigh number.

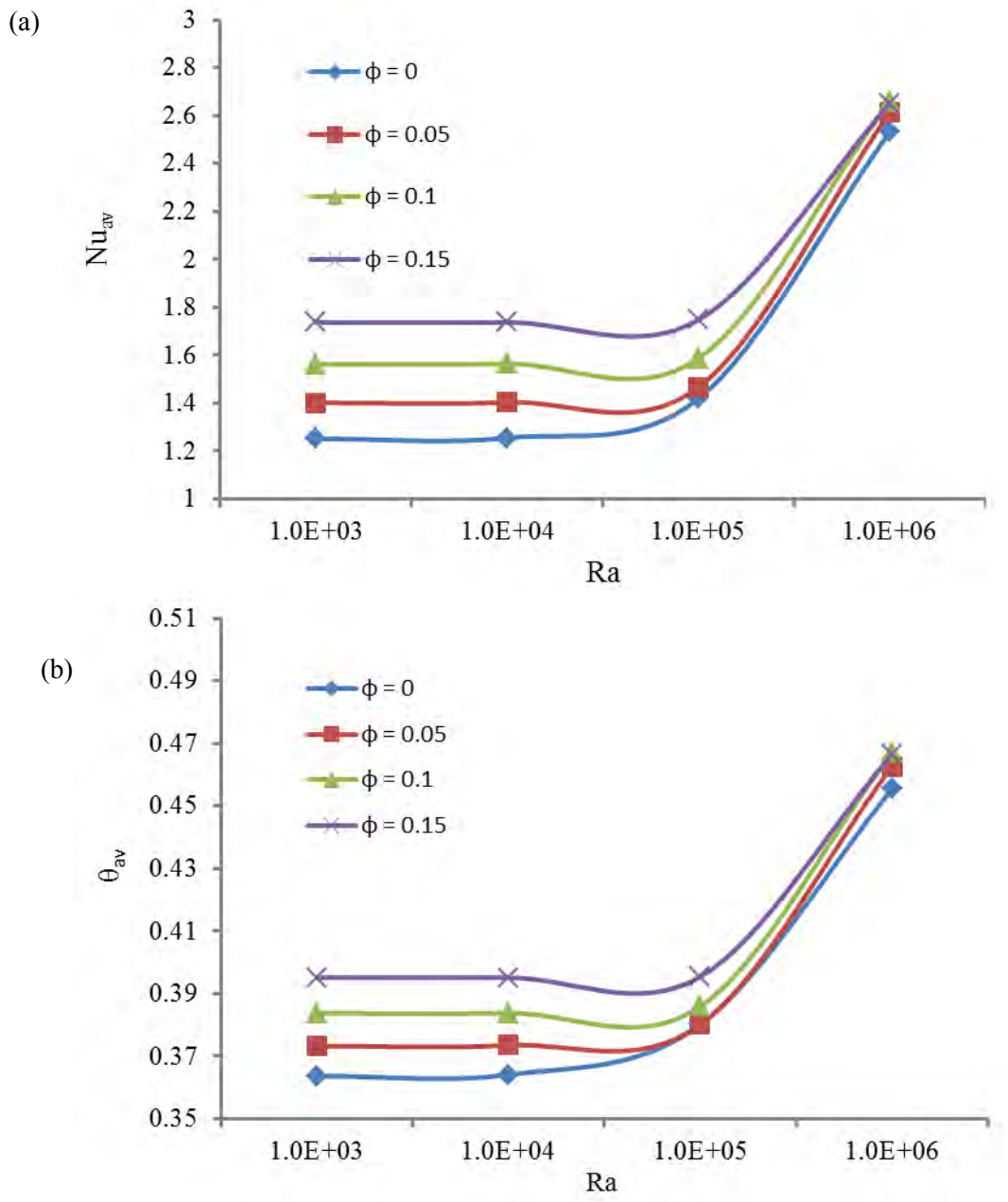

Figure 3.20 Effect of solid volume fraction on (a) average Nusselt number and (b) average fluid temperature for different values of Ra and AR = 1.5, while Re = 100 and Ha = 5.

From Nu_{av} - Ra and θ_{av} – Ra profiles for solid volume Fraction ϕ it is clearly shown that a linear variation of the average Nusselt number and average fluid temperature with the solid volume fraction for Rayleigh number Ra = $10^3$and 10^4but it increases promptly for Rayleigh number 10^6. As clearly be seen that the heat transfer increases with increasing of ϕ. When the solid volume fraction increases from 0% to 15% the heat transfer is increases very commonly.

However, the values of Nu_{av} and θ_{av} are always maximum and almost constant for the highest value of Rayleigh number Ra = 10^6.It is observed that θ_{av} grows up with the variation of ϕ. It is because of thermal conductivity of nanofluidis always higher than base fluid (ϕ = 0%).

3.2.3 Effects of Reynolds Number

The effects of Reynolds number Re on the velocity profile and thermal field in terms of stream lines and isothermal lines are presented in figure 3.21 -3.23 respectively while ϕ = 4%, Ha = 5 and Rayleigh numbers vary from 10^4 to 10^5. The basic flow structure in the absence of natural convection effect is presented in the left bottom corner of figure 3.9 at Re = 100. It is seen clearly that for Ra = 10^4 and low Reynolds number (Re = 100),

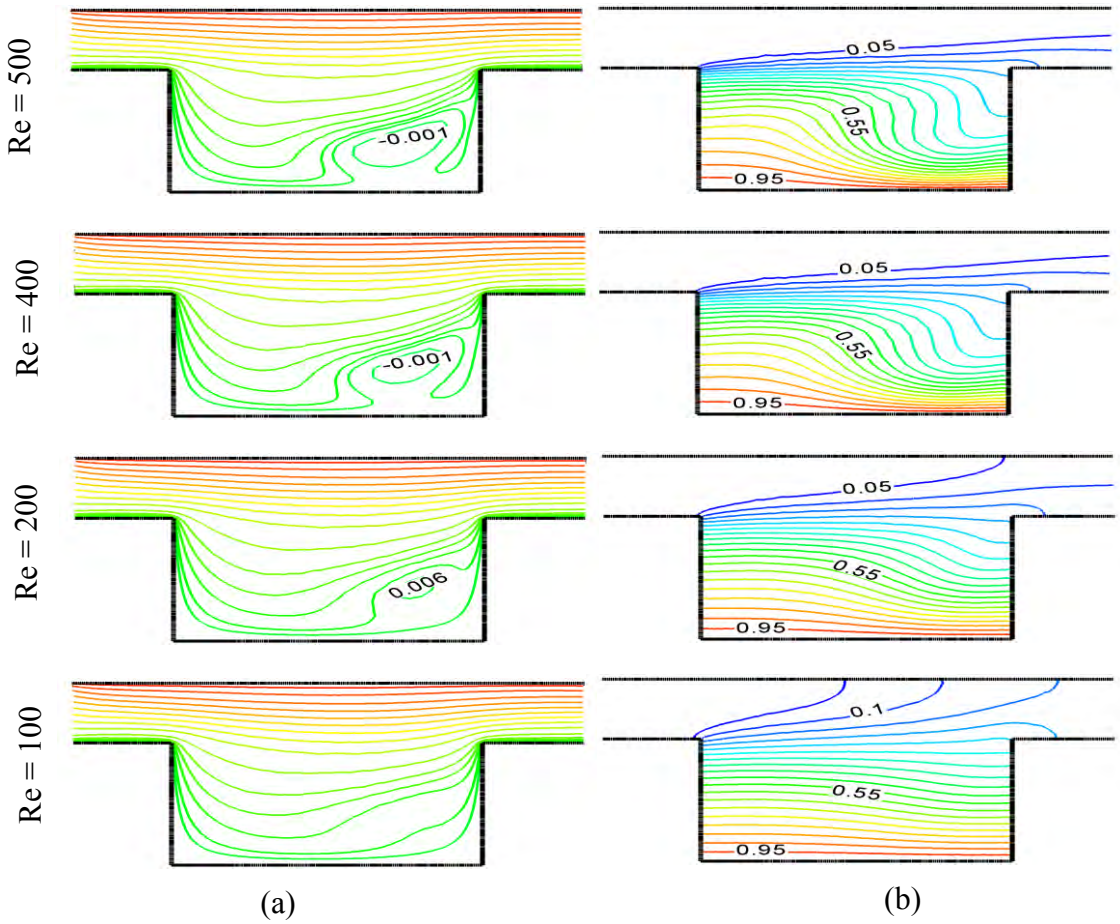

Figure 3.21 Effect of Reynolds number on (a) streamlines and (b) isotherms for AR = 1.5 and Ra = 10^4, while Ha = 5 and ϕ = 0.04.

the forced convection plays a dominant role, and the recirculation flow is mostly generated only by the higher flow.field The fluid flow in a two dimensional horizontal channel with cavity is characterized and a weaker anticlockwise rotating cell close to the right bottom corner.

In the figure 3.21(a), it observe that from the streamlines the rotating cell is formed for higher value of Reynolds number near the right and bottom wall of the cavity gradually disappear for lower values of Reynolds number. As the Reynolds number decreases, as shown in figure 3.21(a) the intensity of the main circulation decreases and fills the entire enclosure. In the velocity vector, initially the flow covers the whole domain of the channel with an open cavity while it goes up from the bottom surface of the cavity and tends to gather to the middle of the channel due to increase inertia force from 100 to 500.

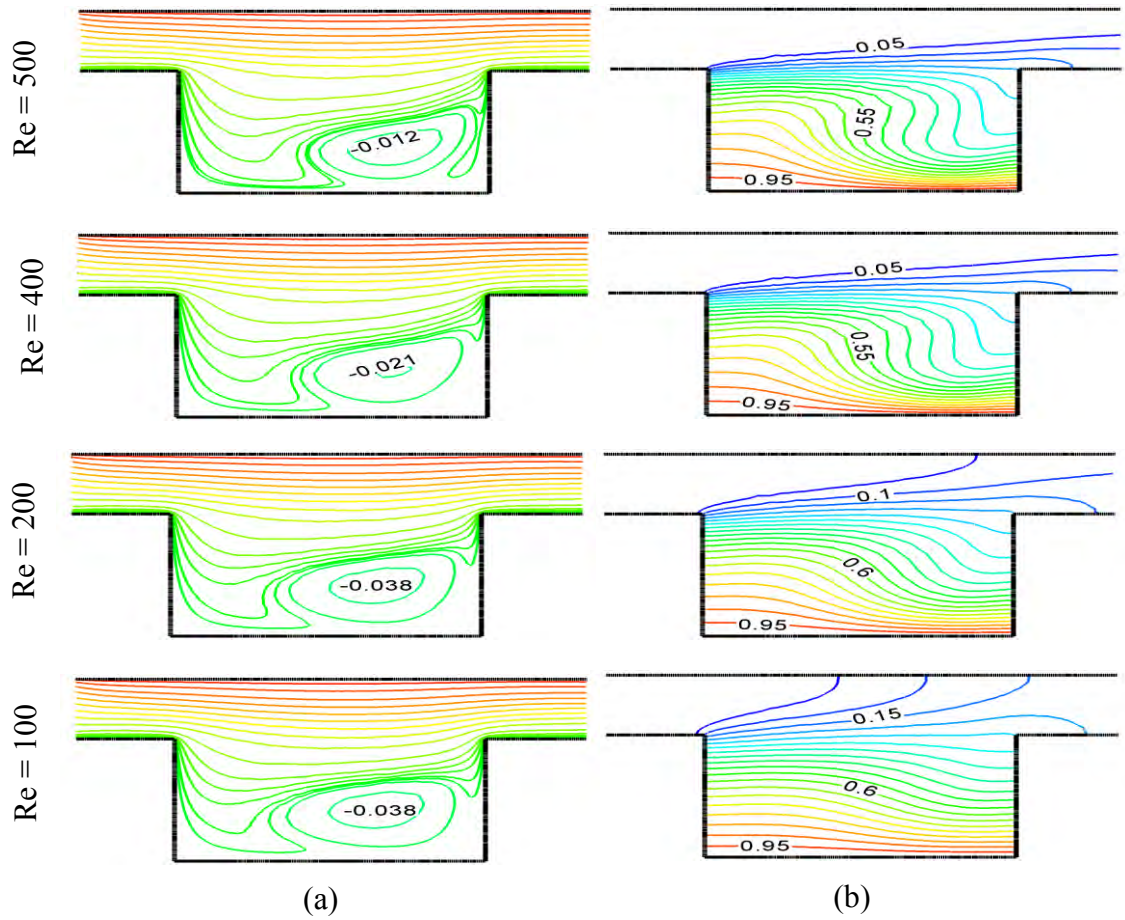

Figure 3.22 Effect of Reynolds number on (a) streamlines and (b) isotherms for AR = 1.5 and Ra = 10^5, while Ha = 5 and ϕ = 0.04.

We also observe that from the figure 3.21(b) as the Reynolds number enhances from 100 to 500, the temperature contours tend to get affected considerably. This figure shows that at low values of Re, the temperature of the nanofluids rapidly reaches to the temperature of heated (by constant temperature) walls due to low viscosity. With increasing Reynolds number, decrement of temperature of Copper- water nonofluids happens slowly which leads to increment of peaks of isothermal lines at the exit port of the channel. Rising Re leads to formation of the thermal boundary layer at the heated surfaces. This means that at higher values of Re, higher heat transfer rate is predicted by the working copper water nanofluids. Isotherms become compressed in a zone close to the hot walls of the open cavity for higher values of Re. Because increasing Re causes more flow of the working nanofluids. Then the average heat transfer enhances by utilizing copper water nanofluids along the channel with an open cavity.

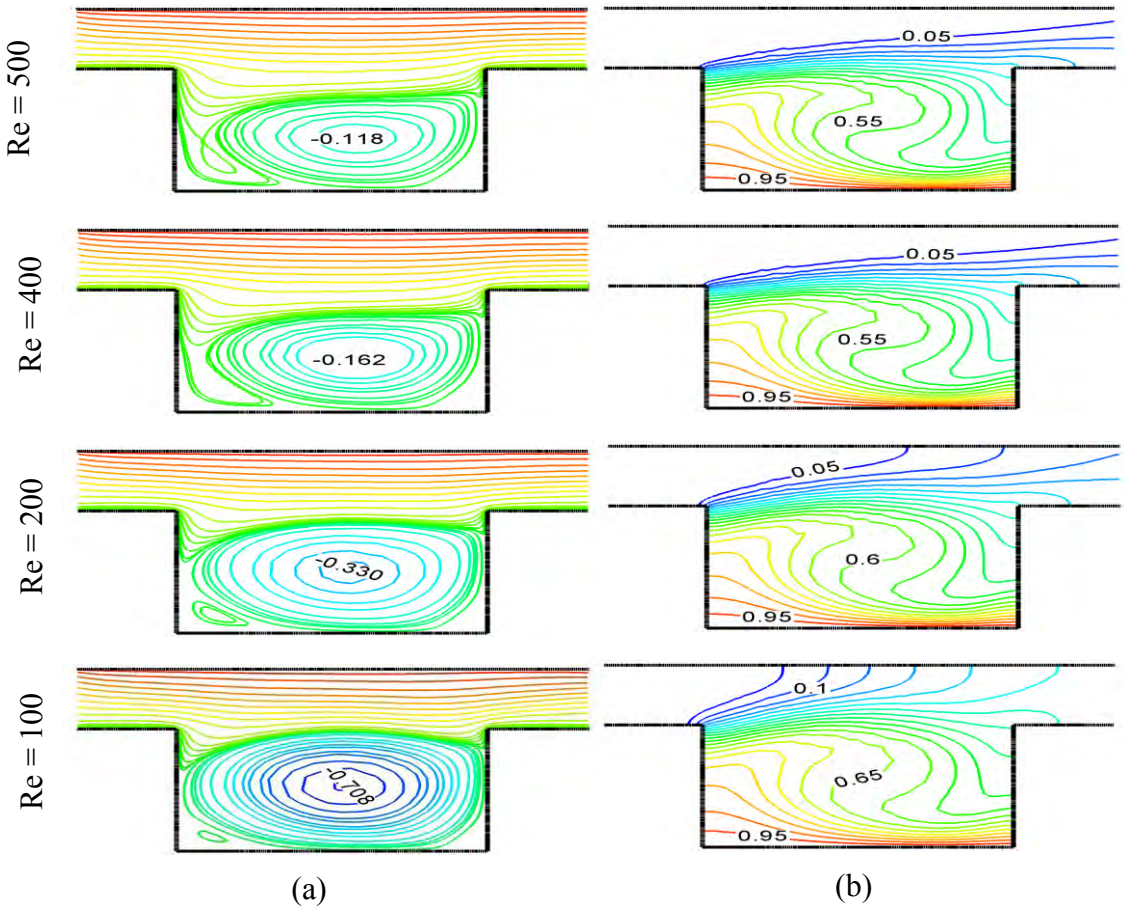

Figure 3.23 Effect of Reynolds number on (a) streamlines and (b) isotherms for AR = 1.5 and Ra = 10^6, while Ha = 5 and ϕ = 0.04.

The effects of Reynolds number on streamlines and isotherms for Ra = 10^5, Ha = 5 and ϕ = 0.04 is described in the figure 3.22. It is observed that the streamlines formed a tiny vortex along right bottom corner of the cavity and it becomes stronger for lower values of Reynolds number but flow field in the channel has no significant change with the figure 3.21. Corresponding temperature field shows that for the grater values of Reynolds number the isothermal lines form a thin thermal boundary layer near the hot bottom wall along the right side of the cavity which are radically changed with decreasing of Reynolds number and at lowest value of Ra = 100 it is totally disappeared due to increasing of temperature difference . There is a little bit of change for the temperature field in the channel due to decreasing of Reynolds numbers. It is because of force convection is dominant.

The figure 3.23 shows the effects of Reynolds number on streamlines and isotherms for Ra = 10^6, Ha = 5 and ϕ = 0.04. Streamlines designed clockwise rotating cells near the middle-right vertical wall. This rotating cells become stronger for lower values of Re and occupies almost total cavity. On the other hand temperature field shows that stronger thermal boundary layer near the hot bottom wall along the right side of the cavity presented in the figure 3.23(b).which are slightly changed with decreasing of Reynolds number. Isothermal lines in the cavity take almost non uniform weave shaped. In the channel isotherm shape is almost linear for higher values of Reynolds number where as for lower values of Reynolds number these lines become wind shape. It means that force convection is dominant on the temperature field.

From the figures 3.21 to 3.23 it is clearly seen that flow field is dominant due to increasing the Rayleigh number. It is because of forced convection gain the strength due to increasing of Reynolds number. Similarly temperature field is dominant in the cavity as well as in the channel for increasing the Rayleigh number.

Figure 3.24(a) and (b) depict the average Nusselt number (Nu_{av}) and average fluid temperature respectively with the variation of Re (Re = 100, 200, 400 and 500). In these figure we consider heat transfer rate as well as average fluid temperature as a function of Rayleigh number.

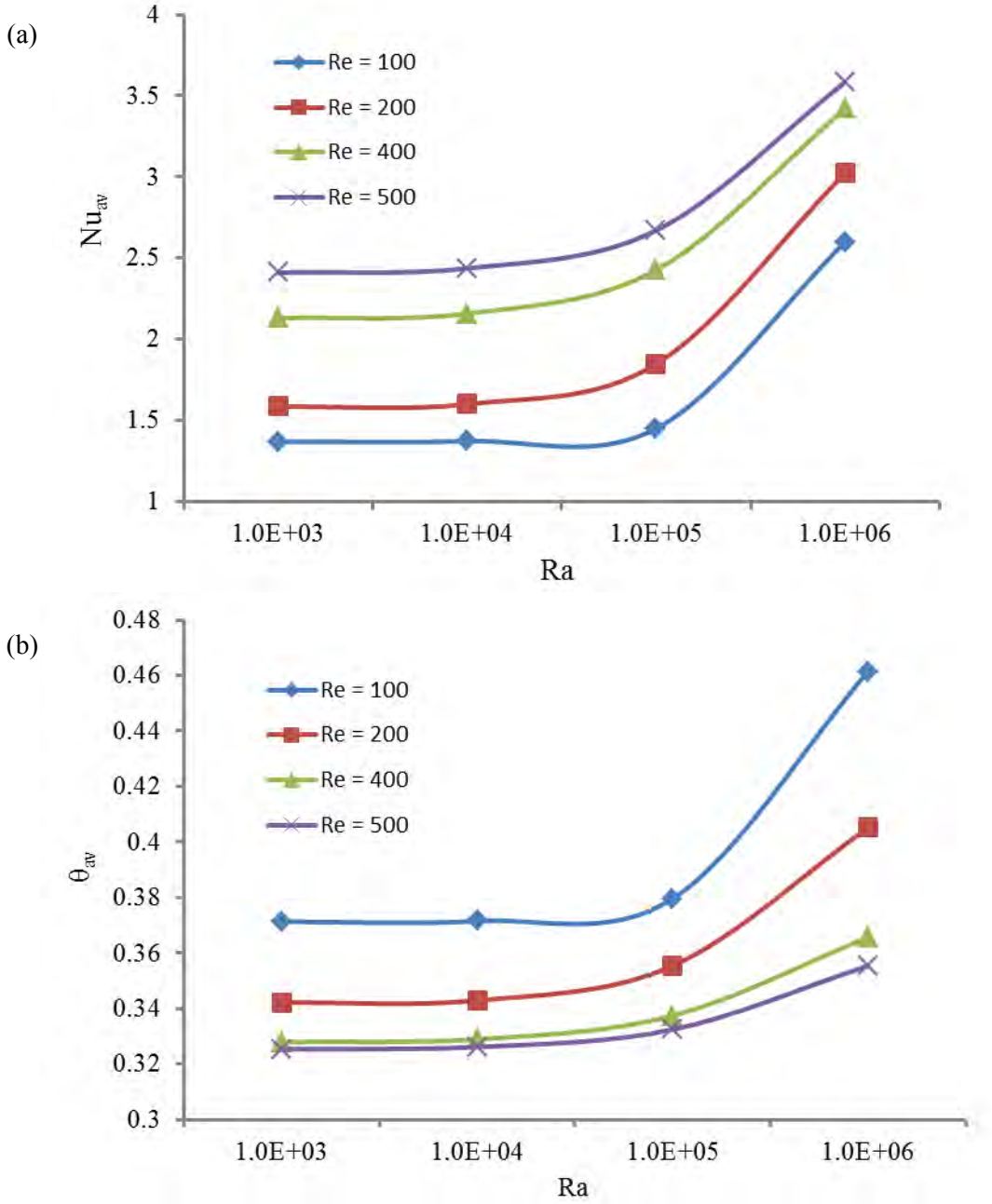

Figure 3.24 Effect of Reynolds number on (a) average Nusselt number and (b) average fluid temperature for different values of Ra and AR = 1.5, while $\phi = 0.04$ and Ha = 5.

From Nu_{av} - Ra profiles for Reynolds number Re it is clearly shown that average Nusselt number increases for higher values of Reynolds number. Also, the average Nusselt number at the heated surface is found to increase as Re increases at fixed Ra. These results are probable because nanoparticles increases heat absorbing capacity of the base fluid.

Therefore, it can be concluded that more heat transfer from the heat source is expected in the case of large parameter value of Re or Ra. Nevertheless, the values of Nu_{av} are always maximum for the higher value of Re (= 500).The effect of Reynolds number Re on average fluid temperature θ_{av} in the cavity is revealed in the figure 3.24(b). From θ_{av} -Ra it can clearly be seen that the value of θ_{av} decreases regularly with the raise of Re for all considered Rayleigh numbers. Because rising inertia force causes the reduction of fluid temperature.

3.3 CASE 3(AR = 1)

3.3.1 Effect of Hartmann number

The influence of Hartman number on the streamlines and isotherms for different values of Ha (= 0, 5, 10, and 20) at Ra (= 10^4.10^5, and 10^6) while the values of ϕ and Re kept fixed at 0.04 and 100 respectively are shown in figures 3.25, 3.26 and 3.27.

The effects of Hartmann number Ha on the thermal and flow fields in terms of streamlines and isothermal for Ra = $10^4$are presented in figures 3.25 (a) and 3.25(b). We observe that as the Hartmann number enhances from 0 to 20, the velocity contours and temperature tend to get affected considerably. Figure 3.25 (a) expresses the velocity (modulus of the velocity vector) field. In the velocity vector, initially the flow covers the whole domain of the channel with an open cavity while it goes up from the bottom surface of the cavity and tends to spread from the middle of the channel due to increase magnetic force from 0 to 20. There is no significant change in streamlines except in the middle of the channel and bottom of the open cavity. Figure 3.25(b) expresses the corresponding temperature profile. This figure shows that there is no significant change is observed to change the Hartmann number. This fact due to magnetic force does not have considerable affect when buoyancy force is low at the convection mode. It is important to note that absence of magnetic field in the figure exactly equal to the presence of magnetic field for lower value of Rayleigh number.

The effect of Hartmann number at Ra = 10^5 is presented in the figure 3.26. A buoyancy-induced clockwise rotating cell is formed by streamlines for lower values of Hartmann number and this cell is gradually became weak and vanishes for higher values of Hartmann number covering the whole domain. Increasing Ha increases the suppression force, which opposes the convection currents and this enables the weakened vortex to penetrate through the cavity grooves. A threshold value of Ha = 5 can be characterized at which the penetration effect starts

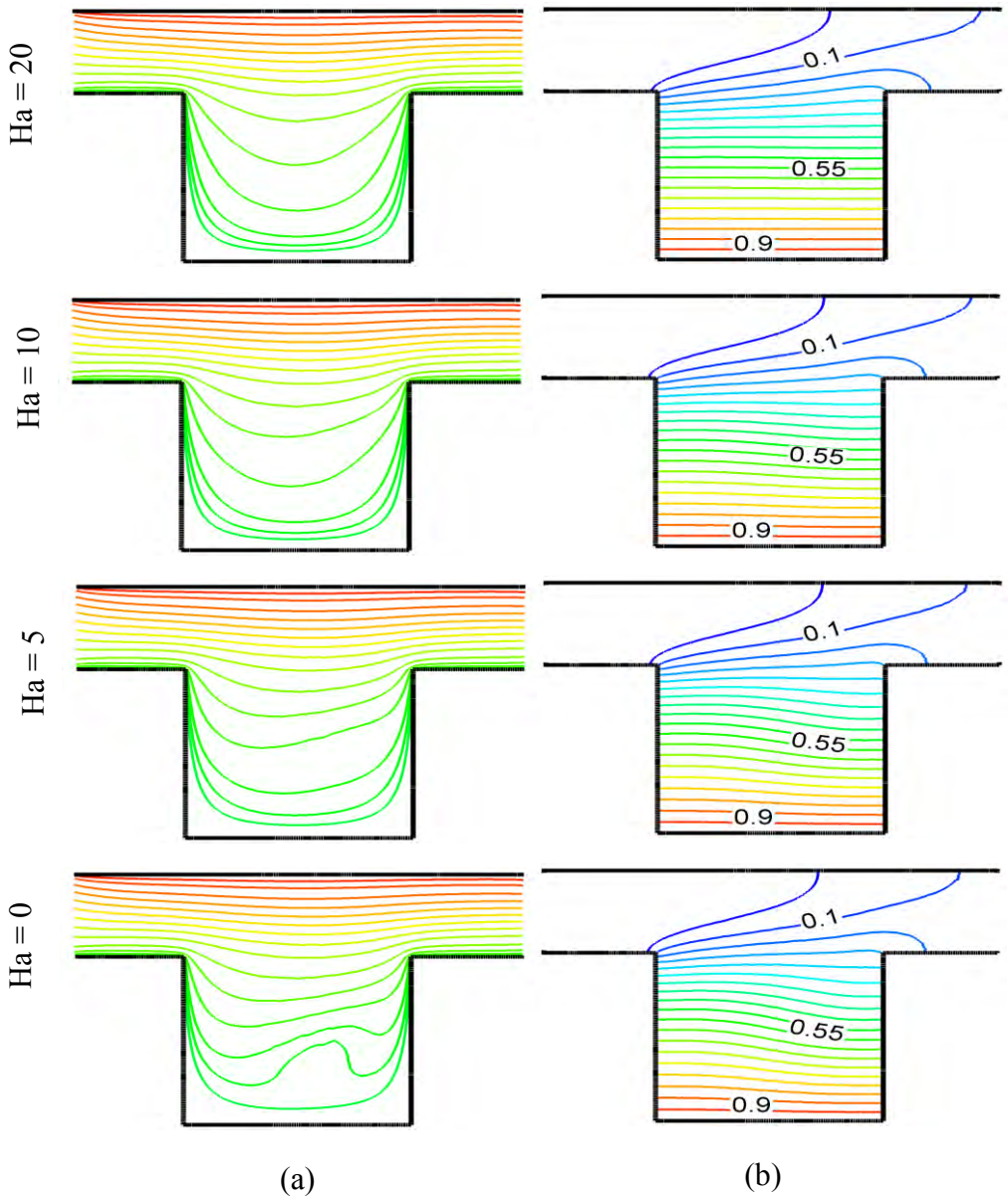

Figure 3.25 Effect of Hartmann number on (a) streamlines and (b) isotherms for AR = 1 and Ra = 10^4, while ϕ = 0.04, Re = 100.

Before this threshold value, the isotherms manifest a disturbed pattern, which is an indication of the convection dominance. Undisturbed isotherms with whole domain behavior is noticed up to Ha = 20. Beyond this value, a small perturbation takes place on the isotherms and crowded isotherms parallel to the channel are seen. However, evenly disturbed isotherms within the whole grooves are still present with all Ha values.

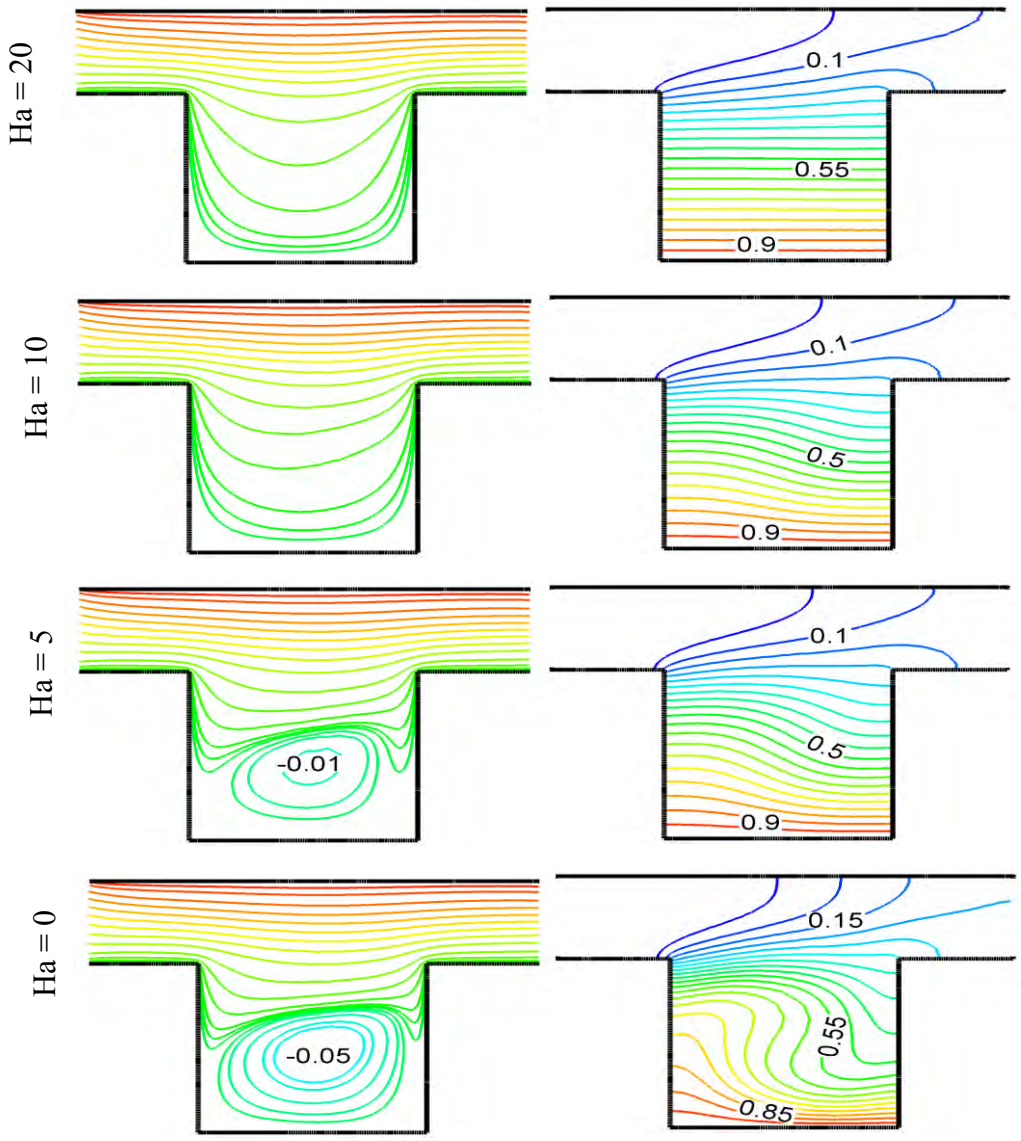

Figure 3.26 Effect of Hartmann number on (a) streamlines and (b) isotherms for AR = 1 and Ra = 10^5, while ϕ = 0.04, Re = 100.

In the figure 3.27 Ra is considered 10^6. The velocity (modulus of the velocity vector) field expresses a continuous reduction in vortex strength with increasing Ha. When Ha = 0, the vortex rotates strongly under the effect of natural convection.

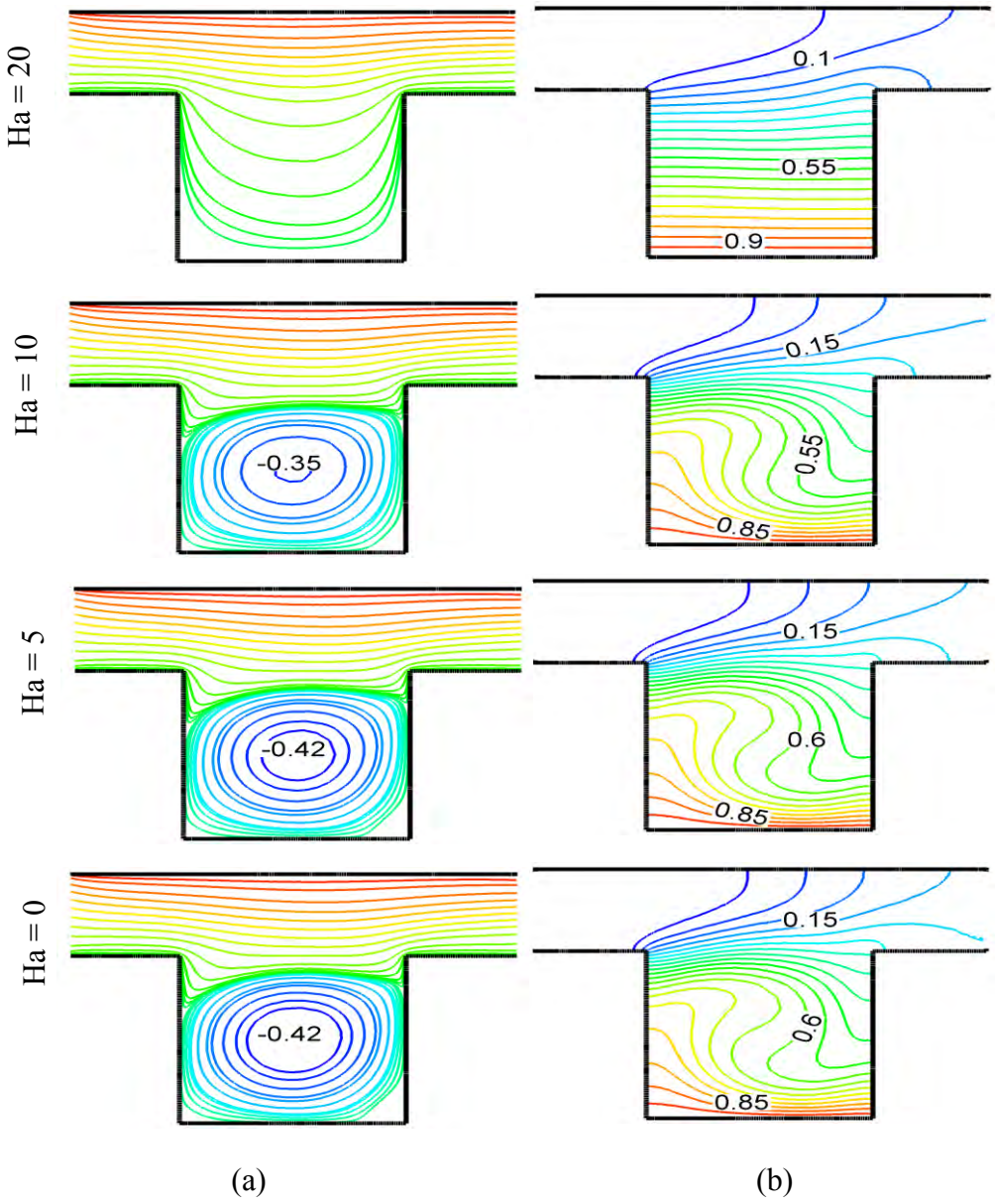

Figure 3.27 Effect of Hartmann number on (a) streamlines and (b) isotherms for AR = 1 and Ra = 10^6, while ϕ = 0.04, Re = 100.

This limit is within the main cavity. Increasing Ha increases the suppression force, which opposes the convection currents and this enables the weakened vortex to penetrate symmetrically through the cavity grooves. For higher values of Ha (Ha = 20) this vortex is vanished and fluid velocity cover the whole domain. On the other hand, the thermal layer becomes thicker with decreasing of Hartmann number. In addition, it is observed that the higher values isotherms are more tightened at the vicinity of the heated wall of the cavity. As Hartmann number increases, isothermal lines inside the cavity approaches more and more towards the conduction-like distribution pattern of isothermal lines appears due to the high convective current inside the cavity. For large Hartmann number Ha = 20 the convection is almost suppressed, and the isotherms are almost parallel to the horizontal wall, indicating that a quasi-conduction regime is reached. However, this parallel distribution is distorted for lower values of Hartmann number. The distortion of isothermal lines appears due to the high convective current inside the cavity.

Contour maps of streamlines and isotherms for different Ra values for different Ha = 0 - 20 at ϕ = 0.04, Re = 100 and AR = 1 are presented in figures 3.25-3.27. The streamlines manifests a single vortex behavior for lower values of Hartmann number. Due to the imposed thermal boundary conditions, the vortex rotates clockwise with its core localized within the main cavity. Increasing Ra from 10^4 to 10^6 leads to strengthening the vortex rotation. Undisturbed isotherms with domain shaped behavior is noticed up to Ra = 10^5.Beyond this value, a small perturbation takes place on the isotherms and crowded isotherms close to the heated wall are seen. However, evenly disturbed isotherms within the cavity grooves are present with Ra = 10^6 values.

Figure 3.28(a) and (b) depict the average Nusselt number (Nu_{av}) and average fluid temperature respectively with the variation of Ha (Ha = 0, 5, 10, 20). In these figure we consider heat transfer rate as well as average fluid temperature as a function of Rayleigh number.

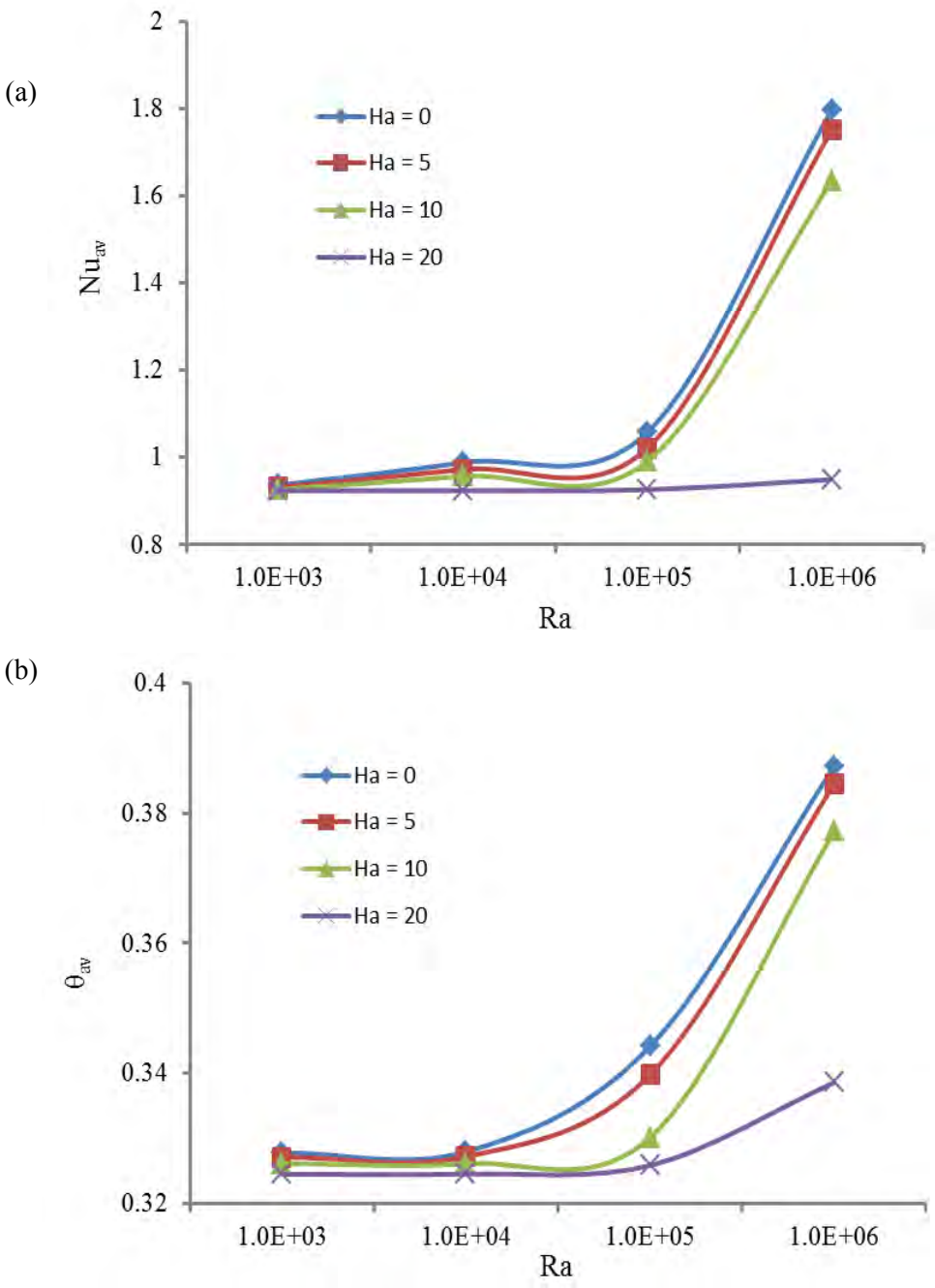

Figure 3.28 Effect of Hartman number on (a) average Nusselt number and (b) average fluid temperature for different values of Ra and AR = 1, while Re = 100 and $\phi = 0.04$.

From Nu_{av} - Ra and θ_{av} – Ra profiles are shown for Hartmann number Ha by escalating Ra. Both heat transfer rate and average fluid temperature are decreased with increasing of Hartmann numbers.

Heat transfer rate and average fluid temperature become almost constant for Ra = 10^3 and 10^4 with the variation of Hartmann number but it drastically increase for higher value of Ra = 10^6 for of all those values of Ha.

Due to decreasing of flow velocity with increasing of strength of magnetic field whereas Heat transfer rate and average temperature quantities increase with increasing of Rayleigh number for all values of Hartmann number. It means that the magnetic field can be used to control the heat transfer phenomena. Maximum heat transfer rate and average fluid temperature is occurred for higher values of Ra (Ra = 10^6)

3.3.2 Effects of solid volume fraction

Here, the effect of the solid volume fractions is investigated in the range of 0% – 15% whiles the Re and Ha are kept fixed at 100 and 5, respectively. Figure 3.29-3.31 shows the streamlines and isotherms in a channel with cavity for various values of the solid volume fractions (ϕ = 0, 0.05, 0.1, and 0.15) for different Ra (= 10^4, 10^5 and 10^6).

From the figure 3.29(a) it is observed that there is no significant change in the streamlines except the middle part of the channel. The streamlines are very similar to those reported in figure 3.25(a) because the solid volume effect is not functional over the size of domain as well as lower bouncy force. The streamlines have very low velocity values in the zone adjacent the bottom heated wall. Figure 3.29(b) shows the influences of solid volume fraction (ϕ) on the temperature profile. The strength of the thermal current activities is not mentionable activated with escalating ϕ from 0% (clear water) to 15%. The temperature lines through the horizontal pipe with an open cavity dense near the inlet for increasing ϕ. But initially (ϕ = 0%) these lines try to gather near the heated walls of the cavity corresponding to physical changes of the working fluid. It is worth noting that as the ϕ increases, the thickness of the thermal boundary layer near the input opening enhances which indicates a steep temperature gradient and hence, an increase in the overall heat transfer through the channel with an open cavity.

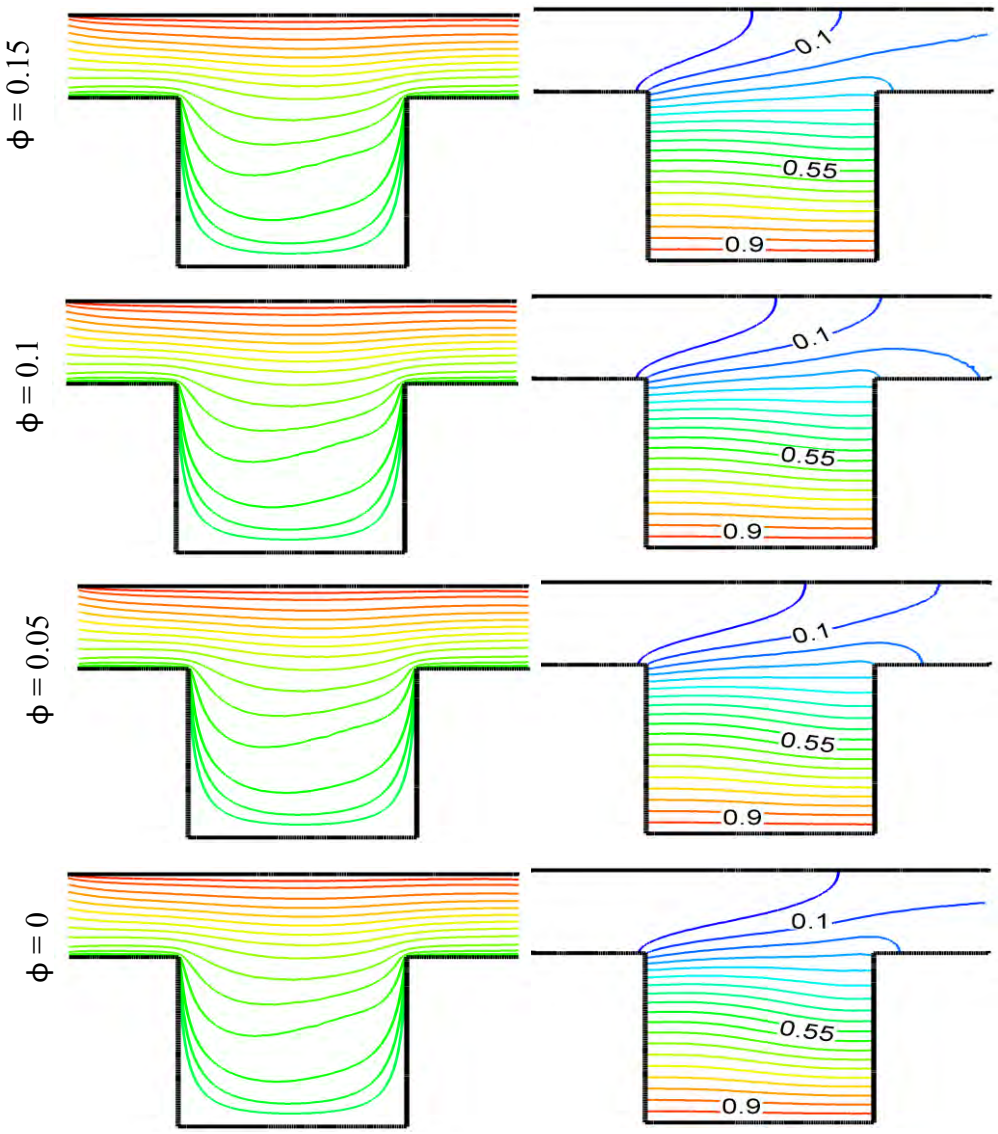

Figure 3.29 Effect of solid volume fraction on (a) streamlines and (b) isotherms for AR = 1 and Ra = 10^4, while Ha = 5, Re = 100.

The outcome of solid volume fraction on the flow field and temperature fields has been revealed in figure 3.30 at Ra = 10^5, Ha = 5, Re = 100 and AR = 1. It can easily be seen that the circulating cell is formed in the clockwise direction and ψ_{min} = -0.03for base fluid (ϕ = 0%). This clockwise rotating cell occupies almost whole of the part of the cavity. It is noticed that flow strength of core of the rotating cell decreasing with the escalating values of solid volume concentration water-Cu.

And, also this cell disappears for higher value of ϕ (ϕ = 15%). This is due to the fact that base fluid (water) moves rapidly than solid concentrated water-Cu nanofluids. Isotherms are parallel to the heated wall for higher values of ϕ due to low flow velocity. However, Wavy temperature distribution is formed for lower value of ϕ.

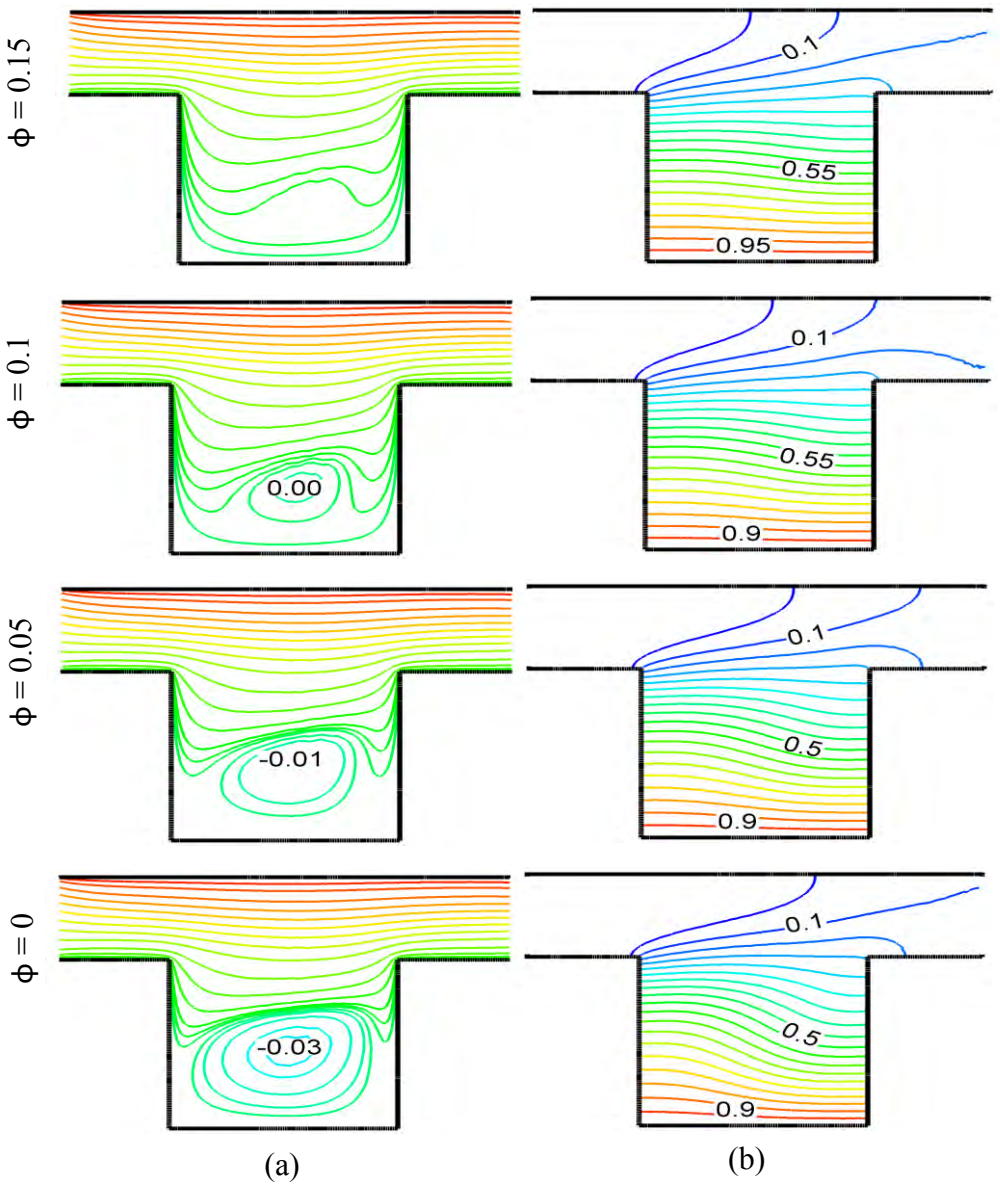

Figure 3.30 Effect of solid volume fraction on (a) streamlines and (b) isotherms for AR = 1 and Ra = 10^5, while Ha = 5, Re = 100.

Figure 3.31 (a) and (b) shows the influences of solid volume fraction (ϕ) on the velocity temperature profile while Ra = 10^6, Ha = 5 and Re = 100. As seen from the left column of this figure, it is noted, for all considered ϕ, the presence of a large clockwise recirculation cell which fills the almost entire cavity. This eddy becomes weaker by increasing solid volume fraction due to intensification of the inertia effects.

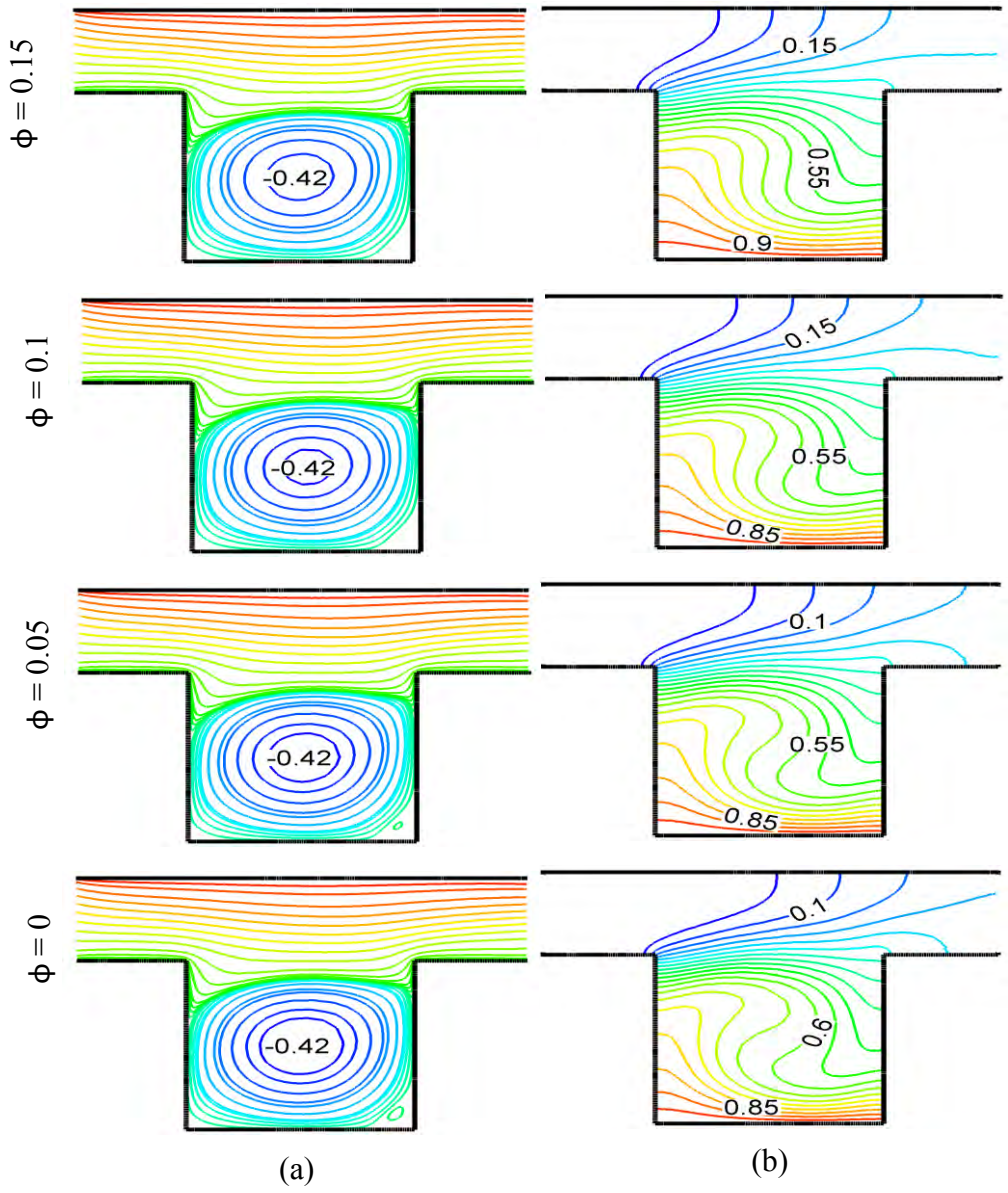

Figure 3.31 Effect of solid volume fraction on (a) streamlines and (b) isotherms for AR = 1 and Ra = 10^6, while Ha = 5, Re = 100.

The isotherms show the formation of thermal boundary layer at the heated wall (thermal stratification), where the temperature gradually varied from the heated wall to the cold part indicating the domination of heat transfer conduction mechanism. By increasing solid volume fraction, the isotherms become stronger showing the increase of temperature gradients, the low temperature areas become thicker and the isotherms become distorted indicating the intensification of convective heat transfer.

From the figure 3.29 to 3.31 it is seen that fluid flow is stronger in the cavity for higher values of Rayleigh numbers in the same vale of ϕ beside this in the channel the flow pattern has no significant change for different values of Rayleigh numbers. But for the lower values of solid volume fraction (ϕ = 0, 0.05) at higher value of Rayleigh number isotherms formed more curvy shaped than the lower values of Rayleigh number. Due to rising values of Ra the temperature distributions and velocity become distorted resulting in an increase in the overall heat transfer and fluid velocity.

Figure 3.32(a) and (b) depict the average Nusselt number (Nu_{av}) and average fluid temperature respectively with the variation of ϕ (ϕ = 0, 0.05, o.1 and 0.15). In these figure we consider heat transfer rate as well as average fluid temperature as a function of Rayleigh number. From Nu_{av} - Ra and θ_{av} – Ra profiles for solid volume fraction ϕ it is clearly shown that similar variation between the average Nusselt number and average fluid temperature with the solid volume fraction for all Rayleigh number. There is no effect is observed for lower values of Ra (Ra = 10^3 and 10^4). But both of these value increases promptly for Rayleigh number 10^6. As clearly be seen that the heat transfer and average temperature increases with increasing of ϕ because thermal conductivity of nanofluids is always higher than base fluid (ϕ = 0%). However, the values of Nu_{av} and θ_{av} are always maximum for the highest value of Rayleigh number Ra = 10^6.

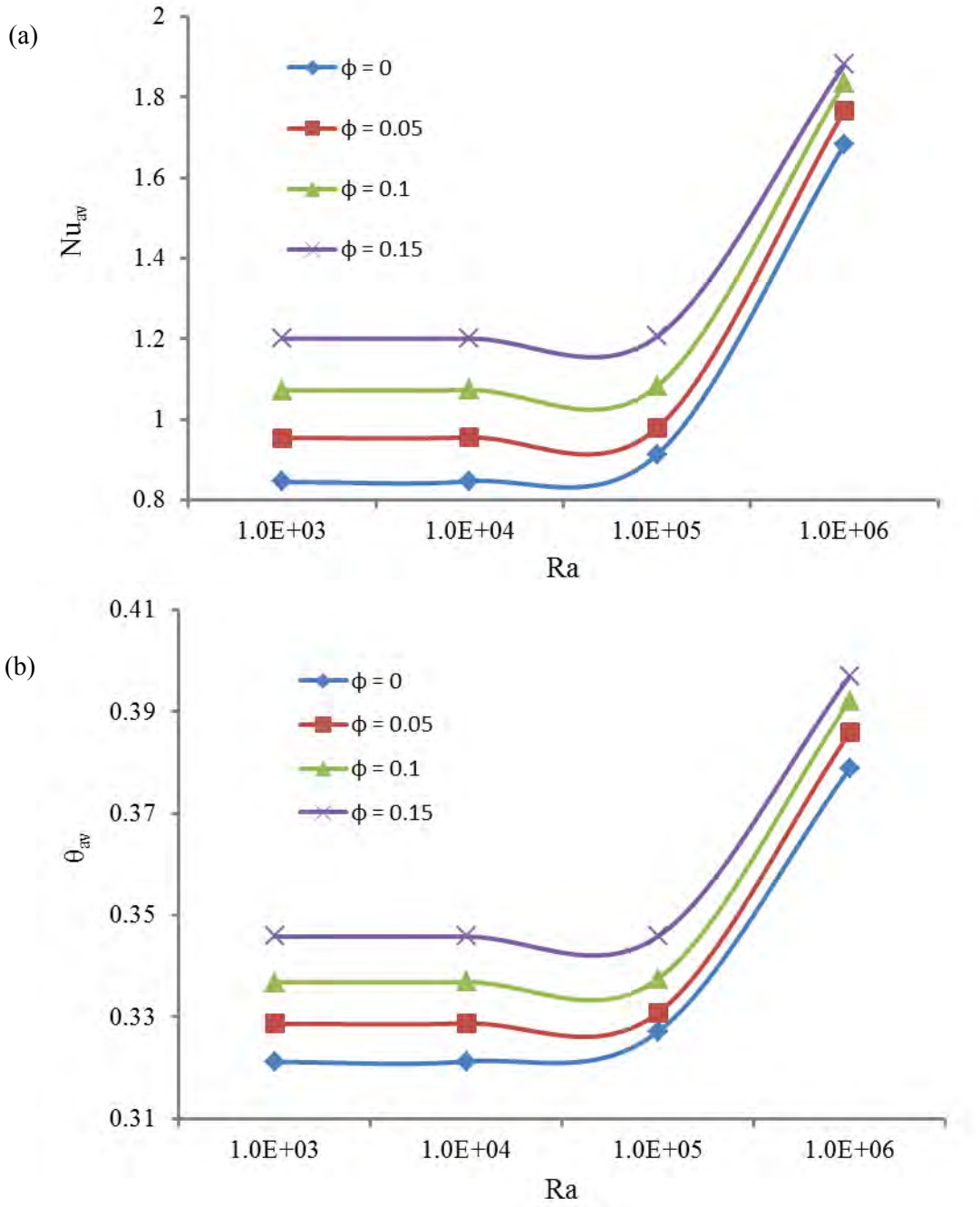

Figure 3.32 Effect of solid volume fraction on (a) average Nusselt number and (b) average fluid temperature for different values of Ra and AR = 1, while Re = 100 and Ha = 5.

3.3.3 Effects of Reynolds Number

To analyze Reynolds number of the flow behavior the streamlines and the isotherms for three values of Rayleigh number: Ra = 10^4, Ra = 10^5 and Ra = 10^6 are illustrated in figures 3.33, 3.34 and 3.35 respectively while ϕ = 4% and Ha = 5 in the form of streamlines and isotherms. As the Reynolds number decreases, as shown in figure 3.33(a), the intensity of the main circulation decreases and fills the entire enclosure.

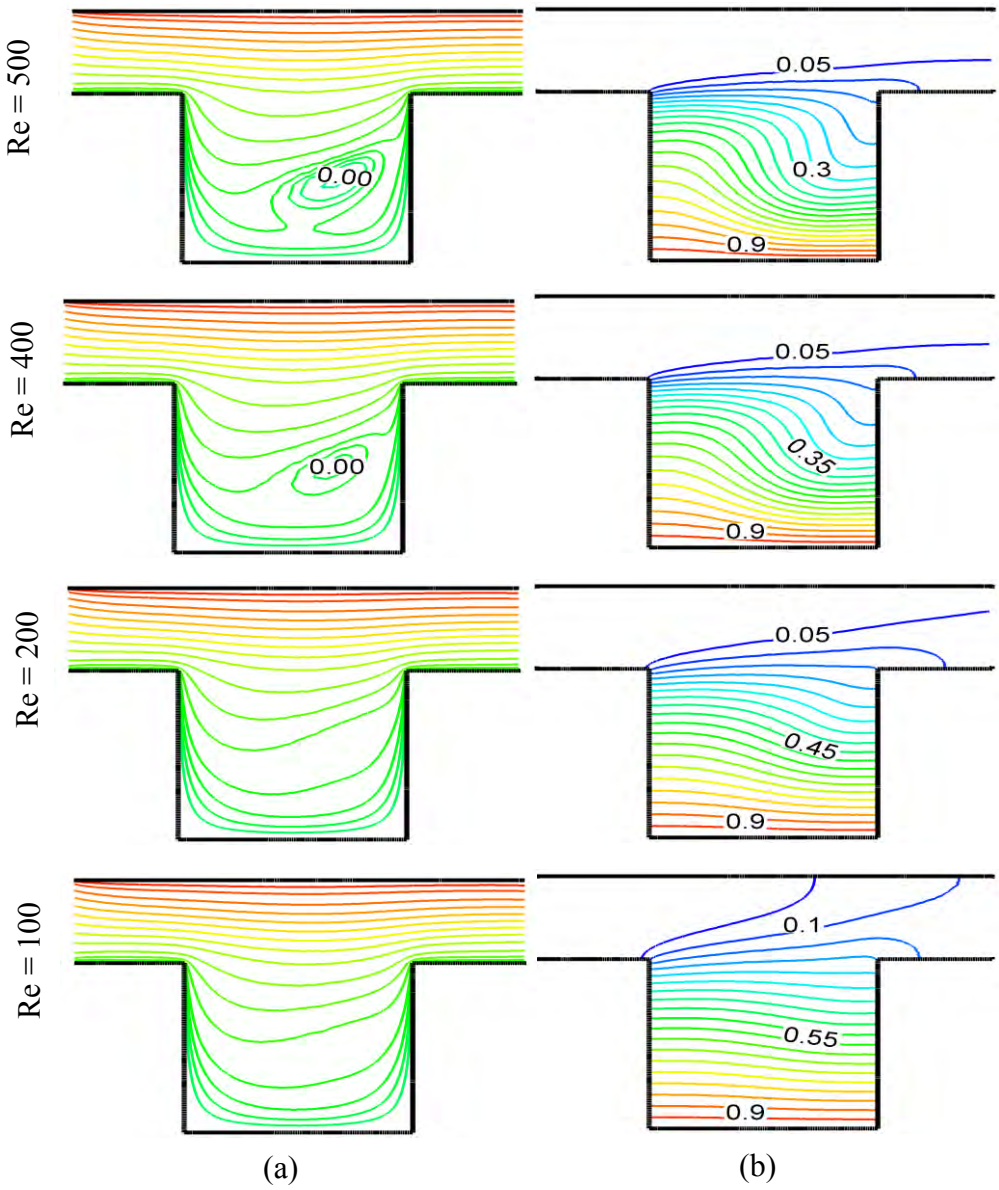

Figure 3.33 Effect of Reynolds number on (a) streamlines and (b) isotherms for AR = 1 and Ra = 10^4, while Ha = 5 and ϕ = 0.04.

In the velocity vector, initially the flow covers the whole domain of the channel with an open cavity while it goes up from the bottom surface of the cavity and tends to gather to the middle of the channel with an anticlockwise circulation cell due to increase inertia force from 100 to 500. Also we observe that from figure 3.33(b) as the Reynolds number enhances from 100 to 500, the temperature contours tend to get affected considerably.

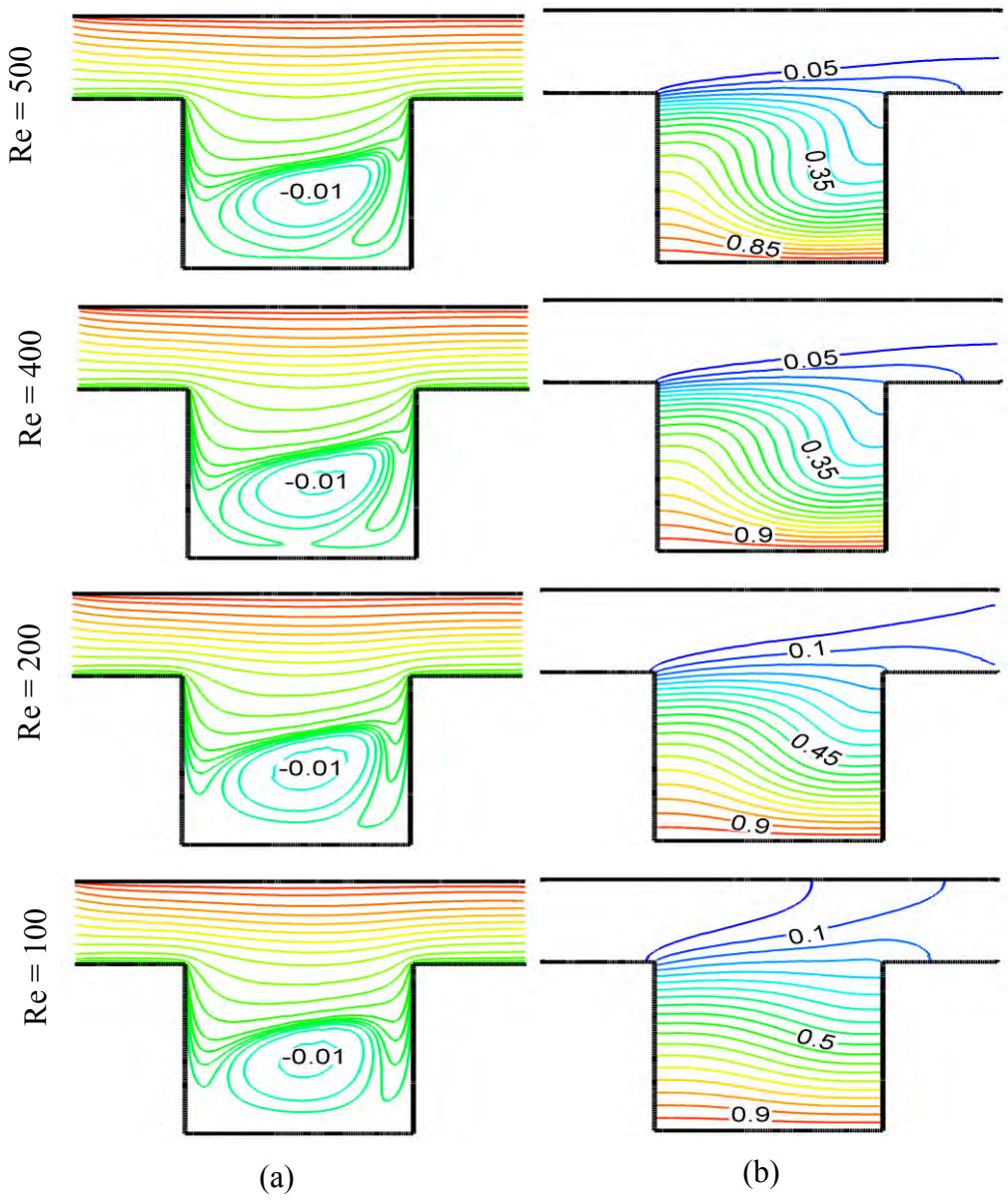

Figure 3.34 Effect of Reynolds number on (a) streamlines and (b) isotherms for AR = 1 and Ra = 10^5, while Ha = 5 and ϕ = 0.04.

This figure shows that at low values of Re, the temperature of the nanofluids rapidly reaches to the temperature of heated walls due to low viscosity. With increasing Reynolds number, decrement of temperature of water-Cu nonofluids happens slowly which leads to increment of peaks of isothermal lines at the exit port of the channel. Rising Re leads to formation of the thermal boundary layer at the heated surfaces. This means that higher heat transfer rate is predicted by the working water- Cu nanofluids. Isotherms become compressed in a zone close to the hot walls of the open cavity for higher values of Re. Because increasing Re causes more flow of the working nanofluids. Then the average heat transfer enhances by utilizing water-Cu nanofluids along the channel with an open cavity.

The effects of Reynolds number on streamlines and isotherms for Ra = 10^5, Ha = 5 and $\phi = 0.04$ is described in the figure 3.34. It is observed that the streamlines formed a tiny vortex along right bottom corner of the cavity and it became stronger for lower values of Reynolds number but flow field in the channel has no significant change with the figure 3.33. Corresponding temperature field shows that for the grater values of Reynolds number the isothermal lines form a thin thermal boundary layer near the hot bottom wall along the right side of the cavity which are radically changed with decreasing of Reynolds number and at lowest value of Ra = 100 it is totally disappeared due to increasing of temperature difference . There is a little bit of change for the temperature field in the channel due to decreasing of Reynolds numbers it is because of force convection is dominant.

The figure 3.35 shows the effects of Reynolds number on streamlines and isotherms for Ra = 10^6, Ha = 5 and $\phi = 0.04$. Streamlines designed clockwise rotating cells and covered the entire cavity. This rotating cells became stronger for lower values of Re. One the other hand temperature field shows that stronger thermal boundary layer near the hot bottom wall along the right side of the cavity presented in the figure 3.35(b) which is slightly changed with decreasing of Reynolds number. Isothermal lines in the cavity formed almost uniform spiral like temperature distribution lower all values of Re.

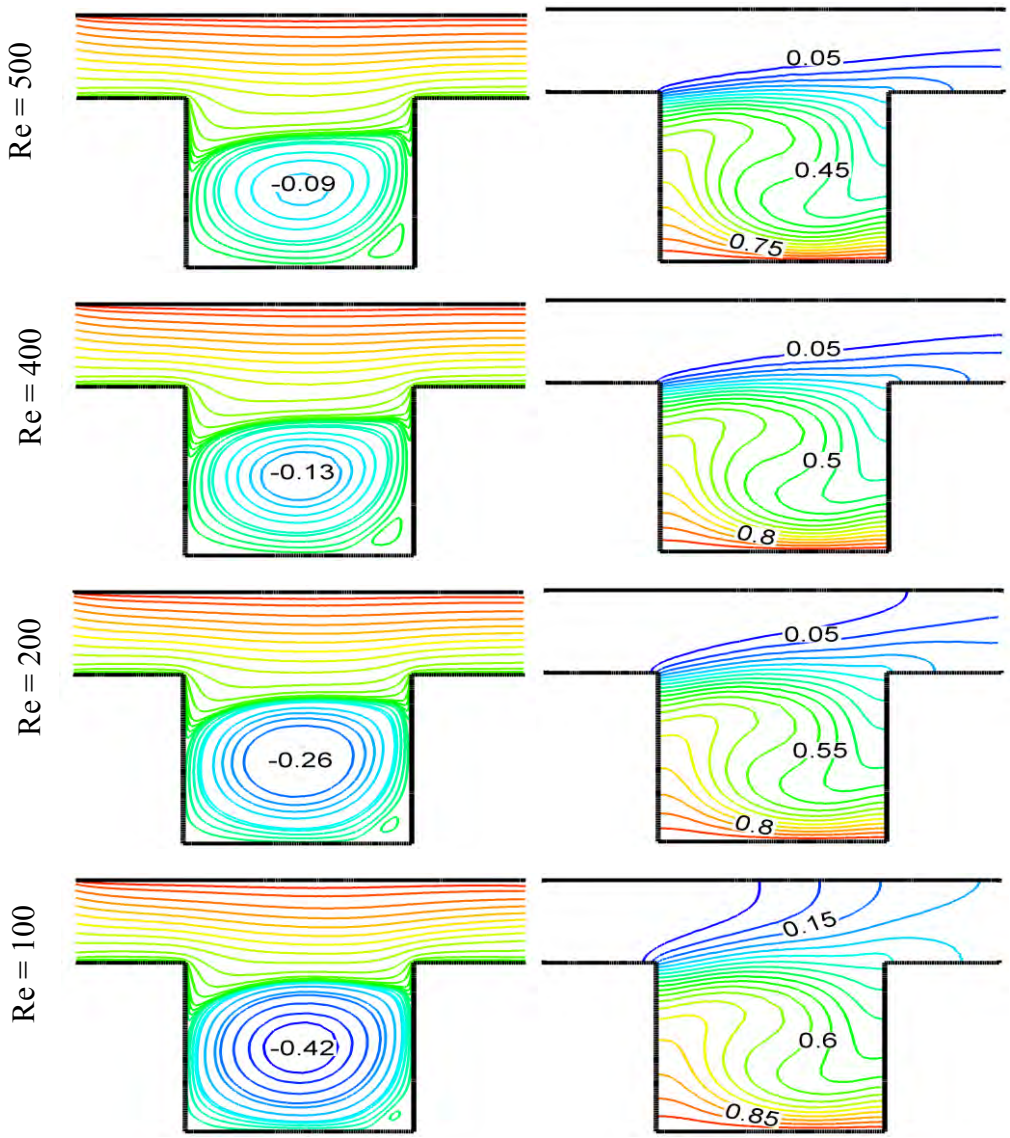

Figure 3.35 Effect of Reynolds number on (a) streamlines and (b) isotherms for AR = 1 and Ra = 10^6, while Ha = 5 and ϕ = 0.04.

Isotherms become compressed in a zone close to the hot walls of the open cavity for higher values of Re. Because increasing Re causes more flow of the working nanofluids then the average heat transfer enhances.

From the figures 3.33 to 3.35 it is clearly seen that flow field is dominant due to increasing the Rayleigh number, it is because of force convection is gain the strength due to increasing of Reynolds number. Similarly temperature field is dominant in the cavity as well as in the channel for increasing the Rayleigh number.

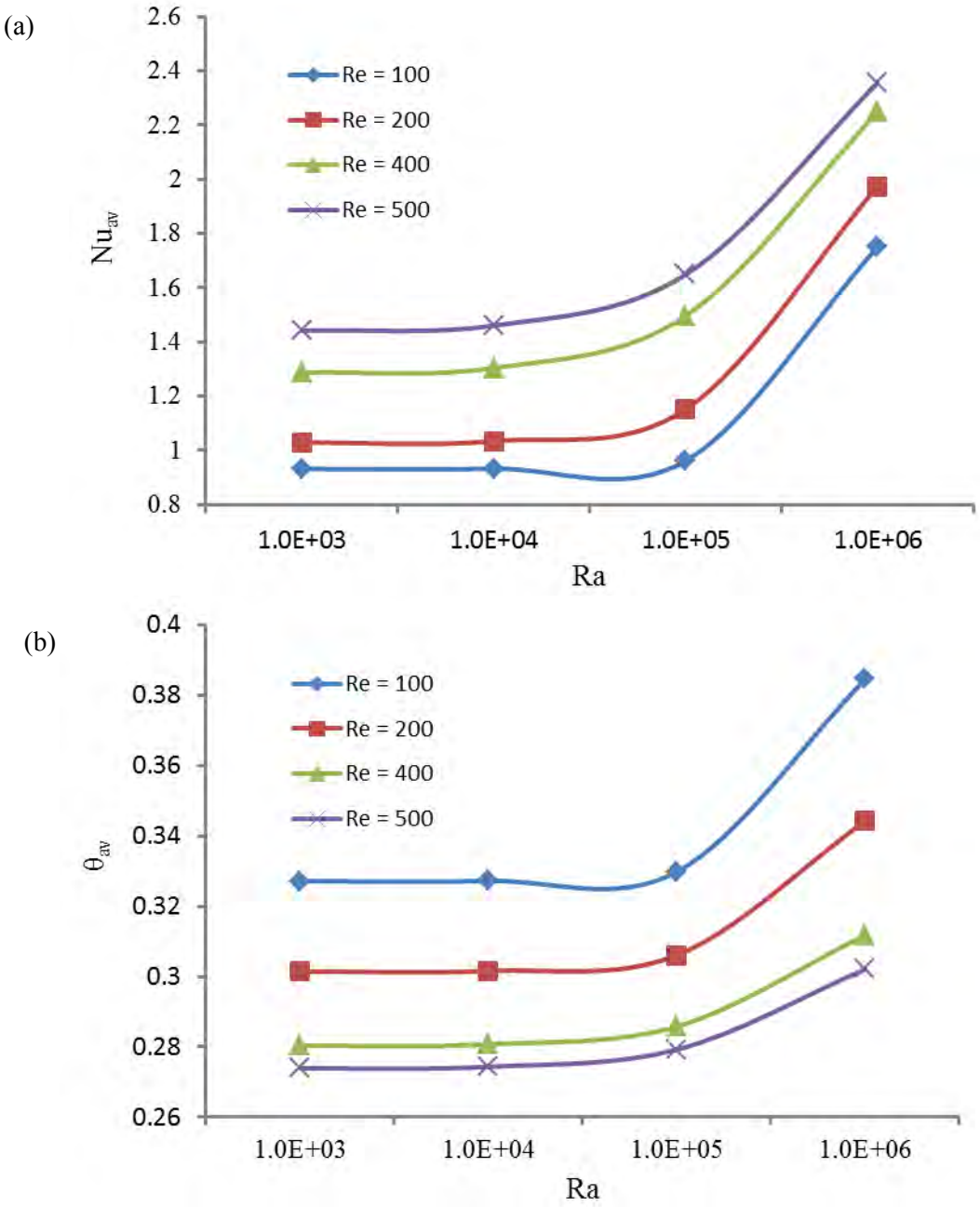

Figure 3.36 Effect of Reynolds number on (a) average Nusselt number and (b) average fluid temperature for different values of Ra and AR = 1, while $\phi = 0.04$ and Ha = 5.

Figure 3.36(a) and (b) depict the average Nusselt number (Nu_{av}) and average fluid temperature θ_{av} respectively with the variation of Re (Re = 100, 200, 400 and 500). In these figure we consider heat transfer rate as well as average fluid temperature as a function of Rayleigh number. From Nu_{av} - Ra profiles for Reynolds number Re it is clearly shown that any specific value of Ra, Nu_{av} increases as the Re increases. This is due to the increase of entering velocity and the strengthening of forced heat transfer. At lower values of Ra the Nu_{av} increases slightly but for higher values of Ra Nu_{av} becomes more significant for any specific value of Re. The reason for this is the lower bouncy force of fluid at lower Ra that provides more time for exchanging heat. The effect of Reynolds number Re on average fluid temperature θ_{av} in the cavity is revealed in the figure 3.36(b). From θ_{av} - Ra it can clearly be seen that the value of θ_{av} decreases regularly with the raise of Re for all considered Rayleigh numbers .Because rising inertia force causes the reduction of fluid temperature. Ra plays the same role upon the θ_{av} like Nu_{av}.

3.4 CASE 4 (AR = 0.5)

3.4.1 Effect of Hartmann number

The Influence of Hartman number on the streamlines and isotherms for different values of Ha (= 0, 5, 10 and 20) at Ra (= 10^4, 10^5 and 10^6) while the values of ϕ and Re kept fixed at 0.04 and 100 respectively are shown in figures 3.37, 3.38 and 3.39.

Figure 3.37 (a) expresses the velocity (modulus of the velocity vector) field in the velocity vector trend to get affected considerably. A buoyancy-induced clockwise rotating cell is formed by streamlines near the upper side of the cavity. And for increasing of Hartmann number this rotating cell becomes weaker and pulled towards the channel. This can be explained that magnetic field is dominant over the velocity field. Figure 3.37(b) expresses the corresponding temperature profile. This figure shows that there is no significant change is observed to change the Hartmann number.

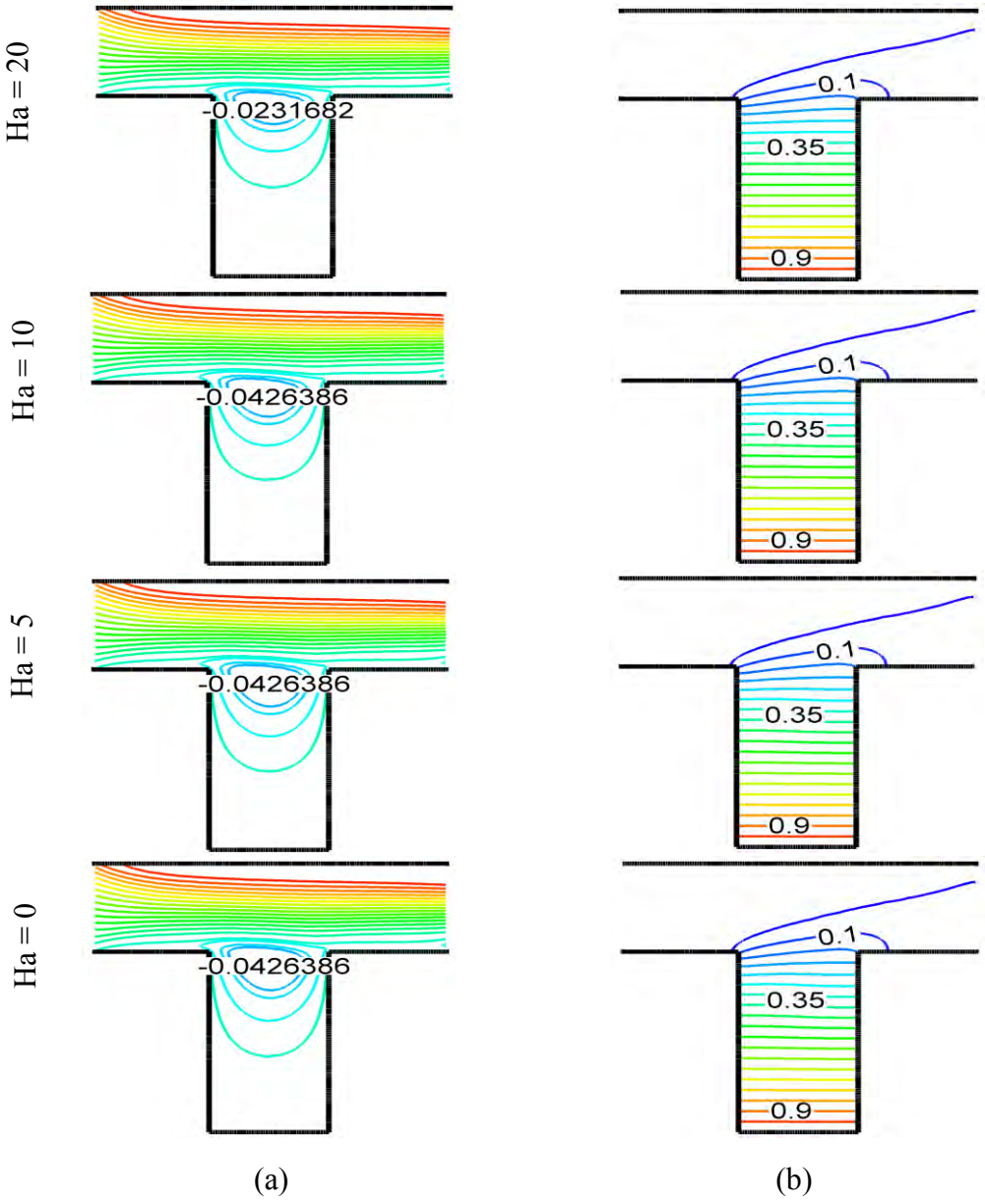

Figure 3.37 Effect of Hartmann number on (a) streamlines and (b) isotherms for AR = 0.5 and Ra = 10^4, while ϕ = 0.04, Re = 100.

This fact due to magnetic force does not have considerable affect when buoyancy force is low at the convection mode. It is important to note that absence of magnetic field in the figure exactly equal to the presence of magnetic field for lower value of Rayleigh number.

The effects of Hartmann number for Ra = 10^5 is presented by the figure 3.38. Stream lines and isotherms patterns are similar with the figure 3.37. This fact due to lower values of Rayleigh number is in significant for variation of Hartmann number while aspect ratio is considered as AR = 0.05.

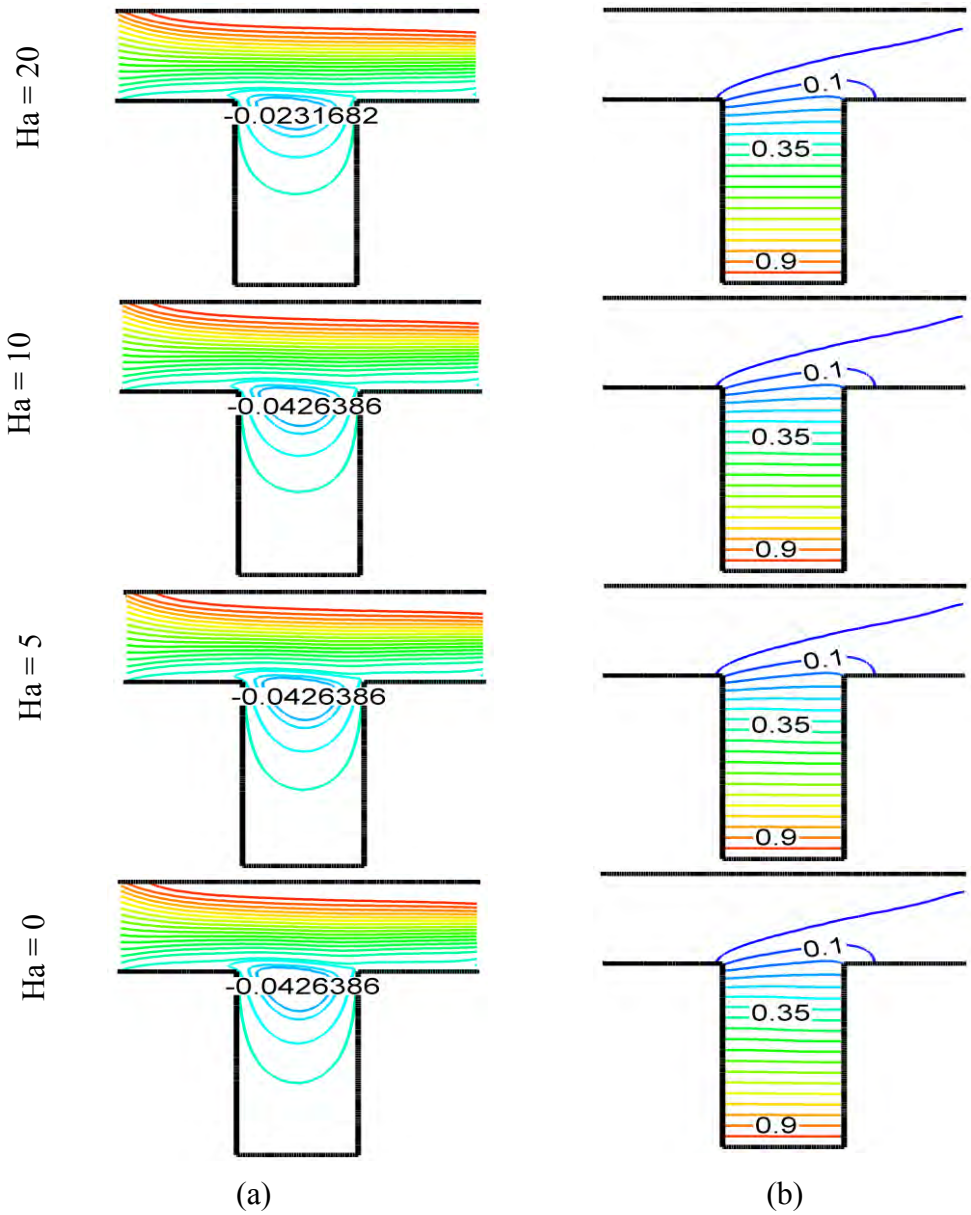

Figure 3.38 Effect of Hartmann number on (a) streamlines and (b) isotherms for AR = 0.5 and Ra = 10^5, while ϕ = 0.04, Re = 100.

In the figure 3.39 Ra is considered 10^6. The velocity (modulus of the velocity vector) field expresses a continuous reduction in vortex strength with increasing Ha.

When Ha = 0, the vortex rotates strongly cover the whole cavity under the effect of natural convection. Increasing Ha increases the suppression force, which opposes the convection currents and this enables the weakened vortex to penetrate symmetrically through the cavity grooves and puss towards the upper side of the cavity. On the other hand, temperature profile becomes still in significant. This is because the length of the temperature travelling path is insufficient before being able to exchange of Hartmann number.

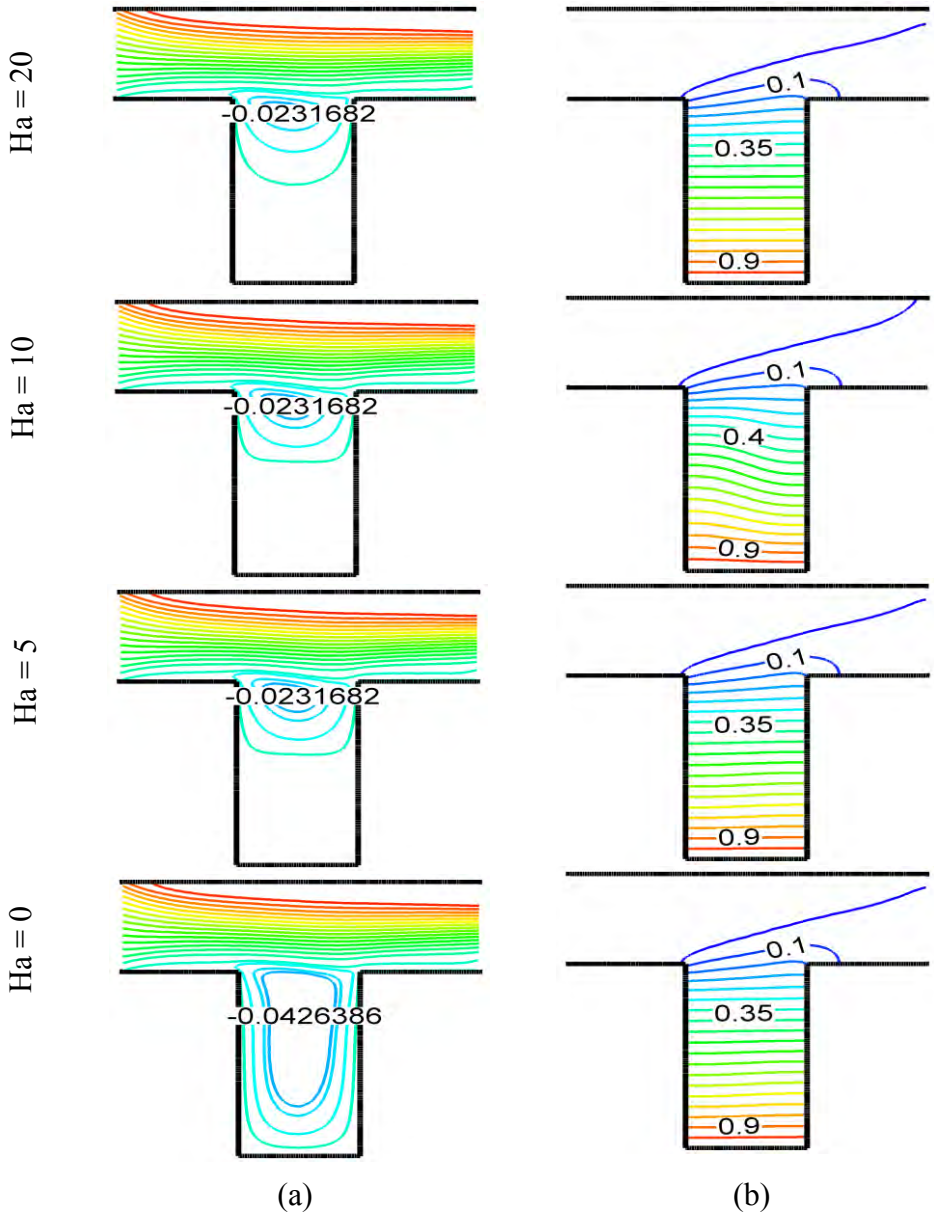

Figure 3.39 Effect of Hartmann number on (a) streamlines and (b) isotherms for AR = 0.5 and Ra = 10^6, while ϕ = 0.04, Re = 100.

Contour maps of streamlines and isotherms for different Ra values for different Ha = 0-20 at ϕ = 0.04, Re = 100 and AR = 1 are presented in figures 3.37-3.39. The streamlines manifests a single vortex behavior for lower values of Hartmann number. Due to the imposed thermal boundary conditions, the vortex rotates clockwise with its core localized within the main cavity. Increasing Ra from 10^4 to 10^6 is not mentionable to strengthening the vortex rotation.

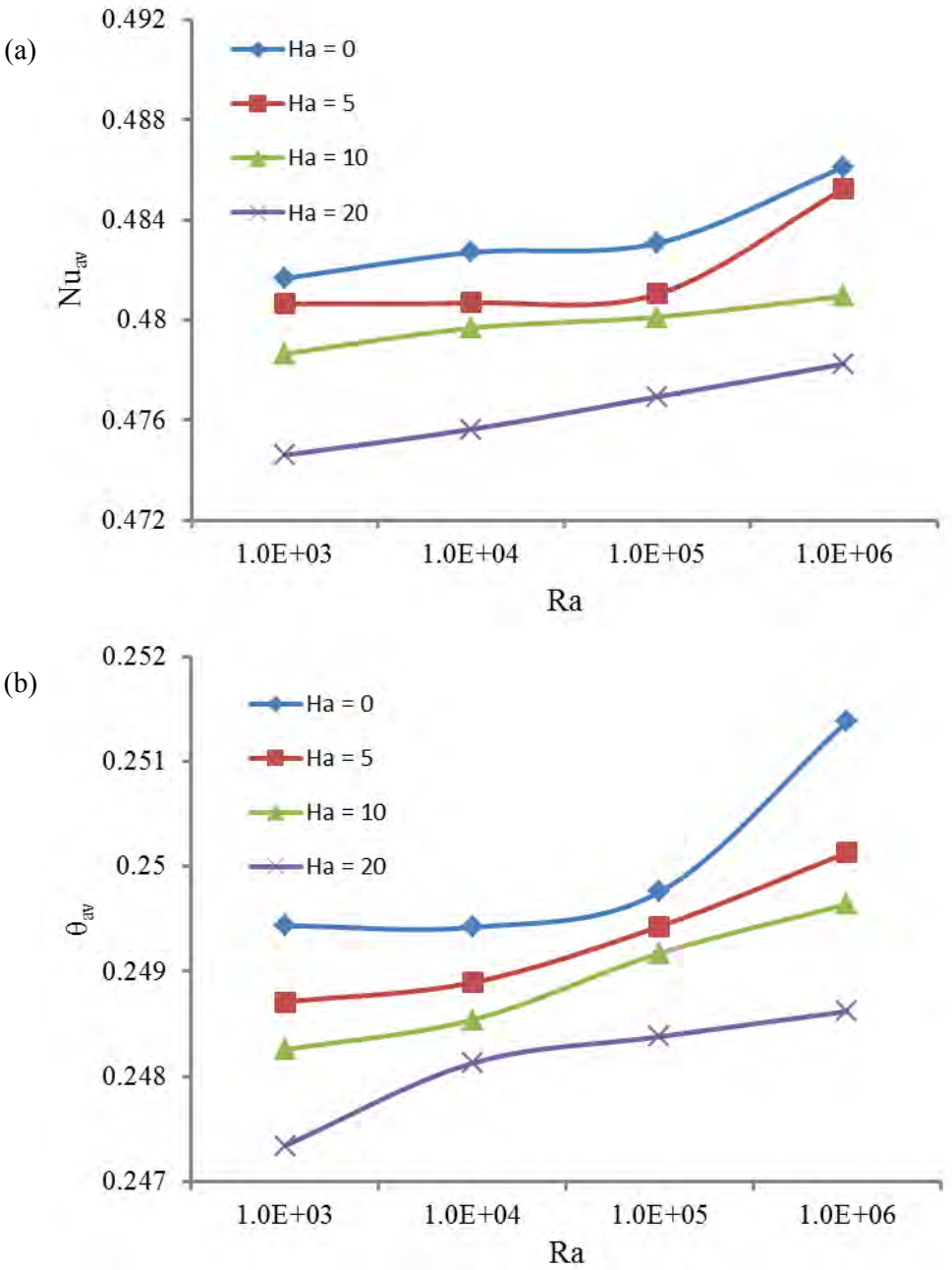

Figure 3.40 Effect of Hartman number on (a) average Nusselt number and (b) average fluid temperature for different values of Ra and AR = 0.5, while Re = 100 and ϕ = 0.04.

Undisturbed isotherms with domain shaped behavior is noticed for all values of Rayleigh number

Figure 3.40(a) and (b) depict the average Nusselt number (Nu_{av}) and average fluid temperature respectively with the variation of Ha (Ha = 0, 5, 10, 20). In these figure we consider heat transfer rate as well as average fluid temperature as a function of Rayleigh number.

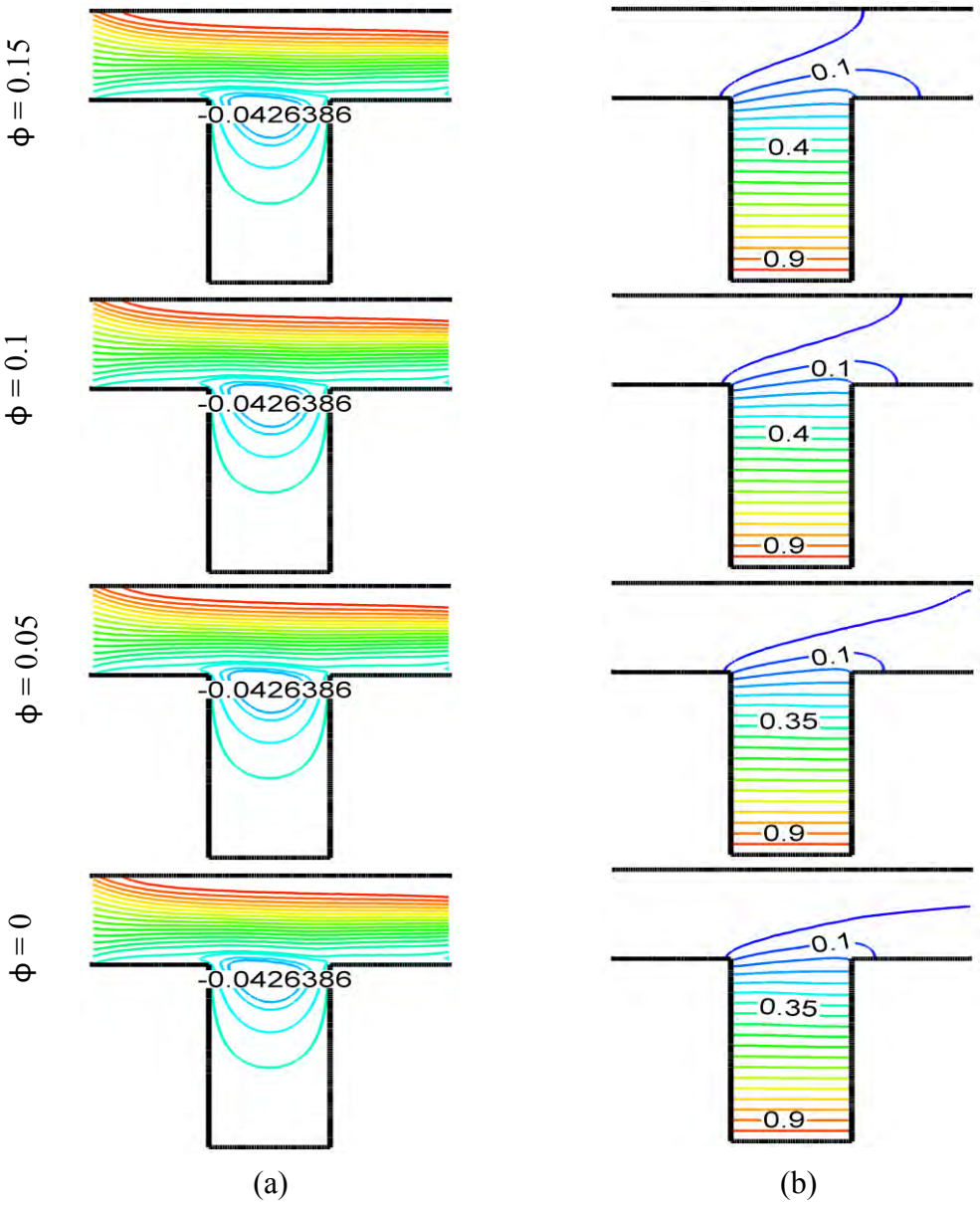

Figure 3.41 Effect of solid volume fraction on (a) streamlines and (b) isotherms for AR = 0.5 and Ra = 10^4, while Ha = 5, Re = 100.

From Nu_{av} - Ra and θ_{av} – Ra profiles are shown for Hartmann number Ha to escalate Ra. Both heat transfer rate and average fluid temperature are decreased with increasing of Hartmann numbers. Because magnetic force control the Heat transfer rate as well as average temperature. For increasing of Ra heat transfer rate and average temperature are increasing in non-consistent way.

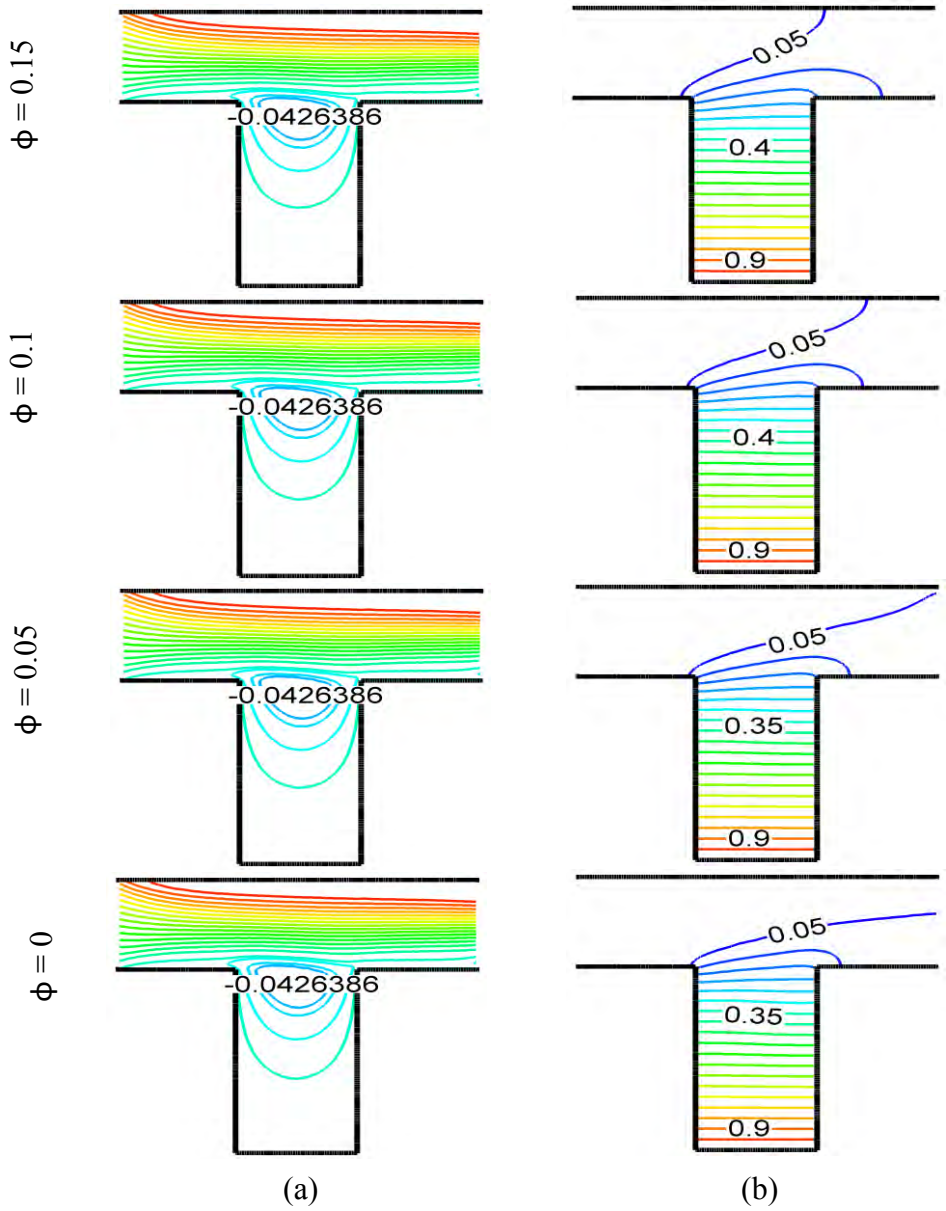

Figure 3.42 Effect of solid volume fraction on (a) streamlines and (b) isotherms for AR = 0.5 and Ra = 10^5, while Ha = 5, Re = 100.

However heat transfer rate is linearly changes to Ra at Ha = 20. Maximum heat transfer rate and average fluid temperature is occurred for higher values of Ra (Ra = 10^6)

3.4.2 Effects of solid volume fraction

Here, the effect of the solid volume fractions is investigated in the range of 0% – 15% whiles the Re and Ha are kept fixed at 100 and 5, respectively. Figure 3.41-3.43 shows the streamlines and isotherms in a channel with cavity for various values of the solid volume fractions (ϕ = 0, 0.05, 0.1, and 0.15) for different Ra (=10^4, 10^5 and 10^6).

From the figure 3.41 it is observed that there is no significant change for solid volume concentration over the streamlines as well as isotherms. For in tiny path way and lower values of Ra solid volume fraction is not functional. Flow velocity creates a clock wise circulation cell along the upper middle side of the cavity. This is the result that fluid velocity does not reach the lower part of the cavity due to insufficient movement path way. The strengths of the thermal current are stronger for higher values of solid volume concentration because the nanofluids increases in the overall heat transfer through the channel with an open cavity.

The outcome of solid volume fraction on the flow field and temperature fields has been revealed in figure 3.42 at Ra = 10^5, Ha = 5, Re = 100 and AR = 1. It can easily be seen that flow field as well as temperature contour show the similar attitude with the figure 3.40. This is the result those of lower bouncy force.

Figure 3.43 (a) and (b) shows the influences of solid volume fraction (ϕ) on the velocity and temperature profile while Ra = 10^6, Ha = 5 and Re = 100. As seen from the left column of this figure, initially (ϕ = 0%) stream lines form a large clockwise recirculation cell with ψ_{min} = -0.0887078 which fills the almost entire cavity. This eddy becomes weaker (ψ_{min} = -0.0231682) by increasing solid volume fraction due to intensification of the inertia effects. On the other hand by increasing solid volume fraction, the isotherms become stronger showing the increase of temperature gradients, the low temperature areas become thicker and the isotherms become distorted indicating the intensification of convective heat transfer.

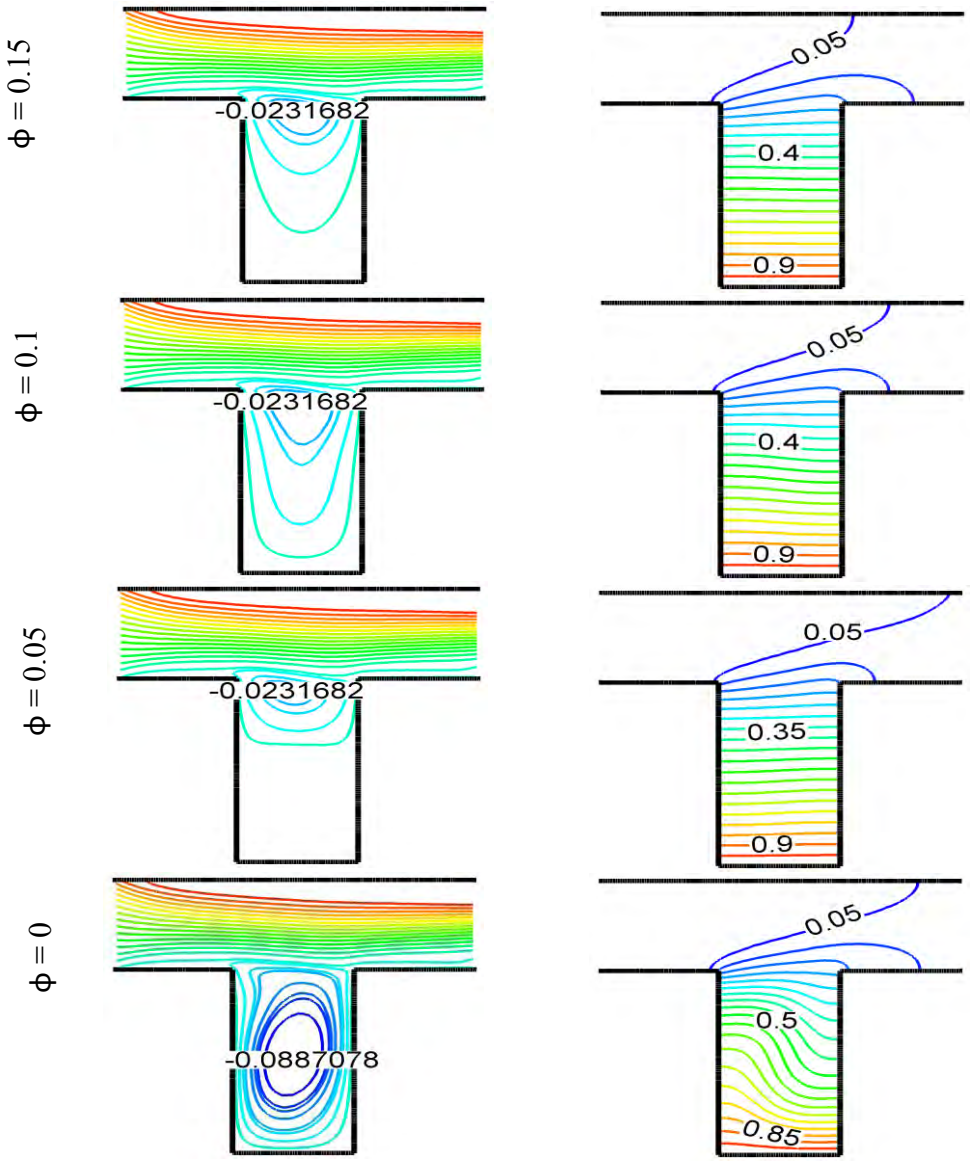

Figure 3.43 Effect of solid volume fraction on (a) streamlines and (b) isotherms for AR = 0.5 and Ra = 10^6, while Ha = 5, Re = 100.

From the figure 3.41 to 3.43 it is seen that fluid flow is stronger in the cavity for higher values of Rayleigh numbers in the same vale of ϕ beside this in the channel the flow pattern has no significant change for different values of Rayleigh numbers. But for the lower values of solid volume fraction (ϕ = 0, 0.05) at higher value of Rayleigh number isotherms formed more curvy shaped than the lower values of Rayleigh number.

Due to rising values of Ra the temperature distributions and velocity become distorted resulting in an increase in the overall heat transfer and fluid velocity.

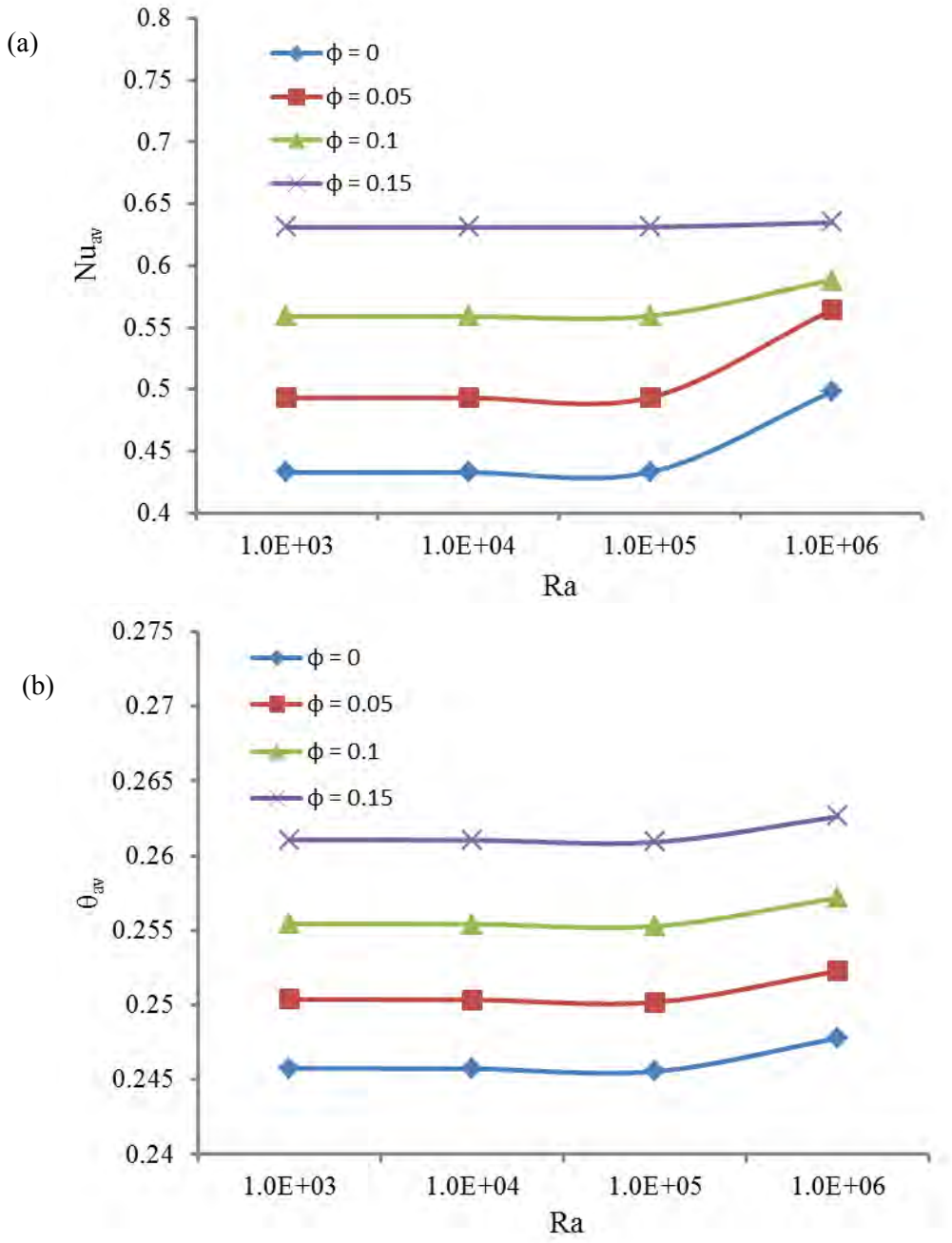

Figure 3.44 Effect of solid volume fraction on (a) average Nusselt number and (b) average fluid temperature for different values of Ra and AR = 0.5, while Re = 100 and Ha = 5.

Figure 3.44(a) and (b) depict the average Nusselt number (Nu_{av}) and average fluid temperature respectively with the variation of ϕ (ϕ = 0, 0.05, o.1 and 0.15). In these figure we consider heat transfer rate as well as average fluid temperature as a function of Rayleigh number. From Nu_{av} - Ra and θ_{av} – Ra profiles for solid volume fraction ϕ it is clearly shown that almost similar variation between the average Nusselt number and

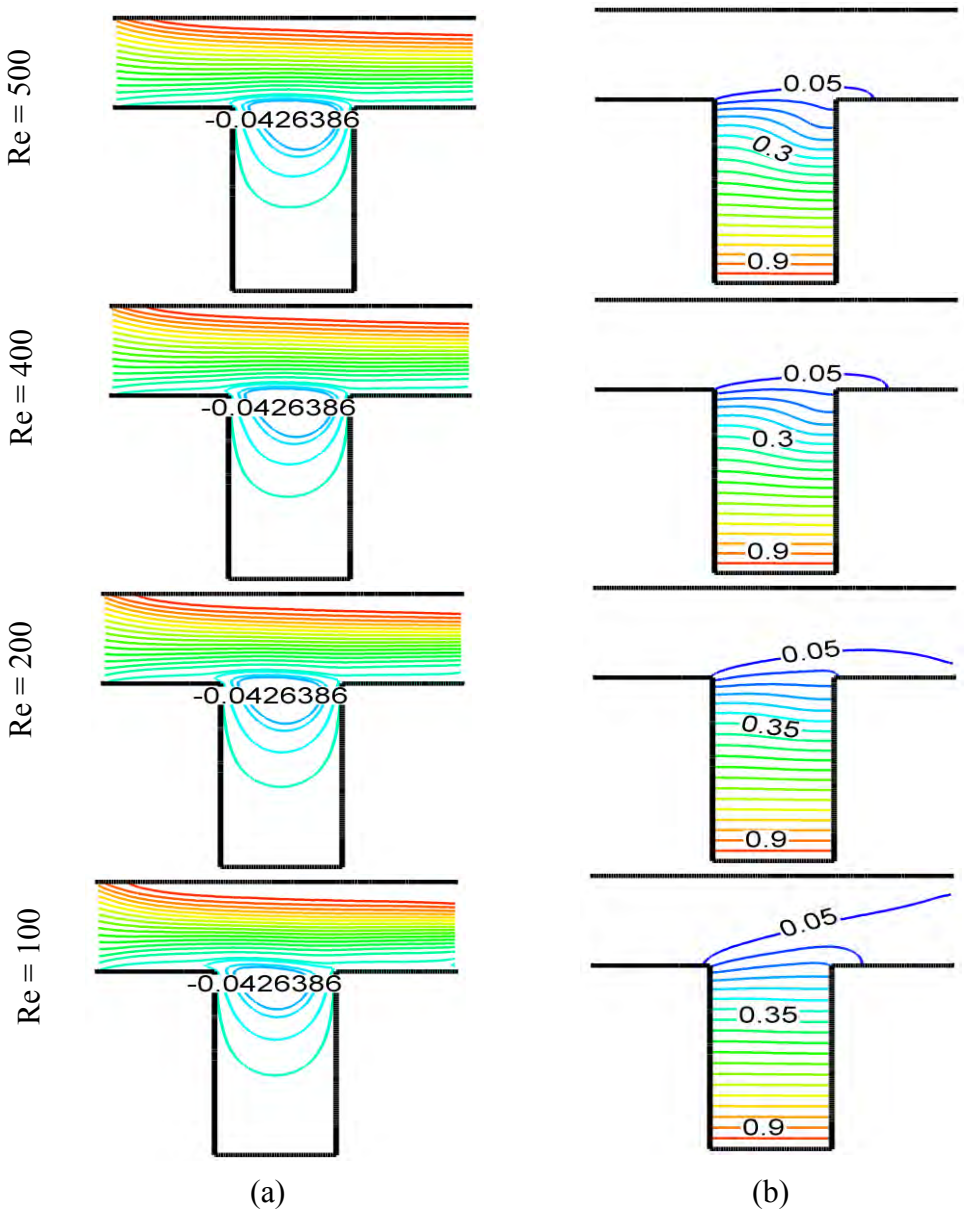

Figure 3.45 Effect of Reynolds number on (a) streamlines and (b) isotherms for AR = 0.5 and Ra = 10^4, while Ha = 5 and ϕ = 0.04.

average fluid temperature with the solid volume fraction is confined for all Rayleigh number. No effect is observed for lower values of Ra (Ra = 10^3 and 10^4). But both of these values gradually increase for higher values of Rayleigh number 10^6. As clearly be seen that the heat transfer and average temperature increases with increasing of ϕ because thermal conductivity of nanofluid is always higher than base fluid (ϕ = 0%). However, the values of Nu_{av} and θ_{av} are always maximum for the highest value of Rayleigh number Ra = 10^6.

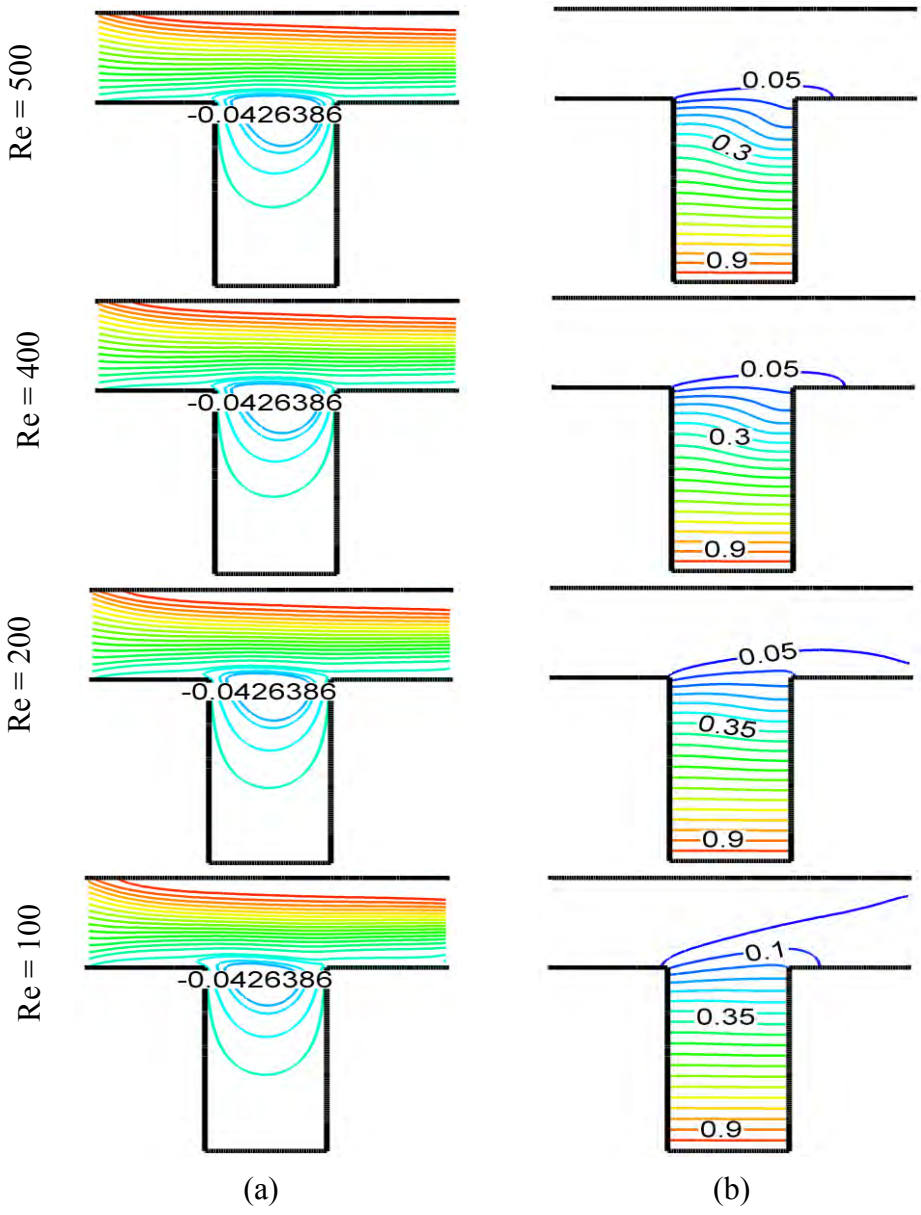

Figure 3.46 Effect of Reynolds number on (a) streamlines and (b) isotherms for AR = 0.5 and Ra = 10^5, while Ha = 5 and ϕ = 0.04.

3.4.3 Effects of Reynolds Number

To analyze Reynolds number of the flow behavior the streamlines and the isotherms for three values of Rayleigh number: Ra = 10^4, Ra = 10^5 and Ra = 10^6 are illustrated in figures 3.45, 3.46 and 3.47 respectively while ϕ = 4% and Ha = 5 in the form of streamlines and isotherms.

From the figure 3.45(a) it is clearly seen that a clockwise circulation cell is formed upper middle side of the cavity and try to gather along the channel because fluid velocity does not reach the lower part of the cavity due to tiny path way and goes quickly along the channel. No significant effect of Re is observed. On the other hand with increasing Reynolds number, decrement of temperature of water-Cu nonofluids happens slowly which leads to increment of peaks of isothermal lines at the exit port of the channel.

The effects of Reynolds number on streamlines and isotherms for Ra = 10^5, Ha = 5 and ϕ = 0.04 is described in the figure 3.46. It is observed that flow field in the channel with the open cavity has no significant change with the figure 3.45(a). Corresponding temperature field shows that in the same way with the figure 3.45(b) there is a little bit of change for the temperature field in the channel as well as cavity due to decreasing of Reynolds numbers it is because that force convection is dominant.

The figure 3.47 shows the effects of Reynolds number on streamlines and isotherms for Ra = 10^6, Ha = 5 and ϕ = 0.04. Streamlines designed clockwise rotating cells and covered the entire cavity. This rotating cell becomes stronger for lower values of Re. On the other hand temperature field shows that strength is decreased for lower values of Reynolds number due to increasing Re causes more flow of the working nanofluids as a result the average heat transfer enhances.

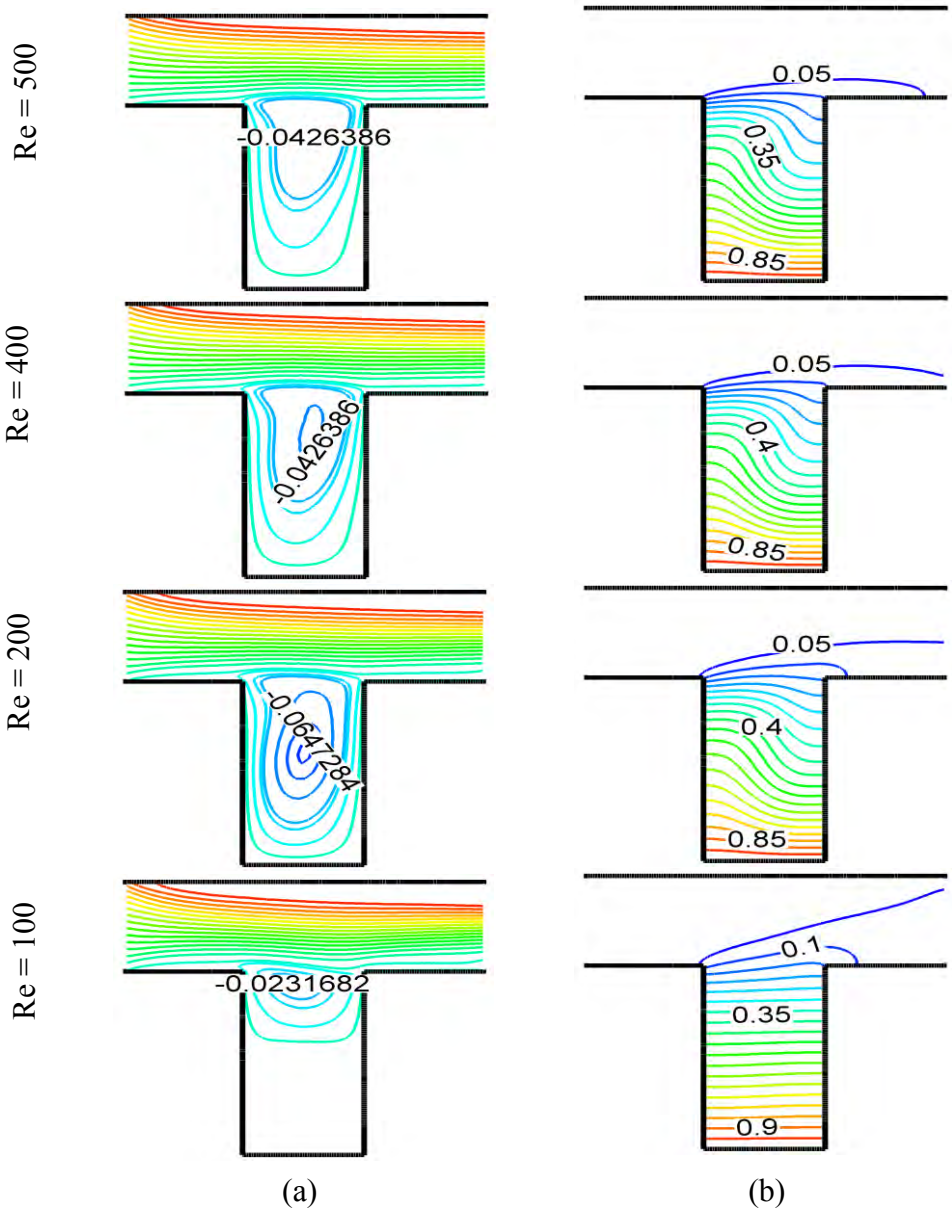

Figure 3.47 Effect of Reynolds number on (a) streamlines and (b) isotherms for AR = 0.5 and Ra = 10^6, while Ha = 5 and ϕ = 0.04.

From the figure 3.45 to 3.47 it is clearly seen that flow field is dominant due to increasing the Rayleigh number, it is because of force convection gain the strength due to increasing of Reynolds number. Similarly temperature field is dominant in the cavity as well as in the channel for increasing the Rayleigh number.

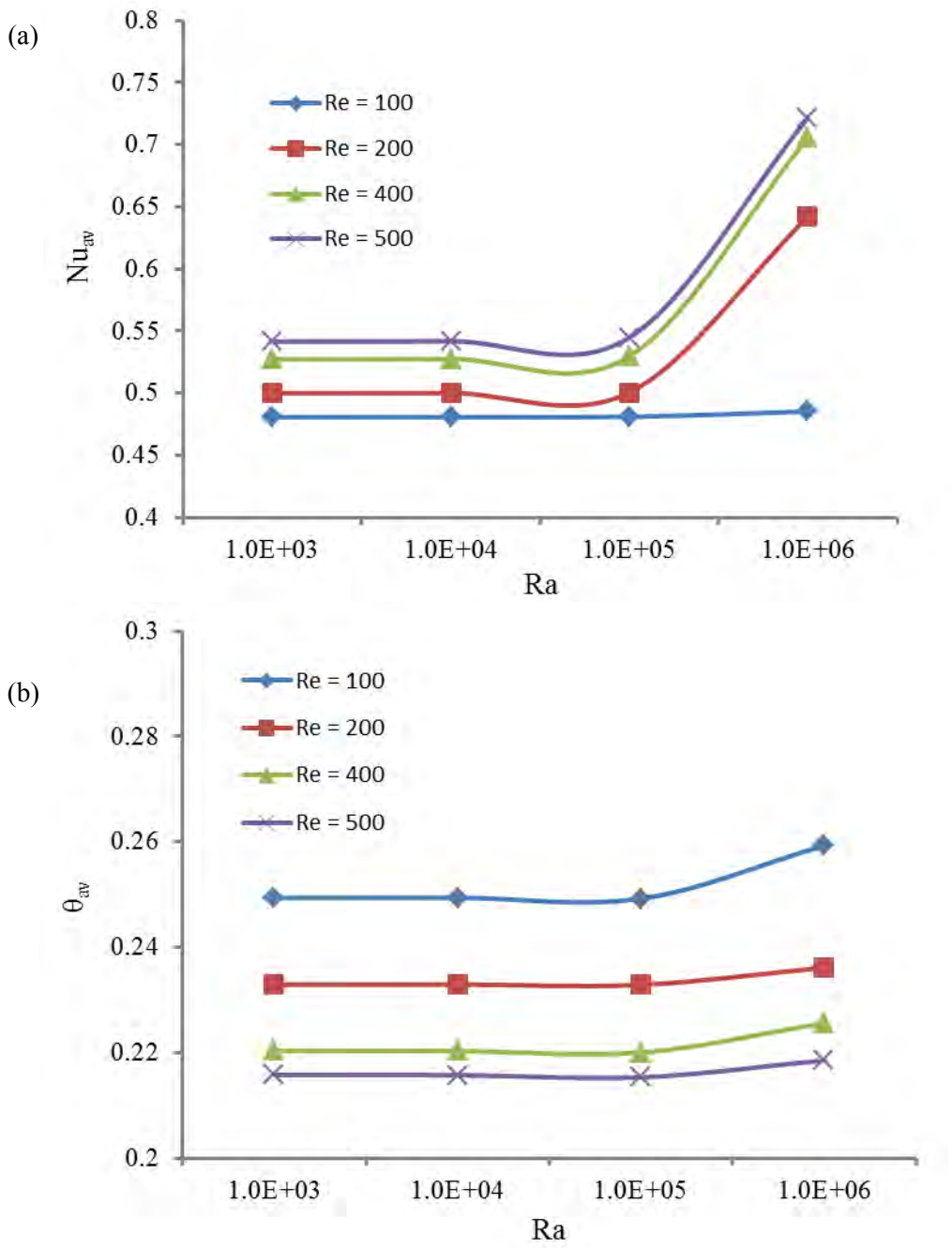

Figure 3.48 Effect of Reynolds number on (a) average Nusselt number and (b) average fluid temperature for different values of Ra and AR = 0.5, while ϕ = 0.04 and Ha = 5.

Figure 3.48(a) and (b) depict the average Nusselt number (Nu_{av}) and average fluid temperature θ_{av} respectively with the variation of Re (Re = 100, 200, 400 and 500). In these figures we consider heat transfer rate as well as average fluid temperature as a function of Rayleigh number.

From Nu_{av} - Ra profiles for Reynolds number Re it is clearly shown that any specific value of Ra, Nu_{av} increases as the Re increases. This is due to the increase of entering velocity strengthening forced heat transfer. At lower values of Ra, the Nu_{av} increases slightly but for higher values of Ra, Nu_{av} becomes more significant for any specific value of Re. The reason for this is the lower buoyancy force of fluid at lower Ra that provides more time for exchanging heat. However heat transfer rate is constant for the lower values of Re = 100. Because the low velocity of the heat transfer rate is not significant. The effect of Reynolds number Re on average fluid temperature θ_{av} in the cavity is revealed in the Figure 3.48(b). From θ_{av} - Ra it can clearly be seen that the value of θ_{av} decreases regularly with the raise of *Re* for all considered Rayleigh numbers. Because rising inertia force causes the reduction of fluid temperature. On the other hand average fluid temperature is not dependent upon Rayleigh number for lower values of Ra (Ra = 10^3 to10^5). But at Ra = 10^6 average temperature slightly drops down for higher values of Re (Re = 400 and 500) due to rising inertia force in rising bouncy force fluid temperature is reduced at the minimum distance between the hot and cold wall.

3.5 COMPARISON OF DIFFERENT NANOFLUIDS

Figures 3.49(a) - 49(d) show comparison between two commonly used nanofluids based on overall Nusselt number at the heated surface for different percentages of nanoparticles in the fluid for Ra = 10^3, 10^4, 10^5, and 10^6 at AR = 1.5, Ha = 5, and Re = 100. From comparison it is evident that water-Cu nanofluid gives the better performance with respect to average Nusselt number and water-Al_2O_3 gives the worse performance between the two nanofluids considered here. Another point to reveal is that the absolute value of Nu_{av} generally increases, though at different rates, with increasing value of solid volume fraction in the fluid. At Ra = 10^3 to 10^5 and solid volume fraction up to 0.1 performances from water-Al_2O_3 and water-Cu becomes almost comparable. But at Ra = 10^6 it is incomparable. So it can be said that, generally, water-Cu nanofluid performs better in terms of convective heat transfer rate than water-Al_2O_3.

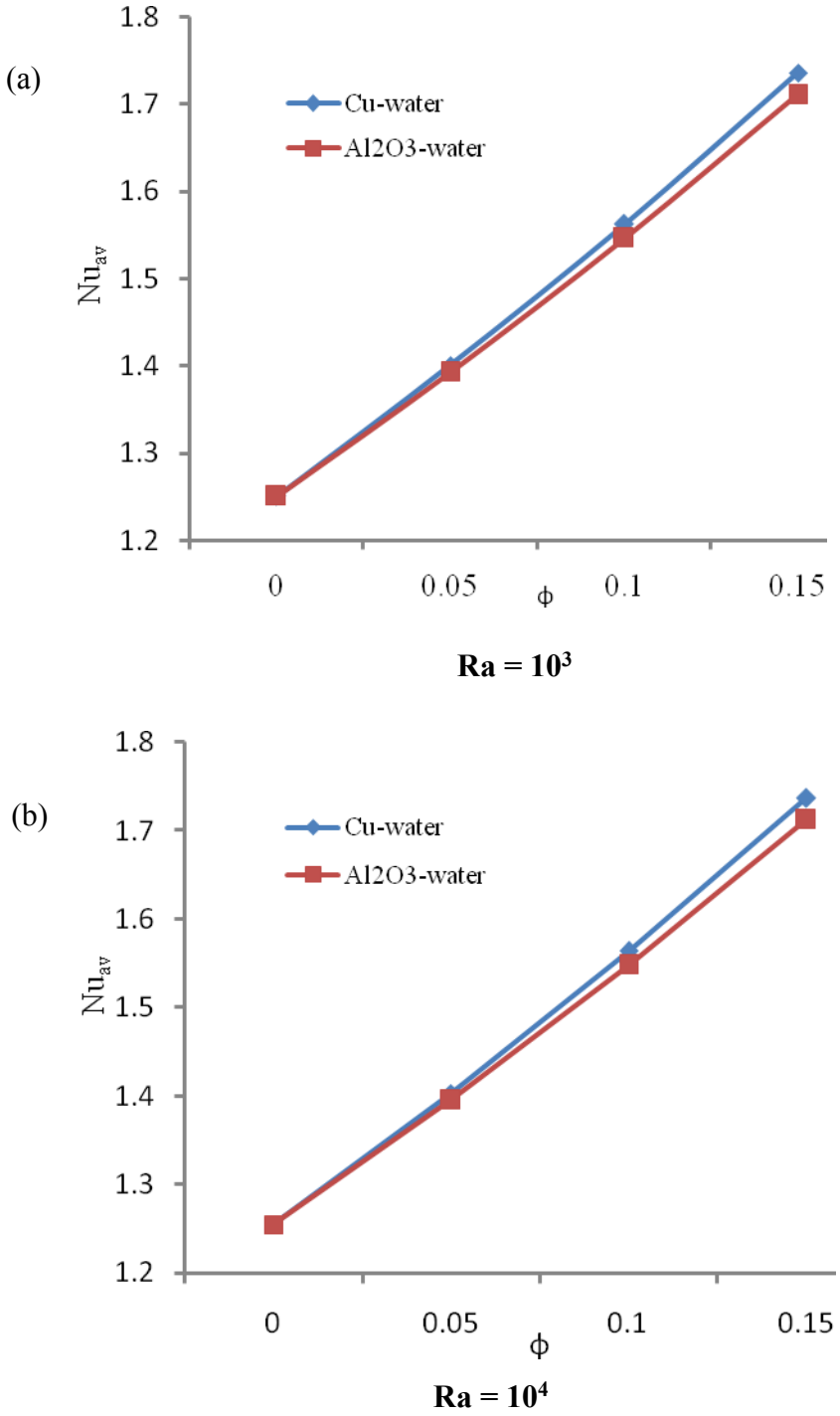

Figure 3.49 Comparison of average Nusselt number at the heated surface between different nanofluids for (a) Ra = 10^3, (b) Ra = 10^4 while AR = 1.5, Re = 100 and Ha = 5.

(c)

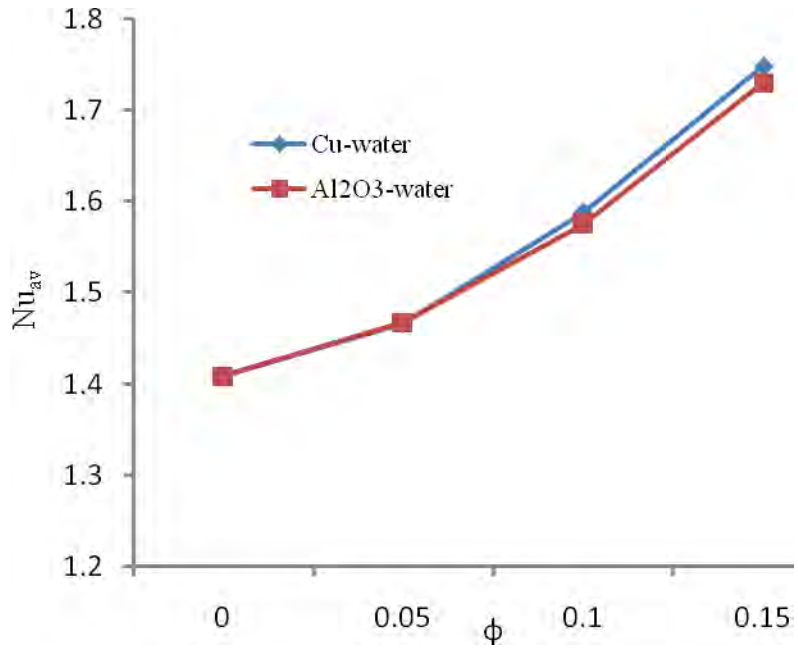

Ra = 10^5

(d)

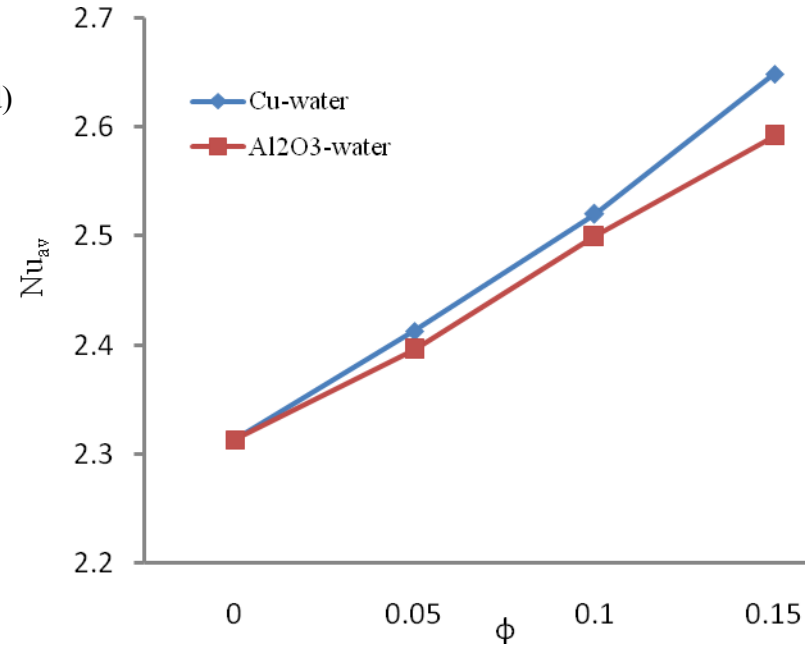

Ra = 10^6

Figure 3.49 Comparison of average Nusselt number at the heated surface between different nanofluids for (c) Ra = 10^5, (d) Ra = 10^6 while AR = 1.5, Re = 100 and Ha = 5.

3.6 COMPARISON FOR THE CONSIDERED PARAMETERS

In this section we compare the values of average Nusselt number Nu_{av} and average fluid temperature θ_{av} between the four above mentioned cases considered for highest, upper intermediate, lower intermediate and lowest considered parameters and tabulated in Table 3.1 – 3.4.

Table -3.1: Comparison for the highest values of the considered parameters

AR		Nu_{av}			Θ_{av}		
	Ra =	10^4	10^5	10^6	10^4	10^5	10^6
0.5	Re = 500	0.54182	0.54488	0.72178	0.21573	0.21631	0.21853
	ϕ =0.15	0.63091	0.63125	0.63481	0.26104	0.26191	0.26262
	Ha = 20	0.47563	0.47693	0.47824	0.24812	0.24838	0.24862
1	Re = 500	1.46053	1.64880	2.35530	0.27434	0.27925	0.30210
	ϕ =0.15	1.20099	1.20592	1.88075	0.34580	0.34587	0.39697
	Ha = 20	0.92423	0.92617	1.00156	0.32453	0.32584	0.33859
1.5	Re = 500	2.43708	2.67087	3.58476	0.32617	0.3324	0.35544
	ϕ =0.15	1.73687	1.74782	2.64908	0.39511	0.39539	0.47647
	Ha = 20	1.30100	1.32645	1.79147	0.36683	0.36765	0.38150
2	Re = 500	2.98781	3.16517	4.22868	0.35029	0.35465	0.37395
	ϕ =0.15	2.23389	2.24803	2.69970	0.42898	0.42954	0.44748
	Ha = 20	1.76337	1.77582	2.20013	0.39538	0.39829	0.40612

From the table 3.1 it is seen that (i) heat transfer rate significantly increases for all cases due to increasing of buoyancy driven force. Among them best case is case 3 (AR = 1) because Nu_{av} increases 13% to 61% for highest value of Re and 0.4% to 56% for highest value of ϕ. But for the Ha value best case is case 2(AR = 1.5) because Nu_{av} increases 1.9% to 38%. On the other hand fluid temperature is also increases for all cases from Ra = 10^4 to 10^6 highest increment is 21% at AR = 1.5

Table 3.2: Comparison for the upper intermediate values of the considered parameters

AR		Nu_{av}			Θ_{av}		
	Ra =	10^4	10^5	10^6	10^4	10^5	10^6
0.5	Re = 400	0.52759	0.52968	0.70572	0.22030	0.22042	0.22561
	ϕ =0.1	0.55899	0.55933	0.58846	0.25542	0.25557	0.25718
	Ha = 10	0.47967	0.48011	0.48095	0.24854	0.24917	0.24964
1	Re = 400	1.30390	1.49642	2.24826	0.28073	0.28583	0.31177
	ϕ =0.1	1.07308	1.08283	1.83553	0.33685	0.33752	0.39216
	Ha = 10	0.95689	0.9917	1.63425	0.32611	0.33715	0.37718
1.5	Re = 400	2.15881	2.42701	3.42197	0.32898	0.33746	0.36569
	ϕ =0.1	1.56371	1.58705	2.52037	0.38377	0.38588	0.46709
	Ha = 10	1.35915	1.47543	2.43359	0.36888	0.37539	0.44979
2	Re = 400	2.70935	2.90906	4.01405	0.35370	0.35966	0.38199
	ϕ =0.1	2.01978	2.03592	2.62730	0.41541	0.41583	0.43472
	Ha = 10	1.77229	1.80692	2.40463	0.39794	0.39988	0.41368

From the table 3.2 it is seen that heat transfer rate significantly increases for all cases. When Rayleigh number is changed lower to higher then Nu_{av} increases highest 15% to 72% for AR = 1 at Re = 400, 1.5% to 61% for AR = 1.5 at ϕ = 0.1 and 9% to 71% for AR = 1.5 at Ha = 10. Fluid temperature is increases very insignificant way from Ra = 10^4 to 10^5 but from 105 to 106 it is increase noticeable way (highest 22% for AR = 1.5).

Table -3.3: Comparison for the lower intermediate values of the considered parameters

AR		Nu_{av}			Θ_{av}		
	Ra =	10^4	10^5	10^6	10^4	10^5	10^6
0.5	Re = 200	0.50015	0.50062	0.64225	0.23293	0.23386	0.23614
	ϕ =0.05	0.49317	0.49353	0.56445	0.25035	0.25049	0.25228
	Ha = 5	0.48068	0.48103	0.48524	0.24889	0.24943	0.250131
1	Re = 200	1.03432	1.15185	1.97335	0.30159	0.30610	0.34422
	ϕ =0.05	0.95512	0.97896	1.76650	0.32872	0.33085	0.38590
	Ha = 5	0.97265	1.02178	1.75081	0.32718	0.33981	0.38454
1.5	Re = 200	1.60048	1.84782	3.02356	0.34295	0.35545	0.40522
	ϕ =0.05	1.40306	1.46614	2.41286	0.37348	0.38008	0.46268
	Ha = 5	1.37240	1.52998	2.59902	0.37154	0.37960	0.46043
2	Re = 200	2.08421	2.25868	3.16481	0.36842	0.37678	0.38851
	ϕ =0.05	1.81900	1.84743	2.50234	0.40302	0.40427	0.42404
	Ha = 5	1.78043	1.84368	2.56140	0.40067	0.40247	0.42038

From the table 3.3 it is observed that that transfer rate pointedly increases for all cases. When Rayleigh number is changed lower to higher then Nu_{av} increases extremely for the case 2 (AR = 1.5) and case 3 (AR = 1). On the other hand flow temperature is increases beastly for case 2 (AR = 1.5) up to 24%.

Table -3.4: Comparison for the lowest values of the considered parameters

AR		Nu_{av}			Θ_{av}		
	Ra =	10^4	10^5	10^6	10^4	10^5	10^6
0.5	Re = 100	0.48068	0.48104	0.48526	0.24939	0.24942	0.25930
	$\phi = 0$	0.43275	0.43312	0.49803	0.24573	0.24585	0.24778
	Ha = 0	0.48269	0.48307	0.48611	0.24942	0.24975	0.25138
1	Re = 100	0.93265	0.96178	1.75081	0.32518	0.32981	0.38454
	$\phi = 0$	0.8464	0.91284	1.68368	0.32125	0.32712	0.37887
	Ha = 0	0.98847	1.05850	1.79741	0.32794	0.34417	0.38727
1.5	Re = 100	1.37240	1.44998	2.59902	0.37154	0.37960	0.46143
	$\phi = 0$	1.25462	1.40864	2.31296	0.3641	0.37014	0.44538
	Ha = 0	1.40367	1.58277	2.69022	0.37314	0.38646	0.46571
2	Re = 100	1.78043	1.81368	2.56140	0.40067	0.40247	0.42138
	$\phi = 0$	1.63148	1.69658	2.42065	0.39165	0.39637	0.41184
	Ha = 0	1.78689	1.88337	2.62467	0.40192	0.40549	0.42277

From the table 3.4 it is observed that in absence of magnetic effect and solid volume concentrate fluid heat transfer rate increases very marginally due to changes of Ra = 10^4 to 10^5(highest 13%) but changing at Ra = 10^6 it changes unevenly (82% to 99%).for case 2 and case 3. Fluid temperature increases normally with the changes of Rayleigh number. Case 2 (AR = 1.5) is the best case for fluid temperature increase (25%).

CHAPTER 4

CONCLUSIONS

Mixed convection in a channel with a cavity heated from bottom wall of the cavity using water-Cu nanofluids under the influence of the applied magnetic force has been investigated numerically. The results are presented for flow and thermal fields as well as heat transfer for the channel with an enclosure subjected to a constant hot temperature at the bottom wall of the cavity while the remaining sidewalls are kept adiabatic. Finite element method is used to solve governing equations. Comparisons with the published work are performed and found to be in excellent agreement. The influences of Rayleigh number, the Hartmann number, Reynolds number, Solid volume fraction and the cavity aspect ratio have been reported. The various ideas and results have been discussed in detail in the relevant chapters of the thesis. In the present chapter an attempt is made to summarize the concepts presented and results obtained in the work reported already. A section on the scope of further work on associated fields of investigation is also included.

4.1 SUMMARY OF THE MAJOR OUTCOMES

Four different aspect ratio as Case-1(AR =. 2), Case-2(AR = 1.5), Case-3(AR = 1) and Case-4(AR =0.5) where Prandtl number is chosen as Pr = 6.2 and water-Cu nanofluids is used.

The following main conclusions are drawn from the present study:

(i) Flow velocity and heat transfer reduces with increasing of Hartmann number. Average Nusselt number at the heated surface and the average fluid temperature changes from highest to lowest as Ha changes lowest to highest. The influence of Hartmann number on streamlines and isotherms are remarkable for the different values of Ra. Buoyancy-induced vortex in the streamlines diminishes and thermal layer near the heated surface becomes thick and less concentrated with growing values of Ha. It is also observed that Ha effect is more noticible for lower values of AR.

(ii) The structure of the fluid flow and temperature field through the cavity is found to be significantly dependent upon the solid volume fraction. Flow velocity decreases for higher values of ϕ. On the other hand temperature gradient is increasing for higher values of ϕ. It is also found that for higher values of solid volume fraction the heat transfer characteristics and fluid tempareture improve. Value of $\phi = 0.15$ with $Ra = 10^6$ proves to be the most effective combination for improving heat transfer as well as fluid temperature. The maximum rate of heat transfer and fluid temperature are obtained for the AR = 1.5.

(iii) Higher Reynolds number strengthens overall flow inside the cavity. It also produces a stronger and larger buoyancy-driven vortex. Temperature distribution is affected by the escalating Re. Temperature distribution reduces for higher values of Re. Average Nusselt number at the heated surface enhances and average fluid temperature is lessen as Re increases. The maximum rate of heat transfer and fluid temperature are observed for the AR = 1.

(iv) Flow strength and heat transfer increase in increasing Rayleigh number in all cases. Higher fluid temperature is formed for the highest value of Rayleigh number except Case 4 when AR = 0.5. The natural convection parameter Ra has significant effects on the flow and temperature fields. The eddy due to bouncy force enhances with increasing Ra. Isothermal lines become denser near the hot surface for rising values of Ra.

(v) The influence of cavity aspect ratio on fluid flow and temperature field is found to be pronounced. As the cavity aspect ratio increases the heat transfer rate as well as the average fluid temperature changes. Best result is found at AR = 1.5.

(vi) It is evident that water-Cu nanofluid gives the better performance with respect to average Nusselt number.

(vii) It is also observed that in absence of magnetic effect and solid volume concentration fluid heat transfer rate increases very marginally due to changes of Ra = 10^4 to 10^5(highest 13%) but changing at Ra = 10^6 it changes unevenly (82% to 99%).for AR = 1.5 and 1. Fluid temperature increases normally with the changes of Rayleigh number. Case 2 (AR = 1.5) is the best case for fluid temperature increase (25%)

It can be said that, generally, water-Cu nanofluid performs better in terms of convective heat transfer rate than water-Al_2O_3. Magnetic field can be a control parameter for heat transfer and fluid flow in open ended channel flow with cavity. Nano fluid can be used to boost the heat transfer rate.

4.2 FURTHER WORKS

The following can be put forward for the further works as follow-ups of the present research as.

- Double diffusive mixed convection can be analyzed through including the governing equation of concentration conservation.
- Investigation can be performed by using magnetic fluid instead of electrically conducting fluid within the porous medium and changing the boundary conditions of the cavity's walls.
- The study can be extended for turbulent flow using different fluids, different thermal boundary conditions such as constant heat flux or radiation and unsteady flow.
- Only two-dimensional fluid flow and heat transfer has been analyzed in this thesis. So this deliberation may be extended to three-dimensional analyses to investigate the effects of parameters on flow fields and heat transfer in cavities.

REFERENCES

Abo-Eldahaband, E. M., and Salem, A. M., "MHD Combined Convection Flow of a Non-Newtonian Power-Law Fluid Due to a Rotating Cone or Disk", Canadian Journal of Physics, Vol. 82(7), pp. 531-540, 2004.

Aminossadati, S. M., and Ghasemib, B., "A Numerical Study of Mixed Convection in a Horizontal Channel with a Discrete Heat Source in an Open Cavity", European Journal of. Mechanics-B/Fluids, Vol. 28(4), pp. 590-598, 2009.

Basak T, Roy, S., Singh, S. K., and Pop, I., "Analysis of Mixed Convection in a Lid-Driven Porous Square Cavity with Linearly Heated Side Wall(s)", International Journal of Heat and Mass Transfer, Vol. 53(9-10), pp. 1819–1840, 2010.

Batchelor, G. K., "The Effect of Brownian Motion on the Bulk Stress in a Suspensions of Spherical Particles", Journal of Fluid Mechanics, Vol. 83(1), pp. 97-117, 1977.

Beck, M. P., Sun, T., and Teja, A. S., "The Thermal Conductivity of Alumina Nanoparticles Dispersed in Ethylene Glycol", Fluid Phase Equilibria, Vol. 260(2), pp. 275-278, 2007.

Bhuvaneswari, M., Sivasankaran, S., and Kim, Y.J., "Magnetoconvection in a Square Enclosure with Sinusoidal Temperature Distributions on Both Side Walls", Numerical. Heat Transfer, Part A, Vol. 59(3), pp 167-184, 2011

Billah, M. M., Rahman, M. M., and Uddin, M.A., "Mixed Convection Inside a Ventilated Cavity Along With a Centered Heat Conducting Horizontal Circular Cylinder'', Engineering e-Transaction, Vol.6(1), pp. 62-69, 2011.

Billah, M. M.,and Rahman, M. M., "A Numerical Study on MHD Mixed Convection in a Ventilated Cavity". The 13th Asian Congress of Fluid Mechanics, ACFM, Dhaka, Bangladesh, pp. 17-21, 2010.

Brinkman, H. C., "The Viscosity of Concentrated Suspensions and Solution", Journal of Chemical Physics, Vol. 20, pp. 571-581, 1952.

Chamkha, A. J., Hussain, S. H., and Abd-Amer, Q. R., "Mixed Convection Heat Transfer of Air inside a Square Vented Cavity with a Heated Horizontal Square Cylinder.", Numerical Heat Transfer, Part A, Vol. 59(1), pp. 58-79, 2011

Chamkha, A. J., Ismael, M. A., Pop, I., "Mixed Convection in a Lid-Driven Square Cavity with Partial Slip", International Journal of Thermal Sciences, Vol. 82(0), pp. 47 – 61, 2014.

Chandrasekar, M., Suresh, S., and Chandra Bose, A., "Experimental Investigations and Theoretical Determination of Thermal Conductivity and Viscosity ofAl_2O_3/water Nanofluid", Experimental Thermal and Fluid Science, Vol. 34(2), pp. 210-216, 2010

Chang, T. S., and Shiau, Y. H., "Flow Pulsation and Baffle's Effects on the Opposing Mixed Convection in a Vertical Channel", International Journal of Heat and Mass Transfer, Vol. 48(19-20), pp. 4190-4204, 2005.

Chatterjee, D., and Mondal, B., "Mixed Convection Heat Transfer From an Equilateral Triangular Cylinder in Cross Flow at Low Reynolds Numbers.", Heat Transfer Engineering, Vol. 36(1), pp. 123-133, 2015

Chen, H., Ding, Y., and Lapkin, A., "Rheological Behavior of Nanofluids Containing Tube/Rode-Like Nanoparticles", Powder Technology, Vol. 194(1-2), pp. 132-141, 2009.

Choi, S. U. S., "Nanofluids: From Vision to Reality Through Research", Journal of Heat Transfer, Vol. 131, pp. 033106-033109, 2009

Chon, C. H., and Kihm, K. D., "Thermal Conductivity of Nanofluids by Brownian Motion", Journal Of Heat Transfer, Vol. 127, pp. 810, 2005.

Chung, Y. C., Chen, C. L., "Numerical Study on Mixed Convection Heat Transfer in Inclined Triangular Cavities", Numerical Heat Transfer, Part A, Vol. 67(6), pp. 651–672, 2015.

Colangelo, G., Favale, E., de Risi, A., & Laforgia, D., "Results of Experimental Investigations on the Heat Conductivity of Nanofluids Based on Diathermic Oil for High Temperature Applications", Applied Energy, Vol. 97, pp. 828-833, 2011.

Corcione, M., "Empircal Correlating Equations for Predicting the Effective Thermal Conductivity and Dynamic Viscosity of Nanofluids", Energy Conversion and Management, Vol. 52(1), pp. 789-793, 2011.

Corcione, M., "Heat Transfer Features of Buoyancy-Driven Nanofluids Inside Rectangular Enclosures Differentially Heated at the Sidewalls", International Journal of Thermal Sciences, Vol. 49, pp.1536-1546, 2010.

Duangthongsuk, E., and Wongwises, S., "Measurement of Temperature-Dependent Thermal Conductivity and Viscosity of Tio_2—Water Based Nanofluids", Experimental Thermal and Fluid Science, Vol. 33(4), pp. 706-714, 2009.

Eastman, J. A., Choi, S. U. S, Li, S., Yu, W., and Thompson, L. J., "Anomalously increased effective thermal conductivities of ethylene glycol-based nanofluids containing copper nanopartices", Applied Physics Letters, Vol. 78(6), pp. 718-720, 2001.

EL-Kabeir, S. M. M., Rashad, A. M., and Gorla, R. S. R., “Unsteady MHD Combined Convection Over a Moving Vertical Sheet in a Fluid Saturated Porous Medium with Uniform Surface Heat Flux.”, Mathematical and Computer Modelling, Vol. 46(3-4), pp. 384–397, 2007.

Farid, S. K., Billah, M. M., Rahman, M. M., and Sharif, U. M., “Numerical Study of Fluid Flow on Magneto-Hydrodynamic Mixed Convection in a Lid Driven Cavity Having a Heated Circular Hollow Cylinder”, Procedia Engineering, Vol. 56, pp. 474 – 479, 2013.

Ganji, D. D., Hosseinizadeh, S.F., Sourtiji, E., Gorji-Bandpy, M., “Numerical Analysis of Mixed Convection Heat Transfer of Al_2O_3-Water Nanofluid in a Ventilated Cavity Considering Different Positions of the Outlet Port”, Powder Technology, Vol. 262, pp. 71–81, 2014.

Garoosi, F., Garoosi, S., Hooman.K., “Numerical Simulation of Natural Convection and Mixed Convection of the Nanofluid in a Square Cavity Using Buongiorno Mode”, Powder Technology, Vol. 268, pp. 279–292, 2014.

Garoosi, F., Hoseininejad, F., “Numerical Study of Natural and Mixed Convection Heat Transfer Between Differentially Heated Cylinders in an Adiabatic Enclosure Filled with Nanofluid”, Journal of Molecular Liquids, Vol. 215, pp. 1-17, 2016.

Ghadimi, A., Saidur, R., and Metselaar, H. S. C., “A Review of Nanofluid Stability Properties and Characterization in Stationary Conditions”, International Journal of Heat and Mass Transfer, Vol. 54(17-18), pp. 4051-4068, 2011.

Guo, G., Sharif, M. A. R., “Mixed Convection in Rectangular Cavities at Various Aspect Ratios with Moving Isothermal Side Walls and Constant Flux Heat Source on the Bottom Wall”, International Journal of Thermal Sciences, Vol. 43, pp. 465-475, 2004.

Gupta, S. K., Chatterjee, D., and Mondal, B., “Investigation of Mixed Convection in a Ventilated Cavity in the Presence of a Heat Conducting Circular Cylinder.”, Numerical Heat Transfer, Part A, Vol. 67(1), pp. 52-74, 2015.

Hasib, M. H., Saha, S., Hossen, S., Saha, S. C., “Onset of Transition in Mixed Convection of a Lid-Driven Trapezoidal Enclosure Filled with Water-Al2O3 Nanofluid”, Proceedings of the 19th Australasian Fluid Mechanics Conference, pp. 177. RMIT University Melbourne, Australia, 2014.

Hussein, A. K., and Hussain, S. H., “Characteristics of Magnetohydrodynamic Mixed Convection in a Parallel Motion Two-Sided Lid- Driven Differentially Heated Parallelogrammic Cavity with Various Skew Angles”, Journal of Thermal Engineering, Yildiz Technical University Press, Istanbul, Turkey, Vol. 1(3), pp. 221-235, 2015.

Hwang, Y. J., Ahn, Y. C., Shin, H. S., Lee, C. G., Kim, G. T., and Park, H. S., "Investigation on Characteristics of Thermal Conductivity Enhanced of Nanofluids", Current Applied Physics, Vol. 6(6), pp. 1068-1071, 2006.

Hwang, Y., Lee, J. K., Lee, J. K., Jeong, Y. M., Cheong, S. I., and Ahn, Y. C., "Production and Dispersion Stability of Nanoparticles in Nanofluids", Powder Technology, Vol. 186(2), pp. 145-153, 2008.

Jang, S. P., and Choi, S. U. S., "Role of Brownian Motion in the Enhanced Thermal Conductivity of Nanofluids", Applied Physics Letters, Vol. 84 (21) 4316-4318, pp. 2004.

Keblinski, P., Eastman, J. A., and Chaill, D. G., "Nanofluids for Thermal Transport", Materials Today, Vol. 8(6), pp. 36-44, 2005.

Khanafer, K. M., Abdalla, M., Amiri, A., Pop, I., "Numerical Simulation of Unsteady Mixed Convection in a Driven Cavity Using an Externally Excited Sliding Lid", European Journal of Fluid Mechanics, Vol. 26.pp. 669-687, 2007.

Khanafer, K., and Vafai, K., "A Critical Synthesis of Thermo Physical Characteristics of Nanofluids", International Journal of Heat and Mass Transfer, Vol. 54(19-20), pp. 4410-4428, 2011.

Khanafer, K., Vafai, K., and Lightstone, M., "Mixed Convection Heat Transfer in Two-Dimensional Open-Ended Enclosure", International Journal of Heat and Mass Transfer, Vol. 45, pp. 5171-5190, 2002.

Kulkarni, D. P., Das, D. K., and Vajjha, R. S., "Application of Nanofluids in Heating Buildings and Reducting Pollution", Applied Energy, Vol. 86(12), pp. 2566-2573, 2009.

Lee, I. H., Hwang, K. S., Jang, S. P., Lee, B. H., Kim, J. H., and Choi, S. U. S., "Effective Viscosities and Thermal Conductivity of Aqueous Nanofluids Containing Low Volume Concentrations of Al_2O_3 Nanoparticles", International Journal of Heat and Mass Transfer, Vol. 51(11-12), pp. 2651-2656, 2008.

Lee, S. W., Park, S. D., Kang, S., Bang, I. C., and Kim, J. H., "Investigation of Viscosity and Thermal Conductivity of Sic Nanofluids for Heat Transfer Applications", International Journal of Heat and Mass Transfer, Vol. 54, pp. 433-438, 2011.

Leong, J. C., Brown, N. M., and Lai, F. C., "Mixed Convection from an Open Cavity in a Horizontal Channel", International Communications in Heat and Mass Transfer Vol. 32, pp 583-592, 2005.

Leong, K. C., Yang, C., and Murshed, S. M. S., "A Model for the Thermal Conductivity of Nanofluids-the Effective of Interfacial Layer", Journal of Nanoparticle Research, Vol. 8, pp. 245-254, 2006.

Lin, C. Y., Wang, J. C., and Chen, T. C., "Analysis of Suspension and Heat Transfer Characteristics of Al_2O_3 Nanofluids Prepared Through Ultrasonic Vibration", Applied Energy, Vol. 88(12), pp. 4527-4533, 2011.

Liu, M. S, Lin, M. C. C., Tsai, C. Y., and Wang C. C., "Enhancement of Thermal Conductivity with Cu for Nanofluids Using Chemical Reduction Method", International Journal of Heat and Mass Transfer, Vol. 49(17-18), pp. 3028-3033, 2006.

Lundgren, T.S., "Slow Flow Through Stationary Random Beds and Suspensions of Spheres", Journal of Fluid Mechanics, Vol. 51(2), pp. 273-299, 1972.

Luo, W. J., and Yang, R. J., "Multiple Fluid Flow and Heat Transfer Solutions in a Two-Sided Lid-Driven Cavity", International Journal of Heat and Mass Transfer, Vol. 50, pp. 2394-2405, 2007.

Mahbubul, I. M., Saidur, R., and Amalina, M. A., "Latest Developments on the Viscosity of Nanofluids", International Journal of Heat and Mass Transfer, Vol. 55(4), pp. 874-885, 2011.

Mamun, M. A. H., Rahman,M. M., Billah, M. M., and R. Saidur, "A Numerical Study on the Effect of a Heated Hollow Cylinder on Mixed Convection in a Ventilated Cavity'', International Communications in Heat and Mass Transfer, Vol.37(9), pp. 1326-1334, 2010.

Manca, O., Nardini, S., and Vafai, K., "Experimental Investigation Mixed Convection in a Channel With an Open Cavity", Experimental Heat Transfer, Vol. 19, pp. 53–68, 2006.

Manca, O.,Nardini, S.,Khanafer, K., and Vafi, K., "Effect of Heated Wall Position on Mixed Convection in a Channel with an Open Cavity", Numerical Heat Transfer, Part A, Vol. 43 pp. 259-282, 2003

Mansour, M. A., Mohamed, R. A., Abd-Elaziz, M. M., and Ahmed, S. E., " Numerical simulation of mixed convection flows in a square lid-driven cavity partially heated from below using nanofluid", International. Communications in. Heat and Mass Transfer, Vol. 37, pp. 1504–1512, 2010.

Maxwell, J. C., "A Treatise on Electricity and Magnetism", second ed., Clarendon Press, Oxford, UK, 1881

Mintsa, H. A., Roy, G., Nguyen, C. T., and Doucet, D., "New Temperature Dependent on Thermal Conductivity Data for Water-Based Nanofluids", International Journal of Thermal Sciences, Vol. 48 (2), pp. 363-371, 2009.

Mukhopadhyay, S., Gorachand, C., Layek, and Gorla, R. S. R., "MHD Combined Convection Flow Past a Stretching Surface", International Journal of Fluid Mechanics Research, Vol. 34(3), pp. 244-257, 2007.

Murshed, S. M. S., Leong, K. C., and Yang, C., "Enhanced Thermal Conductivity of Tio_2—Water Based Nanofluids", International Journal of Thermal Sciences, Vol. 44(4), pp. 367-373, 2005.

Murshed, S. M. S., Leong, K. C., and Yang, C., "Investigation of Thermal Conductivity and Viscosity of Nanofluids", International Journal of Thermal Sciences, Vol. 47(5), pp. 560-568, 2008b.

Murshed, S. M. S., Leong, K. C., and Yang, C., "Thermophysical and Electrokinetic Properties of Nanofluids – a Critical Review", Applied Thermal Engineering, Vol. 28 (17-18), pp. 2109-2125, 2008a.

Muthtamilselvan, M., Kandaswamy, P., and Lee, J., "Heat Transfer Enhancement of Copper-Water Nanofluids in a Lid-Driven Enclosure", Communications in Nonlinear Science and Numerical Simulation, Vol. 15(6), pp. 1501-1510, 2010.

Nada, E. A., and Chamkha, A. J., "Mixed Convection Fow of a Nanofluid in a Lid-Driven Cavity with a Wavy Wall", International Communications in Heat and Mass Transfer, Vol. 57, pp. 36–47, 2014.

Najam, M., Amahmid, A., Hasnaoui, M., and Alami, M. E., "Unsteady Mixed Convection in a Horizontal Channel with Rectangular Blocks Periodically Distributed on its Lower Wall", International Journal of Heat and Fluid Flow, Vol.24, pp. 726-735, 2003.

Namburu, P. K., Kulkarni, D. P., Misra, D., and Das, D. K., "Viscosity of Copper Oxide Nanoparticles Dispersed in Ethylene Glycol and Water Mixture", Experimental Thermal and Fluid Science, Vol. 32(2), pp. 397-402, 2007.

Nasrin, R., Alim, M. A., and Chamkha, A. J., "Effect of Heating Wall Position on Forced Convection Along Two Sided Open Enclosure with Porous Medium Utilizing Nanofluid", International Journal of Energy & Technology, Vol. 5 (9) pp. 1-13, 2013).

Nayak R. K., Bhattacharyya S. and Pop I., "Numerical Study on Mixed Convection and Entropy Generation of a Nanofluid in a Lid-Driven Square Enclosure,", Journal of Heat Transfer, Vol. 138(1), pp. 11, 2015.

Nguyen, C. T., Desgranges, F., Roy, G., Galanis, N., Mare, T., and Boucher, S., "Temperature and Particle-Size Dependent Viscosity Data for Water-Based Nanofluids-Hysteresis Phenomenon", International Journal of Heat and Fluid Flow, Vol. 28(6), pp. 1492-1506, 2007.

Ogot, E.B., "Magnetohydrodynamic Natural Convection Flow in an Enclosure with a Finite Length Heater Using The Differential Quadrature (DQ) Method", Numerical Heat Transfer, Part A, Vol. 58(11), pp. 900-921, 2010.

Omri, A., and Nasrallah, S. B., "Control Volume Finite Element Numerical Simulation of Mixed Convection in an Air-Cooled Cavity", Numerical Heat Transfer, Part A, Vol. 36, pp. 615–637, 1999.

Osalusi, E., Side, J., Harris, R., and Clark, P., "The Effect of Combined Viscous Dissipation and Joule Heating on Unsteady Mixed Convection MHD Flow on a Rotating Cone in a Rotating Fluid with Variable Properties in the Presence of Hall and Ion-Slip Currents.", International Communications in Heat and Mass Transfer, Vol. 35(4), pp. 413–429, 2008.

Oztop H.F., "Influence of Exit Opening Location on Mixed Convection in a Channel with Volumetric Heat Sources", International Communications in Heat and Mass Transfer, Vol. 37(4), pp. 410-415, 2011.

Oztop, H.F., Oztop, M., and Varol, Y., "Numerical Simulation of Magnetohydrodynamic Buoyancy-Induced Flow in a Non-Isothermally Heated Square Enclosure", Communications in Nonlinear Science and Numerical Simulation, Vol. 14, pp 770-778, 2009.

Pantokratoras, A., "Opposing Mixed Convection Along Vertical Isothermal Moving Bodies", International Journal of Heat and Fluid Flow, Vol. 25, pp: 692–696, 2004.

Prasher, R., Bhattacharya, P., and E. Phelan, P., "Brownian Motion Based Convective Conductive Model for the Effective Thermal Conductivity of Nanofluids", Journal of Heat Transfer, Vol. 128, pp. 588-595, 2006.

Rahman, M. M, Parvin, S, Saidur R, and Rahim, N. A., "Magnetohydrodynamic Mixed Convection in a Horizontal Channel with an Open Cavity", International Communications in Heat and Mass Transfer, Vol. 38, pp. 184-193, 2011b

Rahman, M. M., Alim, M. A. and Mamun, M. A. H. "Finite Element Analysis of Mixed Convection in a Rectangular Cavity with a Heat-Conducting Horizontal Circular Cylinder", Nonlinear analysis: Modeling and Control, Vol.14(2), pp. 217-247, 2009.

Rahman, M. M., Alim, M. A., and Chowdhury, M. K., Magnetohydrodynamic Mixed Convection Around a Heat Conducting Horizontal Circular Cylinder in a

Rectangular Lid-Driven Cavity with Joule Heating", Journal of Scientific Research Vol. 1(3), pp. 461-472, 2009.

Rahman, M. M., Alim, M. A., Mamun, M. A. H., Chowdhury, M.K. and Islam, A.K.M.S., "Numerical Study of Opposing Mixed Convection in a Vented Enclosure", ARPN Journal of Engineering and Applied Sciences, Vol. 2(2), pp. 25-36, 2007.

Rahman, M. M., Alim, M. A., Saha, S. and Chowdhury, M. K., "A Numerical Study of Mixed Convection in A Square Cavity with A Heat Conducting Square Cylinder at Different Locations", Journal of Mechanical Engineering, The Institution of Engineers, Bangladesh, Vol. ME 39(2), pp. 78 - 85, 2008a.

Rahman, M. M., Alim, M. A., Saha, S. and Chowdhury, M. K., "Mixed Convection in a vented Square Cavity with a Heat Conducting Horizontal Solid Circular Cylinder", Journal of Naval Architecture and Marine Engineering, Vol. 5(2), pp.37 - 46, 2008b.

Rahman, M. M., Billah, M. M. and Alim, M. A., "Effect of Reynolds and Prandtl Numbers on Mixed Convection in an Obstructed Vented Cavity, "Journal of Scientific Research'', Vol. 3(2), pp.271-281, 2011.

Rahman, M. M., Billah, M. M., Rahim, N. A., Saidur, R., and Hasanuzzaman, M., "Finite Element Simulation of Magnetohydrodynamic Mixed Convection in a Double-Lid Driven Enclosure with a Square Heat-Generating Block", ASME Journal of Heat Transfer,Vol. 134/ 062501-8, 2012.

Rahman, M. M., Billah, M. M.,Mamun, M. A. H., Saidur, R., and Hasanuzzaman, M., "Reynolds and Prandtl Numbers Effects on MHD Mixed Convection in a Lid-Driven Cavity Along with Joule Heating and a Centered Heat Conducting Circular Block" International Journal of Mechanical and Materials Engineering (IJMME), Vol. 5(2), pp. 163-170, 2010.

Rahman, M. M., Öztop, H. F., Saidur, R., Mekhilef, S., and Al-Salem, K., "Finite Element Solution of MHD Mixed Convection in a Channel With a Fully or Partially Heated Cavity" Computers & Fluids; Vol. 79 (25), pp. 53–64, 2013

Rahman, M. M., Parvin, S., Hasanuzzaman, M., Saidur, R., and Rahim, A. N., "Effect of Heat-Generating Solid Body on Mixed Convection Flow in a Ventilated Cavity", Heat Transfer Engineering, Vol. 34(15), pp. 1249 – 1261, 2013.

Rahman, M. M., Saidur, R., Rahim, N. A., "Conjugated Effect of Joule Heating and Magneto-Hydrodynamic on Double-Diffusive Mixed Convection in a Horizontal Channel with an Open Cavity", International Journal of Heat and Mass Transfer, Vol. 54, pp 3201-3213, 2011a.

Saha, L. K., Uddin, K. M. S., and Taher, M. A., “Effect of Internal Heat Generation or Absorption on MHD Mixed Convection Flow in a Lid Driven Cavity.”, American Journal of Applied Mathematics, Vol. 3(1), pp. 20-29, 2015.

Sarit, K. D., Choi, S. U. S., Yu, W., and Pradeep, T., “Nanofluids Science and Technology”, New Jersey: Wiley Interscience. (2007)

Sarris, I. E., Kakarantzas, S. C., Grecos, A. P., and Vlachos, N. S., “MHD Natural Convection in a Laterally and Volumetrically Heated Square Cavity”, International Journal of Heat and Mass Transfer, Vol. 48, pp. 3443-3453, 2005.

Selimefendigil, F., “Numerical Analysis and POD Based Interpolation of Mixed Convection Heat Transfer in Horizontal Channel with Cavity Heated from Below.”, Engineering Applications of Computational Fluid Mechanics, Vol. 7(2), pp. 261-271, 2013

Sharif, U. M., Rahman, M. M., Saklayen, M. A., Billah, M. M., Elias M., “A Numerical Study of Assisting MHD Mixed Convection Inside a Ventilated Cavity”, Engineering e-Transaction, Vol. 7(1), pp. 6-13, 2012.

Shercliff, J. A., A Textbook of Magnetohydrodynamics, First Ed., Pergamon Press, UK, 1965.

Singh, S., and Sharif, M. A. R., “Mixed Convective Cooling of a Rectangular Cavity with Inlet and Exit Openings on Differentially Heated Side Walls”, Numerical Heat Transfer, Part A, Vol. 44, pp. 233–253, 2003.

Sposito, G., and Ciofalo, M., “Fully Developed Mixed Magnetohydrodynamic Convection in a Vertical Square Duct”, Numerical Heat Transfer, Part A, Vol. 53(9), pp. 907-924, 2008.

Vajjha, R. S., and Das, D. K., “Experimental Determination of Thermal Conductivity of Three Nanofluids and Development of New Correlations”, International Journal of Heat and Mass Transfer, Vol. 52(21-22), pp. 4675-4682, 2009.

Wang, X. Q., and Mujumder, A. S., “Heat Transfer Characteristics of Nanofluids: A Review”, International Journal of Thermal Sciences, Vol. 46(1), pp. 1-19, 2007.

Wu, S., Zhu, D., Li, X., Li, H., and Lei, J., “Thermal Energy Storage Behavior of Al_2O_3- H_2O Nanofluids”, Thermochimica Acta, Vol. 483(1-2), pp. 73-77, 2009.

Yapici, K., Obut, S., “Laminar Mixed-Convection Heat Transfer in a Lid-Driven Cavity with Modified Heated Wall”. Heat Transfer Engineering, Vol. 36(3), pp. 303–314, 2015.

Yoo, D. H., Hong, K. S., and Yang, H. S., “Study of Thermal Conductivity of Nanofluids for the Application of Heat Transfer Fluids”, Thermochimica Acta, Vol. 455(1-2), pp. 66-69, 2007.

Yu, W., and Choi, S. U. S., "The Role of Interfacial Layers in the Enhanced Thermal Conductivity of Nanofluids: A Renovated Maxwell Model", Journal of nanoparticle Research, Vol. 5, pp. 167-171, 2003.

Yu, W., and Choi, S. U. S., "The Role of Interfacial Layers in the Enhanced Thermal Conductivity of Nanofluids: A Renovated Hamilton-Crosser Model", Journal of nanoparticle Research, Vol. 6, pp. 355-361, 2004.

Yu, W., France, D. M., Choi, S. U. S., and Routbort, J. L., "Review and Assessment of Nanofluid Technology for Transportation and other Application (No. ANL/ESD/07-9)", Argonne: Energy System Division, Argonne National Laboratoryo. (Document Number), 2007.

Yu, W., Xie, H., Chen, L., and Li, Y., "Investigation of Thermal Conductivity and Viscosity of Ethylene Glycol Based on Zno Nanofluid", Thermochimica Acta, Vol. 491(1-2), pp. 2-96, 2009.

Yu, W., Xie, H., Chen, L., and Li, Y., "Investigation on the Thermal Transport Properties of Ethylene Glycol-Based Nanofluids Containing Copper Nanoparticles", Powder Technology, Vol. 197(3), pp. 218-221, 2010.

Zhang, X., Gu, H., & Fujii, M. "Effective Thermal Conductivity and Thermal Diffusivity of Nanofluids Containing Spherical and Cylindrical Nanoparticles", Experimental Thermal and Fluid Science, 31(6), pp.593-599, 2007.

Zhu, D., Li, X., Wang, N., Gao, J., and Li, H., "Dispersion Behavior and Thermal Conductivity Characteristics of Al_2O_3-H_2O Nanofluids", Current Applied Physics, Vol. 9(1), pp. 131-139, 2009.

Zienkiewicz, O. C. and Taylor, R. L., "The Finite Element Method", Fourth Ed., McGraw-Hill, 1991.